Technische Universität Graz
Institut für Festigkeitslehre
Kopernikusgasse 24/I
8010 Graz

Christoph Ager, BSc

Application of the Extended Finite Element Method for quasi-static crack growth

Masterarbeit

zur Erlangung des akademischen Grades
eines Diplom–Ingenieurs

Technische Universität Graz
Fakultät für Maschinenbau und Wirtschaftswissenschaften

Studienrichtung:
Maschinenbau

Betreuer: Dipl.-Ing. Dr.techn. Stefan Hollerer
Beurteiler: O.Univ.–Prof. Dipl.–Ing. Dr.techn. Christian C. Celigoj

Deutsche Fassung:
Beschluss der Curricula-Kommission für Bachelor-, Master- und Diplomstudien vom 10.11.2008
Genehmigung des Senates am 1.12.2008

EIDESSTATTLICHE ERKLÄRUNG

Ich erkläre an Eides statt, dass ich die vorliegende Arbeit selbstständig verfasst, andere als die angegebenen Quellen/Hilfsmittel nicht benutzt, und die den benutzten Quellen wörtlich und inhaltlich entnommenen Stellen als solche kenntlich gemacht habe.

Graz, am …… ……..
(Unterschrift)

Englische Fassung:

STATUTORY DECLARATION

I declare that I have authored this thesis independently, that I have not used other than the declared sources / resources, and that I have explicitly marked all material which has been quoted either literally or by content from the used sources.

…… ……..
date (signature)

Vorwort

Die vorliegende Arbeit beschreibt den Einsatz der Erweiterten Finiten Elemente Methode für quasi-statisches Risswachstum. Sie wurde als Abschluss meines Masterstudiums am Institut für Festigkeitslehre an der Technischen Universität Graz durchgeführt.

Ich möchte mich an dieser Stelle bei Prof. Christian Celigoj und Dr. Stefan Hollerer bedanken, die mir diese Arbeit ermöglichten und mich dabei in allen Belangen immer bestens unterstützten.

Darüber hinaus möchte ich mich bei Dr. Michael Hammer bedanken, der mich in die Umsetzung der Finiten Elemente Methode einführte und den grundlegenden Programmcode für diese Arbeit zur Verfügung stellte.
Weiterer Dank gilt Matthias Rambausek, BSc der immer Zeit zur Lösung auftretender Probleme fand, sowie Ass.-Prof. Manfred Ulz, der mir bei Fragen immer hilfreich zur Verfügung stand.

Ein ganz besonderer Dank gebührt jedoch meiner Familie, vor allem meinen Eltern Anna und Franz Ager, die mir das Studium ermöglichten und mich während der gesamten Studienzeit unterstützten.

Christoph Ager, Graz, am 16. Mai 2013

Abstract

The Extended Finite Element Method (XFEM) allows the consideration of non-smooth or non-continuous effects in the displacements of arbitrary meshes. This is achieved by enlarging the approximation space of the standard Finite Element Method (FEM) with additional enrichment functions.

In this thesis, the XFEM is used to analyze static cracks and quasi-static crack growth inside of 2-dimensional bodies. Firstly, the basics of the Finite Element Method are given, followed by a selection of required fundamentals in fracture mechanics. Afterwards the basics of the XFEM, with a focus on its application to crack analysis, are shown.

The calculations are implemented using the Python programming language, based on pySoofea, a computer code for the standard FEM. To describe the cracks in the actual implementation, level set functions are used. All additional steps compared with the standard FEM such as finding the crack tip, selection of enriched nodes, calculation of new integration points, assembling of the stiffness matrix, calculation of stress intensity factors and the crack growth method are described in detail.

Results of test cases are compared to analytical solutions in order to evaluate the method. Finally, by quasi-static crack growth the crack paths in a stretched plate and a beam are evaluated and analyzed.

Kurzfassung

Die Erweiterte Finite Elemente Methode (XFEM) ermöglicht die Betrachtung von unstetigen und nicht glatten Verschiebungsfeldern in beliebigen Rechennetzen. Dies wird ermöglicht durch eine Vergrößerung des Approximationsraumes der klassischen Finite Elemente Methode (FEM) mit zusätzlichen Anreicherungsfunktionen.

In dieser Arbeit wird die XFEM angewandt, um statische Risse und quasi-statisches Risswachstum in 2-dimensionalen Bauteilen zu untersuchen. Beginnend mit den Grundlagen der Finiten Elemente Methode und einer Auswahl des benötigten Basiswissens in Bruchmechanik, werden anschließend die zusätzlichen Grundlagen für die hier betrachtete Anwendung der XFEM gezeigt.

Die Berechnungen werden in der Programmiersprache Python, aufbauend auf dem klassischen FEM-Code pySoofea durchgeführt. Für die Beschreibung der Risse werden Level-Set Funktionen verwendet. Alle zusätzlich zur klassischen FEM erforderlichen Schritte wie Positionsbestimmung der Rissspitze, Auswahl der angereicherten Knoten, Bestimmung der neuen Integrationspunkte, Assemblierung der Steifigkeitsmatrix, Berechnung der Spannungsintensitätsfaktoren und die Risswachstumsmethode werden im Detail beschrieben.

Testfälle mit verfügbaren analytischen Lösungen werden benutzt um die Methode zu beurteilen. Abschließend erfolgt durch quasi-statische Risswachstumsberechnungen an einer Scheibe und einem Balken die Ermittlung und Analyse des Risspfades.

Contents

1. Basics of the standard Finite Element Method **1**
- 1.1. Differential 3d stress equilibrium . . . 1
  - 1.1.1. Stress equilibrium inside the body . . . 1
  - 1.1.2. Stress equilibrium on the surface of the body . . . 2
- 1.2. Strain-displacement relations . . . 2
- 1.3. Voigt notation . . . 2
- 1.4. Constitutive law . . . 3
- 1.5. The principle of virtual displacements . . . 4
- 1.6. Fundamental equations for the Finite Element Analysis . . . 4
  - 1.6.1. Displacement approximation . . . 5
  - 1.6.2. Finite Element equilibrium . . . 6
  - 1.6.3. Boundaries . . . 7
- 1.7. Standard shape functions . . . 8
  - 1.7.1. Lagrange polynomials . . . 8
  - 1.7.2. Shape function for quadrilaterals . . . 9
  - 1.7.3. Isoparametric concept, the Jacobian matrix . . . 10
- 1.8. Numerical integration . . . 11
  - 1.8.1. The Gauss formulae . . . 11
  - 1.8.2. 2 dimensional integration . . . 12

2. Selected fundamentals of linear elastic fracture mechanics **13**
- 2.1. The three modes of fracture . . . 13
- 2.2. Crack tip field - stress intensity factors . . . 14
- 2.3. Path independent integral about the crack tip (J-integral) . . . 15
- 2.4. Crack growth criterion . . . 17
  - 2.4.1. The maximal circumferential stress criterion . . . 17

3. Extended Finite Element Method **18**
- 3.1. Local enrichment . . . 18
  - 3.1.1. Shifted enrichment interpolation . . . 19
- 3.2. Modelling of cracks . . . 20
  - 3.2.1. Modelling the crack path . . . 20
  - 3.2.2. Modelling the crack tip . . . 20
- 3.3. Level set functions . . . 22
- 3.4. Numerical integration in the context of XFEM . . . 24

4. Implementation **25**
- 4.1. Calculation process . . . 26
- 4.2. Entry point and exit point of an interface in quadrilaterals . . . 27
- 4.3. Selection of enriched nodes . . . 27

4.4. Finding the crack tip . . . 29
4.5. Global indexing . . . 30
4.6. Integration points for elements with an interface . . . 31
4.6.1. Subelements for quadrilaterals cut by a discontinuity . . . 31
4.6.2. Subelements for quadrilaterals with a crack tip . . . 34
4.6.3. Positions and weights of integration points from subelements . 34
4.7. Formulation of matrices in the FE equilibrium . . . 36
4.7.1. Evaluation of the strain-displacement matrix . . . 37
4.7.2. Evaluation of the interpolation matrix . . . 38
4.8. Evaluation of stress intensity factors . . . 38
4.8.1. Domain form of the interaction integral . . . 38
4.8.2. Implementation of the interaction integral . . . 41
4.9. Crack growth by modification of level set functions . . . 43
4.9.1. Crack growth process . . . 44
4.9.2. Calculate crack growth angle . . . 45
4.9.3. Remove tip enrichment, recover crack path enrichment . . . 45
4.9.4. Calculate element boundary - crack intersection points . . . 45
4.9.5. Modify level set function . . . 46
4.9.6. Selection of enriched nodes . . . 49

5. Numerical examples **52**
5.1. Edge crack under tensile stress in a stretched plate . . . 52
5.1.1. Analytical solution . . . 52
5.1.2. Numerical solution . . . 53
5.2. Rotated, centered crack under tensile stress in a stretched plate (mixed mode crack problem) . . . 57
5.2.1. Analytical solution . . . 57
5.2.2. Numerical solution . . . 57
5.3. Centered, circular crack under biaxial stress in a stretched plate . . . 61
5.3.1. Analytical solution . . . 61
5.3.2. Numerical solution . . . 61
5.4. Crack growth under point force load in a beam . . . 65
5.4.1. Numerical solution . . . 65
5.5. Crack growth from two holes in a plate under tensile stress . . . 68
5.5.1. Numerical solution . . . 68

6. Conclusion **72**

A. Derivations **74**
A.1. Derivation of crack growth direction . . . 74
A.2. Derivatives of enrichment functions . . . 75
A.3. Calculate local coordinates from global coordinates for quadrilaterals 77
A.4. Span of the tip enrichment functions . . . 78
A.5. Details using Gauss' theorem for the interaction integral . . . 79
A.6. Derivatives of the analytical crack tip field . . . 79

Bibliography **81**

List of Figures

1.1. Body discretized with elements 5
1.2. 1d Beam element in natural coordinates 8
1.3. Shape function for 1d beam element in natural coordinates 9
1.4. 2d quadrilateral element in natural coordinates 9
1.5. 2d quadrilateral element with integration points 12

2.1. Modes of fracture 13
2.2. Local crack coordinate system 14
2.3. New crack growth direction 17

3.1. Domain of quadrilaterals with enriched nodes 19
3.2. Enriched nodes for a crack 21
3.3. Enrichment function $\psi_{tip}^{(1)}(\mathbf{x})$ 22
3.4. Enrichment function $\psi_{tip}^{(2)}(\mathbf{x})$ 22
3.5. Enrichment function $\psi_{tip}^{(3)}(\mathbf{x})$ 22
3.6. Enrichment function $\psi_{tip}^{(4)}(\mathbf{x})$ 22
3.7. Enriched nodes for a crack with larger tip enrichment 22
3.8. a) Description of crack path by $\phi(\mathbf{x})$ and b) crack tip by $\phi^t(\mathbf{x})$ 23
3.9. Integration areas for elements split by a discontinuity 24

4.1. Extended Finite Element Method (XFEM) calculation process 26
4.2. Evaluation of element entry point and exit point 27
4.3. Possible interfaces described by level set function values ϕ_i 28
4.4. Types of elements that are cut by two interfaces 28
4.5. Quadrilateral cut by two interfaces 29
4.6. Quadrilateral subelements for the reference configuration of case a) in all three occurring coordinate systems 32
4.7. Quadrilateral subelements for the reference configuration of case b) in all three occurring coordinate systems 33
4.8. Quadrilateral subelements for the reference configuration of a crack tip interface in all three occurring coordinate systems 34
4.9. Integration points for a structured grid of quadrilaterals with a crack discontinuity 36
4.10. Paths around crack tip and coordinate system 39
4.11. Weighting function $q(\mathbf{x})$ around the crack tip 40
4.12. Weighting function $q(\mathbf{x})$ created from nodal values $\hat{q}_i$, for a grid around the crack tip 41
4.13. Local crack coordinate system 43
4.14. XFEM crack growth process 44

4.15. Crack growth 45
4.16. Recover crack path enrichment 46
4.17. Element cut by a new crack segment 47
4.18. Modification of the level set function $\phi(\mathbf{x})$ for crack growth in a quadrilateral; configuration a) 47
4.19. Effect of varying the level set value ϕ_n on the crack interface 49
4.20. Modification of the level set function $\phi(\mathbf{x})$ for crack growth in a quadrilateral; configuration b) 49
4.21. Modification of the level set function $\phi(\mathbf{x})$ (illustrated by color) with actual crack for a crack growth example; a) 1st step (inital state), b) 2nd step, c) 3rd step, d) 4th step), e) 10th step 50

5.1. Edge crack under tensile stress in a stretched plate 52
5.2. Meshes for the calculation of the edge crack (marked) - a) coarse structured; b) fine structured; c) unstructured 53
5.3. Deformed plate with an edge crack under tensile stress (displacements multiplied by factor 10^3); color shading shows y - displacement 54
5.4. Rotated, centered crack under tensile stress in a stretched plate . . . 57
5.5. Unstructured mesh for the calculation of the rotated, centered crack (marked) under tensile stress with refined zone in the crack area . . . 58
5.6. Detail of the deformed plate with a rotated, centered crack under tensile stress (displacements multiplied by factor 5); color shading shows y - displacement; a) $\beta = 0°$, b) $\beta = 45°$, c) $\beta = 90°$ 59
5.7. K_I and K_{II} - numerical solution compared to analytical solution for rotated, centered crack under tensile stress 59
5.8. Normalized K_I and K_{II} with reference to the analytical solution for both crack tips, for rotated, centered crack under tensile stress 60
5.9. Centered, circular crack under biaxial stress in a stretched plate . . . 61
5.10. Unstructured mesh for the calculation of the centered, circular crack under biaxial stress with refined zone in the crack area 62
5.11. Detail of the deformed plate with a centered, circular crack under biaxial stress (displacements multiplied by factor 10); color shading shows y - displacement; a) $\beta = 45°$, b) $\beta = 60°$, c) $\beta = 90°$ 64
5.12. Initial configuration for crack growth analysis under point force load in a beam 65
5.13. Unstructured mesh for the crack growth analysis under point force load in a beam 66
5.14. Position of the crack tip for the different crack growth lengths l_c . . . 66
5.15. Detail of deformed beam under point force load for different crack growth steps with growth length $l_c = 0.025\,mm$ (displacements multiplied by factor 3); color shading shows the magnitude of the displacement ; a) Step 1 (inital configuration), b) Step 5, c) Step 10, d) Step 15, e) Step 20 67
5.16. Initial configuration for crack growth analysis from two holes in a plate under tensile stress 68
5.17. Unstructured coarse mesh with 4874 quadrilaterals for crack growth analysis from two holes in a plate under tensile stress 69

5.18. Unstructured, refined mesh with 28726 quadrilaterals for crack growth analysis from two holes in a plate under tensile stress 69
5.19. Positions of the crack tip for the different crack growth lengths l_c and varying meshes; top: tip 2, bottom: tip 1 70
5.20. Detail of deformed plate with two holes for different crack growth steps with growth length $l_c = 0.1\,mm$ (displacements multiplied by factor 5); color shading shows y - displacement; a) Step 1(inital configuration), b) Step 2, c) Step 10, d) Step 20, e) Step 40 71

A.1. Tip coordinate systems 76

List of Tables

4.1. Quadrilateral subelements with their node points for case a) 32
4.2. Quadrilateral subelements with their node points for case b) 33
4.3. Quadrilateral subelements with their node points for elements with a crack tip 35

5.1. Calculated K_I for structured coarse mesh, for different enrichment zone and weight functions of the interaction integral 55
5.2. Calculated K_I for structured fine mesh, for different enrichment zone and weight functions of the interaction integral 55
5.3. Calculated K_I for unstructured mesh, for different enrichment zone and weight functions of the interaction integral 56
5.4. Analytic solutions of K_I and K_{II} for the centered, circular crack . . . 62
5.5. Calculated K_I and K_{II} for different enrichment zones of the circular crack with $\beta = 45°$ 63
5.6. Calculated K_I and K_{II} for different angles β of the circular crack. Thereby, only the crack tip element is enriched by the crack tip enrichment functions 63

1. Basics of the standard Finite Element Method

The aim of the Finite Element Method (FEM) is to calculate the response of solid bodies with any boundary conditions aligned. Especially for cases with no available analytical solution, which is the case for most technical problems, this is the favoured method. Therefore, the body is split into a finite number of elements. By calculating the displacement values in the nodes of these elements, the solution can be obtained.

In the following section, the differential 3d stress equilibrium by using the principle of virtual displacements will lead to the basic equation of the displacement-based FEM. Additionally, the constitutive law and the stress-strain relation are required. In the last section, the numerical integration will be shown.

The following derivations in this chapter are based on [5, 6, 2], although we will use some different notations with regard to the Extended Finite Element Method.

1.1. Differential 3d stress equilibrium

The stress equilibrium is satisfied in every point inside the body as well as on the surface of the entire domain.

1.1.1. Stress equilibrium inside the body

We think of an infinitesimal cube (dimensions $\mathrm{d}x$, $\mathrm{d}y$ and $\mathrm{d}z$) that is cut out of an arbitrary body. The edges are aligned to the x, y, z - Cartesian coordinate system. The propriate partial derivatives of the stress vectors $\boldsymbol{\sigma}_x$, $\boldsymbol{\sigma}_y$, $\boldsymbol{\sigma}_z$ on each surface have to be in equilibrium with the body force $\mathbf{f}^B$ and the inertial force $(-\rho\mathbf{a})$:

$$\frac{\partial \boldsymbol{\sigma}_x}{\partial x} + \frac{\partial \boldsymbol{\sigma}_y}{\partial y} + \frac{\partial \boldsymbol{\sigma}_z}{\partial z} + \mathbf{f}^B - \rho\mathbf{a} = \mathbf{0} \tag{1.1}$$

Stress vectors ($i = x, y, z$), body force and inertial force have components in all three Cartesian coordinate directions:

$$\boldsymbol{\sigma}_i = \begin{bmatrix} \sigma_{ix} \\ \sigma_{iy} \\ \sigma_{iz} \end{bmatrix} \qquad \mathbf{f}^B = \begin{bmatrix} f_x^B \\ f_y^B \\ f_z^B \end{bmatrix} \qquad -\rho\mathbf{a} = \begin{bmatrix} -\rho a_x \\ -\rho a_y \\ -\rho a_z \end{bmatrix} \tag{1.2}$$

All stress vectors can be arrayed in the stress tensor:

$$\mathbf{S} = \begin{bmatrix} \sigma_{xx} & \sigma_{xy} & \sigma_{xz} \\ \sigma_{yx} & \sigma_{yy} & \sigma_{yz} \\ \sigma_{zx} & \sigma_{zy} & \sigma_{zz} \end{bmatrix} \tag{1.3}$$

The first index of the stress components defines the direction of the surface normal vector, the second index specifies the direction of the component. As the stress tensor is symmetric it has only 6 independent components. This fact results from the rotational equilibrium.

1.1.2. Stress equilibrium on the surface of the body

Imagine an arbitrary body with a force load on the surface. For a local point with normal vector $\mathbf{n}$ (components n_x, n_y, n_z), the local surface force $\mathbf{f}^S$ satisfies the local equilibrium (Cauchy formula):

$$\mathbf{f}^S = \boldsymbol{\sigma}_x n_x + \boldsymbol{\sigma}_y n_y + \boldsymbol{\sigma}_z n_z = \mathbf{S}^T \cdot \mathbf{n} \tag{1.4}$$

The surface force has components in all three Cartesian coordinate directions:

$$\mathbf{f}^S = \begin{bmatrix} f_x^S \\ f_y^S \\ f_z^S \end{bmatrix} \tag{1.5}$$

1.2. Strain-displacement relations

Generated by the displacement $\mathbf{u}$ (u, v, w in Cartesian coordinate directions x,y,z respectively), a mesasure for the deformation called strain can be defined. There are different ways to define strain and, particularly, for small strains we get a simple form. If displacements and their derivatives are small we can set up equilibrium on the undeformed body and as a result, the analysis gets linear. In the following, the strains are specified:

$$\epsilon_{xx} = \frac{\partial u}{\partial x} \qquad \epsilon_{yy} = \frac{\partial v}{\partial y} \qquad \epsilon_{zz} = \frac{\partial w}{\partial z} \tag{1.6}$$

$$\epsilon_{xy} = \frac{1}{2}\left(\frac{\partial u}{\partial y} + \frac{\partial v}{\partial x}\right) \qquad \epsilon_{yz} = \frac{1}{2}\left(\frac{\partial v}{\partial z} + \frac{\partial w}{\partial y}\right) \qquad \epsilon_{zx} = \frac{1}{2}\left(\frac{\partial w}{\partial x} + \frac{\partial u}{\partial z}\right) \tag{1.7}$$

These strains can be combined in the linear strain tensor:

$$\mathbf{V} = \begin{bmatrix} \epsilon_{xx} & \epsilon_{xy} & \epsilon_{xz} \\ \epsilon_{yx} & \epsilon_{yy} & \epsilon_{yz} \\ \epsilon_{zx} & \epsilon_{zy} & \epsilon_{zz} \end{bmatrix} \tag{1.8}$$

Also this tensor is symmetric, but has only 3 independent components, which is a result of constraints that prohibit gaps and overlapping.

1.3. Voigt notation

Taking the symmetry of the stress-tensor and strain-tensor into account, the components of these tensors can be set up in 1-dimensional (1d) arrays (Voigt

notation), respectively. As a consequence, handling the following steps will get easier.

$$\boldsymbol{\sigma} = \begin{bmatrix} \sigma_{xx} \\ \sigma_{yy} \\ \sigma_{zz} \\ \sigma_{xy} \\ \sigma_{yz} \\ \sigma_{zx} \end{bmatrix} \qquad \boldsymbol{\epsilon} = \begin{bmatrix} \epsilon_{xx} \\ \epsilon_{yy} \\ \epsilon_{zz} \\ 2\epsilon_{xy} \\ 2\epsilon_{yz} \\ 2\epsilon_{zx} \end{bmatrix} \tag{1.9}$$

1.4. Constitutive law

With (1.1) and (1.4) the state of stress for a body under force load is described. With (1.6) and (1.7) strain can be evaluated out of the displacements. The connection between stress and strain is given by the material behavior. In general this has the following form:

$$\mathbf{S} = \mathbb{C} : \mathbf{V} \tag{1.10}$$

in index notation:

$$\sigma_{ij} = \mathbb{C}_{ijkl}\, \epsilon_{kl} \tag{1.11}$$

Here $\mathbb{C}$ is the elasticity tensor, which is a symmetric, forth-order tensor. In general it can be a function of the strains. For linear elastic materials a constitutive law is given by Hooke's law. With Young's modulus E, specifying the stiffness, Poisson's ratio ν, describing lateral deformation, and the shear modulus G, it can be written as follows:

$$\begin{aligned}
\epsilon_{xx} &= \frac{1}{E}\left(\sigma_{xx} - \nu\sigma_{yy} - \nu\sigma_{zz}\right) \\
\epsilon_{yy} &= \frac{1}{E}\left(-\nu\sigma_{xx} + \sigma_{yy} - \nu\sigma_{zz}\right) \\
\epsilon_{zz} &= \frac{1}{E}\left(-\nu\sigma_{xx} - \nu\sigma_{yy} + \sigma_{zz}\right) \qquad (1.12) \\
2\epsilon_{xy} &= \frac{1}{G}\sigma_{xy} \\
2\epsilon_{yz} &= \frac{1}{G}\sigma_{yz} \\
2\epsilon_{zx} &= \frac{1}{G}\sigma_{zx} \qquad (1.13)
\end{aligned}$$

$$\text{with} \qquad G = \frac{E}{2(1+\nu)} \tag{1.14}$$

Introducing the elasticity matrix and using the Voigt notation this can be rewritten in a compact form:

$$\boldsymbol{\sigma} = \mathbf{C} \cdot \boldsymbol{\epsilon} \tag{1.15}$$

$$\text{with} \qquad \mathbf{C} = \frac{E}{(1+\nu)(1-2\nu)} \begin{bmatrix} 1-\nu & \nu & \nu & 0 & 0 & 0 \\ \nu & 1-\nu & \nu & 0 & 0 & 0 \\ \nu & \nu & 1-\nu & 0 & 0 & 0 \\ 0 & 0 & 0 & \frac{1-2\nu}{2} & 0 & 0 \\ 0 & 0 & 0 & 0 & \frac{1-2\nu}{2} & 0 \\ 0 & 0 & 0 & 0 & 0 & \frac{1-2\nu}{2} \end{bmatrix} \tag{1.16}$$

With this last equation it is possible to solve the system, the 15 unknowns can be determined by the 3 equations (1.1) or (1.4), the 6 Equations (1.6) and (1.7) and the 6 Equations (1.15).

1.5. The principle of virtual displacements

In the FEM a weak formulation of the equilibrium is used. Therefore we imagine small, virtual displacements which fulfill the kinematic restrictions. The virtual work resulting from these deformations inside the body and on the surface has to be zero.

$$\int_V \delta\mathbf{u}^T \cdot \left(\frac{\partial \boldsymbol{\sigma}_x}{\partial x} + \frac{\partial \boldsymbol{\sigma}_y}{\partial y} + \frac{\partial \boldsymbol{\sigma}_z}{\partial z} + \mathbf{f}^B - \rho\mathbf{a} \right) \mathrm{d}V + \int_S \delta\mathbf{u}^T \cdot \left(\mathbf{f}^S - \boldsymbol{\sigma}_x n_x - \boldsymbol{\sigma}_y n_y - \boldsymbol{\sigma}_z n_z \right) \mathrm{d}S = 0 \tag{1.17}$$

By applying Gauss' theorem and using the symmetry of the stress tensor, the following form in Voigt notation can be achieved:

$$\underbrace{-\int_V \delta\boldsymbol{\epsilon}^T \boldsymbol{\sigma} \, \mathrm{d}V}_{\delta W_{int}} + \underbrace{\int_V \delta\mathbf{u}^T \mathbf{f}^B \, \mathrm{d}V + \int_S \delta\mathbf{u}^T \mathbf{f}^S \, \mathrm{d}S}_{\delta W_{ext}} + \underbrace{\int_V \delta\mathbf{u}^T \rho(-\mathbf{a}) \, \mathrm{d}V}_{\delta W_{inertia}} = 0 \tag{1.18}$$

For static problems $\delta W_{inertia}$ is not present. Using (1.15) δW_{int} can be written as follows:

$$\delta W_{int} = -\int_V \delta\boldsymbol{\epsilon}^T \mathbf{C} \boldsymbol{\epsilon} \, \mathrm{d}V \tag{1.19}$$

We have now derived a second form of the equilibrium, which is valid in a domain and not in a point.

1.6. Fundamental equations for the Finite Element Analysis

Up to now the whole derivation is exact and could be used for analytical solutions. But for lots of real problems this is not possible. Therefore a method which is able

to generate approximate solutions for any case is desired, which leads to a linear system of algebraic equations.

We split up the whole body into elements, which are connected through their common nodes (see Figure 1.1).

To get a finite number of unknowns only the displacements in the nodes will be evaluated. But to calculate $\boldsymbol{\epsilon}$ in (1.19) the displacements in the whole domain are required. By interpolating the nodal displacements of the element, the displacements in every point of the element are available. Using at least a linear interpolation allows to calculate $\boldsymbol{\epsilon}$ in every point.

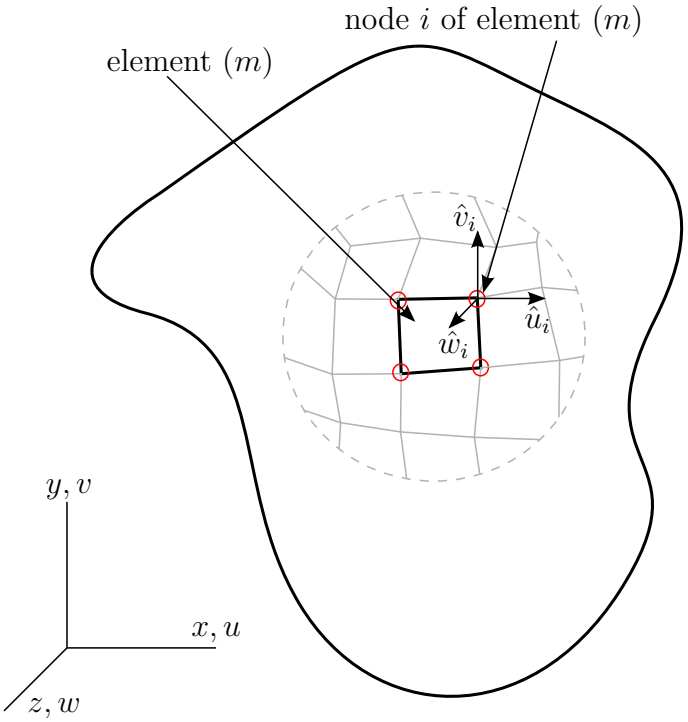

Figure 1.1. Body discretized with elements

1.6.1. Displacement approximation

The interpolation of a displacement in a point with coordinates $\mathbf{x}$ (x, y, z) inside element m (with $n_{el}^{(m)}$ nodes) can be written as:

$$\mathbf{u}^{(m)}(\mathbf{x}) = \sum_{i=1}^{n_{el}^{(m)}} N_i^{(m)}(\mathbf{x}) \cdot \hat{\mathbf{u}}_i \qquad \text{with} \qquad \hat{\mathbf{u}}_i = \begin{bmatrix} \hat{u}_i \\ \hat{v}_i \\ \hat{w}_i \end{bmatrix} \tag{1.20}$$

Thereby $N_i^{(m)}(\mathbf{x})$ are called shape functions and these functions are described in Section 1.7. This can also be written with an interpolation matrix $\mathbf{H}^{(m)}$ (to improve

readability the superscript (m) is not denoted in the matrix):

$$\mathbf{u}^{(m)}(\mathbf{x}) = \mathbf{H}^{(m)}(\mathbf{x}) \cdot \hat{\mathbf{u}} \qquad \text{with} \qquad \hat{\mathbf{u}} = \begin{bmatrix} \hat{u}_1 \\ \hat{v}_1 \\ \hat{w}_1 \\ ... \\ \hat{u}_{n_{el}} \\ \hat{v}_{n_{el}} \\ \hat{w}_{n_{el}} \end{bmatrix} \tag{1.21}$$

$$\mathbf{H}^{(m)}(\mathbf{x}) = \begin{bmatrix} N_1(\mathbf{x}) & 0 & 0 & ... & N_{n_{el}}(\mathbf{x}) & 0 & 0 \\ 0 & N_1(\mathbf{x}) & 0 & ... & 0 & N_{n_{el}}(\mathbf{x}) & 0 \\ 0 & 0 & N_1(\mathbf{x}) & ... & 0 & 0 & N_{n_{el}}(\mathbf{x}) \end{bmatrix} \tag{1.22}$$

1.6.2. Finite Element equilibrium

For derivable functions $N_i^{(m)}(\mathbf{x})$ it will be possible to define a strain-displacement matrix $\mathbf{B}^{(m)}(\mathbf{x})$ to evaluate the strains from the displacements:

$$\boldsymbol{\epsilon}^{(m)}(\mathbf{x}) = \mathbf{B}^{(m)}(\mathbf{x}) \cdot \hat{\mathbf{u}} \tag{1.23}$$

$$\mathbf{B}^{(m)}(\mathbf{x}) = \begin{bmatrix} \frac{\partial N_1(\mathbf{x})}{\partial x} & 0 & 0 & ... & \frac{\partial N_{n_{el}}(\mathbf{x})}{\partial x} & 0 & 0 \\ 0 & \frac{\partial N_1(\mathbf{x})}{\partial y} & 0 & ... & 0 & \frac{\partial N_{n_{el}}(\mathbf{x})}{\partial y} & 0 \\ 0 & 0 & \frac{\partial N_1(\mathbf{x})}{\partial z} & ... & 0 & 0 & \frac{\partial N_{n_{el}}(\mathbf{x})}{\partial z} \\ \frac{\partial N_1(\mathbf{x})}{\partial y} & \frac{\partial N_1(\mathbf{x})}{\partial x} & 0 & ... & \frac{\partial N_{n_{el}}(\mathbf{x})}{\partial y} & \frac{\partial N_{n_{el}}(\mathbf{x})}{\partial x} & 0 \\ 0 & \frac{\partial N_1(\mathbf{x})}{\partial z} & \frac{\partial N_1(\mathbf{x})}{\partial y} & ... & 0 & \frac{\partial N_{n_{el}}(\mathbf{x})}{\partial z} & \frac{\partial N_{n_{el}}(\mathbf{x})}{\partial y} \\ \frac{\partial N_1(\mathbf{x})}{\partial z} & 0 & \frac{\partial N_1(\mathbf{x})}{\partial x} & ... & \frac{\partial N_{n_{el}}(\mathbf{x})}{\partial z} & 0 & \frac{\partial N_{n_{el}}(\mathbf{x})}{\partial x} \end{bmatrix} \tag{1.24}$$

By using the constitutive law, the stresses can be evaluated:

$$\boldsymbol{\sigma}^{(m)}(\mathbf{x}) = \mathbf{C}^{(m)} \cdot \left(\boldsymbol{\epsilon}^{(m)}(\mathbf{x}) - \boldsymbol{\epsilon}^{I(m)}(\mathbf{x}) \right) + \boldsymbol{\sigma}^{I(m)}(\mathbf{x}) \tag{1.25}$$

Here $\boldsymbol{\sigma}^{I(m)}(\mathbf{x})$ are the initial stresses and $\boldsymbol{\epsilon}^{I(m)}(\mathbf{x})$ the initial strains. For our further steps we will set $\boldsymbol{\sigma}^{I(m)}(\mathbf{x}) = 0$ and $\boldsymbol{\epsilon}^{I(m)}(\mathbf{x}) = 0$. Now, the Finite Element (FE) formulation of the equilibrium Equation (1.18) can be gathered. For static problems with no initial stresses the following equation results:

$$\begin{aligned} &\delta\hat{\mathbf{u}}^T \left[\sum_m \underbrace{\int_{V^{(m)}} \mathbf{B}^T \cdot \mathbf{C} \cdot \mathbf{B} \, \mathrm{d}V^{(m)}}_{\mathbf{K}^{(m)}} \right] \hat{\mathbf{u}} = \\ &\delta\hat{\mathbf{u}}^T \left[\sum_m \underbrace{\int_{V^{(m)}} \mathbf{H}^T \cdot \mathbf{f}^B \, \mathrm{d}V^{(m)}}_{\mathbf{F}_{ext}^{B(m)}} + \underbrace{\sum_m \int_{S^{(m)}} (\mathbf{H}^S)^T \cdot \mathbf{f}^S \, \mathrm{d}S^{(m)}}_{\mathbf{F}_{ext}^{S(m)}} + \mathbf{F}_{ext}^C \right] \end{aligned} \tag{1.26}$$

$$\mathbf{K} = \sum_m \mathbf{K}^{(m)} \quad , \quad \mathbf{F}^B_{ext} = \sum_m \mathbf{F}^{B(m)}_{ext} \quad , \quad \mathbf{F}^S_{ext} = \sum_m \mathbf{F}^{S(m)}_{ext} \tag{1.27}$$

To improve readability the superscript (m) in the integrals was omitted (all quantities in the integrals are from the specific element m). Here $\mathbf{H}^S$ is the surface displacement interpolation matrix, which can be gathered from $\mathbf{H}$. We call $\mathbf{K}$ the global stiffness matrix, $\mathbf{F}^B_{ext}$ the body forces, $\mathbf{F}^S_{ext}$ the surface forces and $\mathbf{F}^C_{ext}$ are the concentrated nodal forces.

To calculate the displacements $\hat{\mathbf{u}}$ we apply the principle of virtual displacements for every unknown. Therefore we set $\delta u_i = 1$ and $\delta u_{j \neq i} = 0$ for all δu_i. Collecting all these equations we get a system of linear equations:

$$\mathbf{K} \cdot \hat{\mathbf{u}} = \mathbf{F} \qquad \text{with} \qquad \mathbf{F} = \mathbf{F}^B_{ext} + \mathbf{F}^S_{ext} + \mathbf{F}^C_{ext} \tag{1.28}$$

This formulation implies that the stiffness matrices $\mathbf{K}^{(m)}$ have the same shape as the global stiffness matrix and the forces $\mathbf{F}^{(m)}$ have got the same shape as the global one. Then, the method is called direct stiffness method. This approach has a big disadvantage, namely, very big element matrices that only have very few non-zero entries have to be summed up.

Therefore, the size of the local stiffness matrices and the size of the forces are defined by the number of degrees of freedom for each element. To use this approach, it is necessary to calculate the global index of a local matrix entry, which can be achieved with an index list.

1.6.3. Boundaries

Until now the matrix $\mathbf{K}$ is singular, because no boundary conditions have been considered implemented yet. An easy way presented by Wu et al. [25] to implement basic displacement (Dirichlet) boundaries, which sets a specific degree of freedom (DOF) to a defined value, will be described. To implement a fixed value for the displacement u_i, the following steps have to be applied on the system of equations (1.28):

- Substract the desired displacement value multiplied by the concerned entry in the stiffness matrix for every row in the load vector $\mathbf{F}$.
  $(F^{new}_j = F_j - K_{ji} \cdot \ u_i \quad \forall j \neq i)$
- Enter the value of the displacement multiplied by the main diagonal entry of the stiffness matrix for the considered DOF row in the load vector.
  $(F_i = K_{ii} \cdot u_i)$
- Set the whole row and column of the concerned DOF in the global stiffness matrix to zero, whereby the element on the main diagonal stays untouched.
  $(K_{ij} = 0 \quad \text{and} \quad K_{ji} = 0 \quad \forall j \neq i)$

These steps show the principle approach to implement a boundary condition, nevertheless, for a computer implementation it may be necessary to adopt this procedure.

For the implementation of more general boundary conditions see [2].

The second type of boundary conditions are force boundary conditions. In the displacement based FEM these boundaries can be implemented straight forward by calculation of the load vector $\mathbf{F}$ for the concerned DOFs.

1.7. Standard shape functions

In Section 1.6.1 we use shape functions $N_i(\mathbf{x})$ to evaluate the displacement $\mathbf{u}$ on a specific point $\mathbf{x}$ from the displacements $\hat{\mathbf{u}}_i$ in the nodes i of an element. In most implemented computer codes, these functions are evaluated in a local coordinate system (r, s, t) for every element. This is advantageous, because for all elements of the same type the same shape functions $N_i(r, s, t)$ can be used. In the following, starting with Lagrange polynomials, the shape functions for a first-order quadrilateral will be shown.

1.7.1. Lagrange polynomials

For the principle considerations we think of a 1d beam (see Figure 1.2).

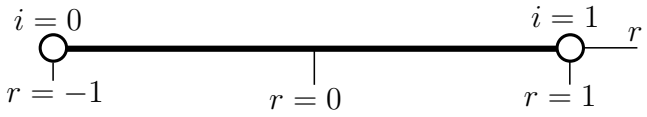

Figure 1.2. 1d Beam element in natural coordinates

A shape function needs the following attributes at the position r_i of node i:

- The shape function $N_i(r_i)$ should be 1.
- All other shape functions $N_{j\neq i}(r_i)$ should be 0.
- The sum of all shape functions $\sum_j N_j(r)$ for the element should be 1.

This enforces that the displacement at node i is exactly the displacement u_i and, in between the nodes, displacements get interpolated.

Functions which are able to fulfill these requirements are the Lagrange polynomials. A general form is given here:

$$l_j^{n-1}(r) = \prod_{\substack{i=0 \\ i\neq j}}^{n-1} \frac{r - r_i}{r_j - r_i} \tag{1.29}$$

For the 1d beam the shape functions which are Lagrange polynomials are specified below:

$$N_0(r) = \frac{r-1}{-2} \qquad \text{and} \qquad N_1(r) = \frac{r+1}{2} \tag{1.30}$$

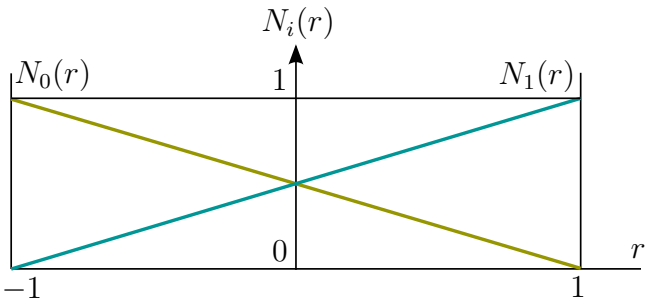

Figure 1.3. Shape function for 1d beam element in natural coordinates

1.7.2. Shape function for quadrilaterals

For a 2-dimensional (2d) quadrilateral element of first order (see Figure 1.4), the Lagrange polynomials for each direction can be multiplied to get the shape functions. The resulting shape functions are:

$$N_0(r,s) = \frac{1}{4}(1-r)(1-s) \qquad N_1(r,s) = \frac{1}{4}(1+r)(1-s)$$
$$N_2(r,s) = \frac{1}{4}(1+r)(1+s) \qquad N_3(r,s) = \frac{1}{4}(1-r)(1+s) \tag{1.31}$$

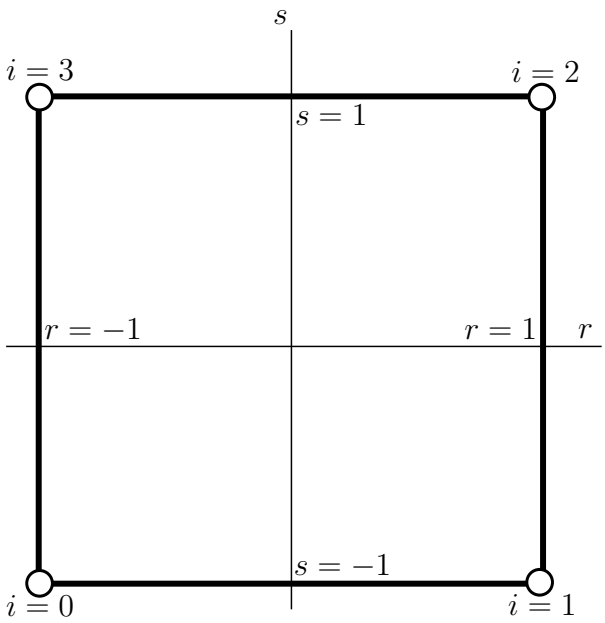

Figure 1.4. 2d quadrilateral element in natural coordinates

1.7.3. Isoparametric concept, the Jacobian matrix

If the same interpolation for geometry and displacements is used, it is called isoparametric concept. The following derivations are shown for the 2d case, nevertheless an extension to the 3-dimensional (3d) case is straight forward.

Equation (1.32) shows the interpolation of the node positions $\hat{\mathbf{x}}_j$ with shape functions to get the position $\mathbf{x}$. In (1.33) this is given in compact form with the interpolation matrix $\mathbf{H}^{(m)}(r,s)$.

$$\mathbf{x} = \sum_j N_j(r,s) \cdot \hat{\mathbf{x}}_j \qquad \text{with} \qquad \hat{\mathbf{x}}_j = \begin{bmatrix} \hat{x}_j \\ \hat{y}_j \end{bmatrix} \tag{1.32}$$

$$\mathbf{x} = \mathbf{H}^{(m)}(r,s) \cdot \hat{\mathbf{x}} \qquad \text{with} \qquad \hat{\mathbf{x}} = \begin{bmatrix} \hat{x}_1 \\ \hat{y}_1 \\ \hat{x}_2 \\ \hat{y}_2 \\ \dots \\ \hat{x}_{n_{el}} \\ \hat{y}_{n_{el}} \end{bmatrix} \tag{1.33}$$

To be able to calculate derivatives of the displacements, the inverse Jacobian matrix $\mathbf{J}^{-1}$ is needed. The definition of $\mathbf{J}$ and $\mathbf{J}^{-1}$ is shown in the following:

$$\mathbf{J}(r,s) = \begin{bmatrix} \frac{\partial x}{\partial r} & \frac{\partial x}{\partial s} \\ \frac{\partial y}{\partial r} & \frac{\partial y}{\partial s} \end{bmatrix} \tag{1.34}$$

$$\mathbf{J}^{-1}(r,s) = \begin{bmatrix} \frac{\partial r}{\partial x} & \frac{\partial r}{\partial y} \\ \frac{\partial s}{\partial x} & \frac{\partial s}{\partial y} \end{bmatrix} \tag{1.35}$$

$\mathbf{J}$ can easily be evaluated by using (1.32) or (1.33):

$$\mathbf{J}(r,s) = \begin{bmatrix} \sum_j \frac{\partial N_j(r,s)}{\partial r} \cdot \hat{\mathbf{x}}_j & \sum_j \frac{\partial N_j(r,s)}{\partial s} \cdot \hat{\mathbf{x}}_j \end{bmatrix} \tag{1.36}$$

$$\mathbf{J}(r,s) = \begin{bmatrix} \frac{\partial \mathbf{H}^{(m)}(r,s)}{\partial r} \cdot \hat{\mathbf{x}} & \frac{\partial \mathbf{H}^{(m)}(r,s)}{\partial s} \cdot \hat{\mathbf{x}} \end{bmatrix} \tag{1.37}$$

If $\det(\mathbf{J}) \neq 0$, $\mathbf{J}$ can be inverted to get $\mathbf{J}^{-1}$. Considering the integrals in Equation (1.26), it is more effective to integrate in the natural coordinate system. For example the $\mathrm{d}V^{(m)}$ has to be calculated in this system as follows (h is the height of the 2d body):

$$\mathrm{d}V^{(m)} = \det(\mathbf{J}(r,s)) \cdot \mathrm{d}r \cdot \mathrm{d}s \cdot h = \det(\mathbf{J}(r,s)) \cdot \mathrm{d}V^r \tag{1.38}$$

1.8. Numerical integration

The following derivation is based on [2] and covers only the most important elements. For the FEM it is necessary to solve integrals of the form:

$$\int F(r)\,\mathrm{d}r \qquad \int F(r,s)\,\mathrm{d}r\,\mathrm{d}s \qquad \int F(r,s,t)\,\mathrm{d}r\,\mathrm{d}s\,\mathrm{d}t \tag{1.39}$$

They occur for example in (1.26), in combination with the remarks in (1.38) these integrals will be solved numerically, with the following basic approach (for 1d):

$$\int_{-1}^{+1} F(r)\ \mathrm{d}r \approx \sum_i \alpha_i \cdot F(r_i) \tag{1.40}$$

Here α_i is the weighting factor and $F(r_i)$ is the value of the function F at the point r_i. For a general function $F(r)$ this approach cannot be exact, but by the choice of more points r_i the accuracy of the results can be improved. Now the two unknowns in (1.40) α_i and r_i have to be evaluated.

There are different methods to do this, for example the Newton-Cotes formulae with equidistant points r_i, where only the α_i are solved for. We will use the Gauss formulas as this approach is very accurate and therefore widely used.

1.8.1. The Gauss formulae

With this method both, α_i and r_i, have to be calculated. We will use n sampling points $r_i\,(i = 1, ..., n)$. Lagrange polynomials are used to approximate the function F, using (1.29) we can identify that the order of these polynomials is $n-1$. The function $\Psi(r)$ is shown in the following, which has the values of F in the sampling points:

$$\Psi(r) = \sum_{i=1}^{n} F(r_i) \cdot l_i^{n-1}(r) \tag{1.41}$$

A polynomial $P(r)$ of order n is defined, which vanishes at all sampling points:

$$P(r) = \prod_{i=1}^{n} (r - r_i) \tag{1.42}$$

To approximate the function $F(r)$ the following approach is used:

$$F(r) \approx \underbrace{\underbrace{\Psi(r)}_{n-1} + \underbrace{P(r)}_{n} \cdot \underbrace{\sum_{k=0}^{n-1} (\beta_k r^k)}_{n-1}}_{\text{order } (2n-1)} \tag{1.43}$$

This polynomial has the order $(2n-1)$ and its integration leads to:

$$\int_{-1}^{+1} F(r)\,\mathrm{d}r \approx \underbrace{\sum_{i=1}^{n} \int_{-1}^{+1} l_i^{n-1}(r)\,\mathrm{d}r}_{I}\, F(r_i) + \underbrace{\sum_{k=0}^{n-1} \int_{-1}^{+1} P(r) r^k\,\mathrm{d}r}_{II} \beta_k \tag{1.44}$$

By condition, the integral II in (1.44) should vanish, n equations for the sampling points r_i can be gathered. This implies that the desired integral is approximated by the integration of a polynomial of order $(2n-1)$. As a result, polynomials of order $\leq (2n-1)$ are integrated exactly. To calculate the weighting factors α_i we use (1.40) and replace $F(r)$ with $\Psi(r)$ from (1.41) and integrate the equation.

$$\alpha_i = \int_{-1}^{1} l_i^{n-1}(r)\,\mathrm{d}r \tag{1.45}$$

The (α_i)s and (r_i)s evaluated for the natural interval have been published by [18].

1.8.2. 2 dimensional integration

For multidimensional integration in rectangular elements, the 1d integral is combinded for each direction by multiplying the weighting factors of the 1d case:

$$\int_{-1}^{1}\int_{-1}^{1} F(r,s)\,\mathrm{d}r\,\mathrm{d}s = \sum_{i,j}\alpha_i\alpha_j F(r_i,s_j) \tag{1.46}$$

In Figure 1.5, the integration points for a quadrilateral element are shown.

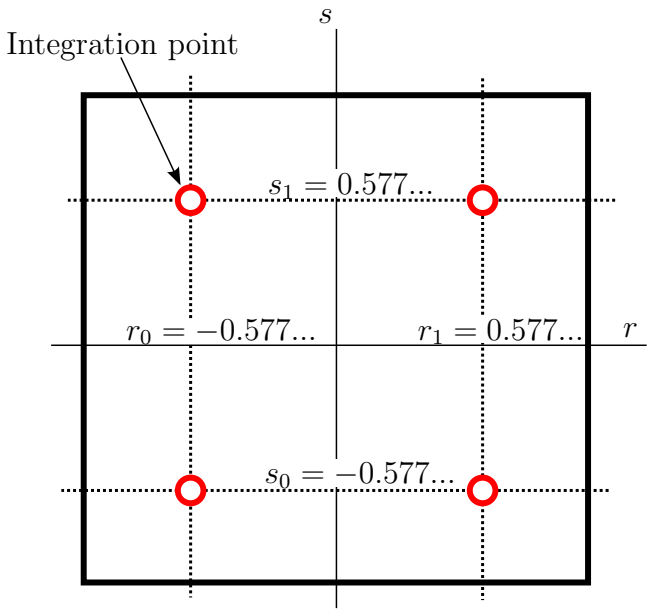

Figure 1.5. 2d quadrilateral element with integration points

2. Selected fundamentals of linear elastic fracture mechanics

In this chapter, the description of crack behavior from a macroscopic view should be presented. This is the 'view', which is used for the crack calculations in the XFEM.

A crack is a separation through a body, creating a new surface, which is free of load in most cases. The crack ends in the crack front or for 2d cases in the crack tip.
The following formulations are based on [13, 17].

2.1. The three modes of fracture

To describe the deformation of a crack, three fracture modes are distinguished (see Figure 2.1):

- Mode I describes a symmetric crack opening.
- Mode II describes an antisymmetric deformation, where both crack surfaces move against each other inside the crack plane.
- Mode III desribes a deformation in direction of the crack front. Therefore, this mode only exists for 3d cases.

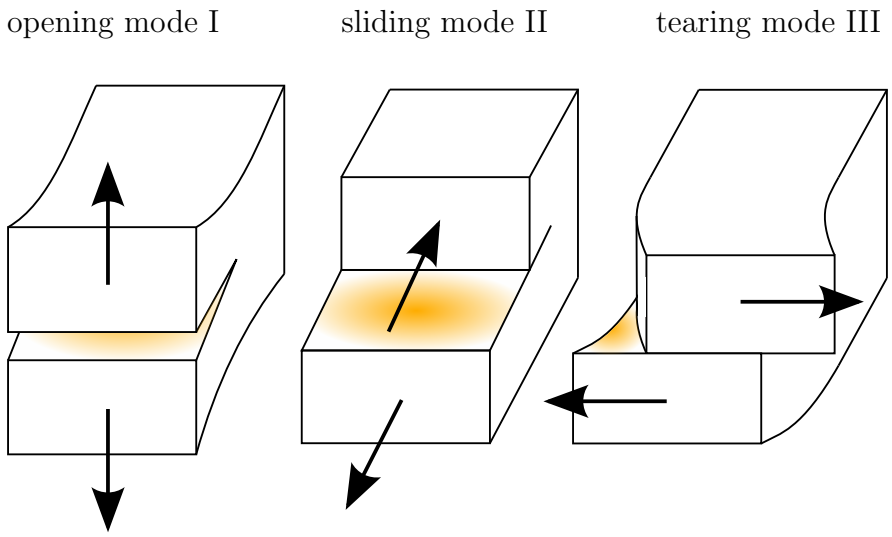

Figure 2.1. Modes of fracture

These modes of fracture describe the situation near the crack front, but for some special cases they can be used for the whole body.

2.2. Crack tip field - stress intensity factors

Stress intensity factors (SIFs) will be used to describe the deformations and stresses near the crack tip for each mode. Since later on only 2d case will be considered, mode III is not shown. A complete description for all modes is given in.

The following solutions for the near tip field in the local Cartesian and polar coordinate system (see Figure 2.2) can be derived. Here K_I is the stress intensity factor (SIF) for mode I and K_{II} for mode II. We can see that they characterize a kind of the amplitude for the near tip solutions.

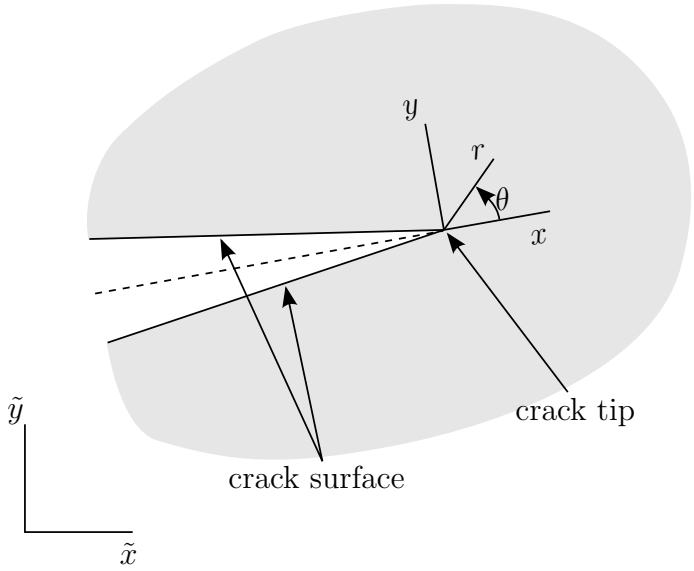

Figure 2.2. Local crack coordinate system

Mode I:

$$\begin{pmatrix}\sigma_{xx}\\ \sigma_{yy}\\ \sigma_{xy}\end{pmatrix} = \frac{K_I}{\sqrt{2\pi r}}\cos\left(\frac{\theta}{2}\right)\begin{pmatrix}1-\sin(\frac{\theta}{2})\sin(\frac{3\theta}{2})\\ 1+\sin(\frac{\theta}{2})\sin(\frac{3\theta}{2})\\ \sin(\frac{\theta}{2})\cos(\frac{3\theta}{2})\end{pmatrix} \tag{2.1}$$

$$\begin{pmatrix}\sigma_{rr}\\ \sigma_{\theta\theta}\\ \sigma_{r\theta}\end{pmatrix} = \frac{K_I}{\sqrt{2\pi r}}\begin{pmatrix}\cos(\frac{\theta}{2})[1+\sin^2(\frac{\theta}{2})]\\ \cos^3(\frac{\theta}{2})\\ \sin(\frac{\theta}{2})\cos^2(\frac{\theta}{2})\end{pmatrix} \tag{2.2}$$

$$\begin{pmatrix}u\\ v\end{pmatrix} = \frac{K_I}{2G}\sqrt{\frac{r}{2\pi}}(\kappa-\cos(\theta))\begin{pmatrix}\cos(\frac{\theta}{2})\\ \sin(\frac{\theta}{2})\end{pmatrix} \tag{2.3}$$

Mode II:

$$\begin{pmatrix}\sigma_{xx}\\ \sigma_{yy}\\ \sigma_{xy}\end{pmatrix} = \frac{K_{II}}{\sqrt{2\pi r}} \begin{pmatrix}-\sin(\frac{\theta}{2})[2+\cos(\frac{\theta}{2})\cos(\frac{3\theta}{2})]\\ \sin(\frac{\theta}{2})\cos(\frac{\theta}{2})\cos(\frac{3\theta}{2})\\ \cos(\frac{\theta}{2})[1-\sin(\frac{\theta}{2})\sin(\frac{3\theta}{2})]\end{pmatrix} \tag{2.4}$$

$$\begin{pmatrix}\sigma_{rr}\\ \sigma_{\theta\theta}\\ \sigma_{r\theta}\end{pmatrix} = \frac{K_{II}}{\sqrt{2\pi r}} \begin{pmatrix}\sin(\frac{\theta}{2})[1-3\sin^2(\frac{\theta}{2})]\\ -3\sin(\frac{\theta}{2})\cos^2(\frac{\theta}{2})\\ \cos(\frac{\theta}{2})[1-3\sin^2(\frac{\theta}{2})]\end{pmatrix} \tag{2.5}$$

$$\begin{pmatrix}u\\ v\end{pmatrix} = \frac{K_{II}}{2G}\sqrt{\frac{r}{2\pi}} \begin{pmatrix}\sin(\frac{\theta}{2})[\kappa+2+\cos(\theta)])\\ -\cos(\frac{\theta}{2})[\kappa-2+\cos(\theta)])\end{pmatrix} \tag{2.6}$$

$$\begin{aligned}&\text{with} \quad \kappa = 3-4\nu \quad \text{and} \quad \sigma_{zz} = \nu(\sigma_{xx}+\sigma_{yy}) \quad \text{for plane strain case}\\ &\text{with} \quad \kappa = \frac{3-\nu}{1+\nu} \quad \text{and} \quad \sigma_{zz} = 0 \quad \text{for plane stress case}\end{aligned} \tag{2.7}$$

In the derivation of these solutions there are some restrictions as it is only valid for load free crack surfaces. For the v-component in (2.3) it can be seen that this is only possible for $K_I \geq 0$,because then there is no contact between the crack sufaces.

The complete solution would have parts with higher order terms of r. As we are only interested in the near tip field, these terms can be neglected.

Linear elastic behavior of the material is assumed, although this assumption cannot be exact. In the crack tip, stresses would get infinite, which no material is able to stand. In a small zone around the crack tip there are plastic deformations. If this zone is small enough in comparison to the near tip field, this effect can be neglected, too.

With the XFEM we will be able to calculate the SIFs and, consequently, have a description of the near tip field.

2.3. Path independent integral about the crack tip (J-integral)

Another criterion to describe fracture behavior is the J-integral.

A body of homogeneous, linear elastic material (for a more general derivation see [13]) with an arbitrary surface ∂V inside, normal vector components to the surface n_j and the volume inside the surface V should be considered without any body force $\mathbf{f}^B$. With the stress components σ_{ij}, the strains components ϵ_{ij} and the Kronecker delta δ_{jk}, the J-Integral in index notation is defined as:

$$J_k = \int_{\partial V} (\frac{1}{2}\sigma_{mn}\epsilon_{mn}\delta_{jk} - \sigma_{ij}\frac{\partial u_i}{\partial x_k})n_j \,\mathrm{d}A \tag{2.8}$$

Using Gauss' theorem we can find:

$$J_k = \int_V \left(\frac{1}{2}\sigma_{mn}\frac{\partial \epsilon_{mn}}{\partial x_j}\delta_{jk} + \frac{1}{2}\frac{\partial \sigma_{mn}}{\partial \epsilon_{op}}\frac{\partial \epsilon_{op}}{\partial x_j}\epsilon_{mn}\delta_{jk} - \frac{\partial \sigma_{ij}}{\partial x_j}\frac{\partial u_i}{\partial x_k} - \sigma_{ij}\frac{\partial^2 u_i}{\partial x_k \partial x_j}\right) \mathrm{d}V \tag{2.9}$$

Using (1.1), (1.6), (1.7), (1.10) and the symmetry of the stress tensor we get:

$$J_k = \int_V \left(\sigma_{mn} \frac{\partial^2 u_m}{\partial x_n \partial x_k} - \sigma_{ij} \frac{\partial^2 u_i}{\partial x_k \partial x_j} \right) \mathrm{d}V = 0 \tag{2.10}$$

As Gauss' theorem demands that the gradient can be calculated, this result is only valid for bodies without any singularities or discontinuities (for example cracks). In other cases $J_k \neq 0$ in general.

Additionally, it can be shown that for linear elastic material behavior, there is a connection between the SIFs and the J-integral (see [13]):

$$J = \frac{1}{E'}(K_I^2 + K_{II}^2) + \frac{1}{2G} K_{III}^2 \tag{2.11}$$

$$\text{with} \qquad E' = \frac{E}{1-\nu^2} \qquad \text{for plane strain case}$$

$$\text{with} \qquad E' = E \qquad \text{for plane stress case}$$

2.4. Crack growth criterion

To describe the crack growth process, a criterion which describes the crack growth direction from the evaluated displacements is required.

Here, the maximal circumferential stress criterion should be used, which allows the calculation of the crack growth direction from the SIFs. In Section 4.8.1, it will be shown, how to calculate the SIFs out of the displacements.

2.4.1. The maximal circumferential stress criterion

This criterion, [7], implies that the crack grows in direction r_c, where the circumferential stress $\sigma_{\theta\theta}$ is maximal.

As $\sigma_{\theta\theta}$ is a principal stress in growth direction and the fact that on principal stress planes, no shearing stresses occur, θ_c can be evaluated from $\sigma_{r\theta} = 0$ by addition of the shear stresses $\sigma_{r\theta}$ in (2.2) and (2.5) (a detailed derivation can be found in Appendix A.1).

$$\frac{K_I}{\sqrt{2\pi r}}\sin\left(\frac{\theta_c}{2}\right)\cos^2\left(\frac{\theta_c}{2}\right) + \frac{K_{II}}{\sqrt{2\pi r}}\cos\left(\frac{\theta_c}{2}\right)\left[1 - 3\sin^2\left(\frac{\theta_c}{2}\right)\right] = 0 \tag{2.12}$$

$$K_I\sin(\theta_c) + K_{II}\big(3\cos(\theta_c) - 1\big) = 0 \tag{2.13}$$

$$\theta_c = 2\arctan\left\{\frac{1}{4}\left[\frac{K_I}{K_{II}} \pm \sqrt{\left(\frac{K_I}{K_{II}}\right)^2 + 8}\right]\right\} \tag{2.14}$$

Figure 2.3 shows the new crack direction in the local crack coordinate system (x, y), starting from the actual crack tip.

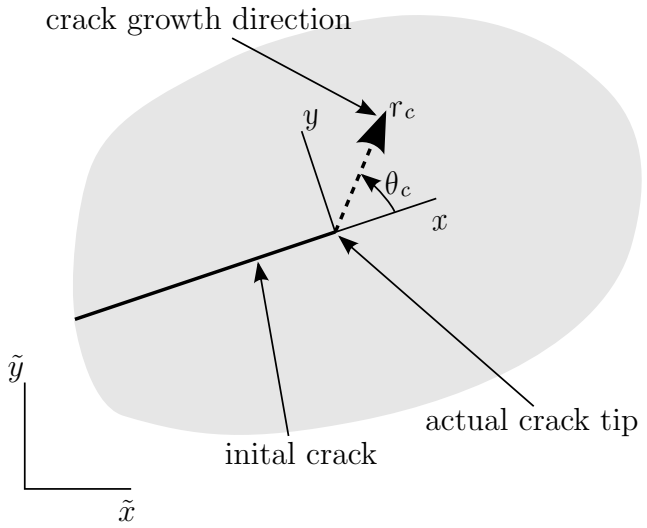

Figure 2.3. New crack growth direction

3. Extended Finite Element Method

A polynomial approximation space which is used in the standard FEM, describes a smooth solution very well. But in many real problems, solutions are non-smooth, for example discontinuities, singularities, high gradients or other non-smooth solutions can exist. In solid mechanics some examples for such behavior are cracks, shear bands, dislocations, inclusions and voids.

There are two approaches to calculate such solutions. The first one is to use a polynomial approximation space and refine the mesh size in the area of high gradients or singularities and to orientate the elements to discontinuities. For this method the mesh has to be adapted if different non-smooth solutions should be described.

The second approach is to enrich the approximation space with problem specific shape functions. This allows to describe non-smooth solutions independent of the mesh.

First possibility to change the approximation space is to replace the polynomial shape functions by problem specific shape functions. This approach is called intrinsic (see [10]).

We will use another method, where extra shape functions with new unknowns are added to the standard approximation space, called an extrinsic approach. As a result of such a method, the number of unknowns is increased.

If all nodes in the entire domain are enriched, it is called 'global enrichment'. Most phenomena in solid mechanics are local (cracks, kinks, ...). To implement these non-smooth effects in the solution only nodes nearby have to be enriched ('local enrichment'). This approach is called Extended Finite Element Method (XFEM). We will focus on fracture mechanics and, therefore, use local enrichments.

All formulations in this chapter are based on [11, 3, 19].

3.1. Local enrichment

Starting from (1.20) the approximation space gets locally enriched. For one extra enrichment function, the XFEM approximation has the form:

$$\mathbf{u}(\mathbf{x}) = \underbrace{\sum_{i \in I} N_i(\mathbf{x}) \cdot \hat{\mathbf{u}}_i}_{\text{standard FE approximation}} + \underbrace{\sum_{i \in \breve{I}} \breve{N}_i(\mathbf{x}) \cdot \psi(\mathbf{x}) \cdot \hat{\mathbf{a}}_i}_{\text{enrichment}} \tag{3.1}$$

Thereby, I is the set of all nodes and $\breve{I}$ is the set of nodes to be enriched, which is a subset of all nodes ($\breve{I} \subset I$). $N_i(\mathbf{x})$, $\breve{N}_i(\mathbf{x})$ are standard shape functions and are often chosen to be equal. These functions build a partition of unity (PU) over the

whole domain, if they are considered in all nodes.

$$\sum_{i \in I} N_i(\mathbf{x}) = 1 \qquad \sum_{i \in I} \breve{N}_i(\mathbf{x}) = 1 \tag{3.2}$$

In this expression, $\hat{\mathbf{u}}_i$ are the unknowns for the standard FEM, $\hat{\mathbf{a}}_i$ the additional unknowns from the enrichment. The enrichment function $\psi(\mathbf{x})$ implements the problem specific insight into the approximation space.

In Figure 3.1, a domain is shown, where some of the nodes are enriched to add the problem specific information in this local area (e.g. a crack).

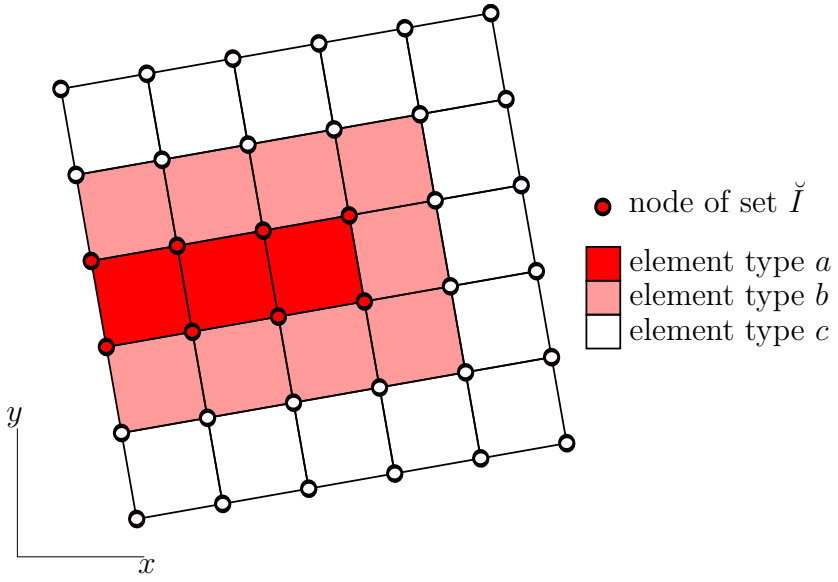

Figure 3.1. Domain of quadrilaterals with enriched nodes

Depending on the number of enriched nodes in an element, three types of enrichment can be distinguished.

- type a: Here all nodes are enriched, therefore $\breve{N}_i(\mathbf{x})$ builds a PU and $\psi(\mathbf{x})$ can be exactly reproduced.
- type b: Only some of the nodes are enriched. As a consequence of this, $\breve{N}_i(\mathbf{x})$ does not build a PU and therefore, in general $\psi(\mathbf{x})$ cannot be exactly reproduced. These elements are called 'blending elements'.
- type c: There are no enriched nodes. Here, the classical FEM approximation is used.

3.1.1. Shifted enrichment interpolation

In (3.1), it can be seen that this approximation generally does not have the Kronecker-delta property. As a result it cannot be ensured that $\mathbf{u}(\mathbf{x}_i) = \hat{\mathbf{u}}_i$. This fact makes it more diffucult to apply displacement boundary conditions. In addition, the effort to get displacement data is increased, because for every single point, (3.1) has to be evaluated.

To avoid these disadvantages, a shifted form of (3.1) is used (first suggested in [4]).

$$\mathbf{u}(\mathbf{x}) = \sum_{i \in I} N_i(\mathbf{x}) \cdot \hat{\mathbf{u}}_i + \sum_{i \in \breve{I}} \breve{N}_i(\mathbf{x}) \cdot (\psi(\mathbf{x}) - \psi(\mathbf{x}_i)) \cdot \hat{\mathbf{a}}_i \tag{3.3}$$

Here the enrichment part vanishes at the nodes and, therefore, $\mathbf{u}(\mathbf{x}_i) = \hat{\mathbf{u}}_i$. As the enrichment part in (3.3) is only shifted with a constant value, it can be compensated by the classical FE approximation so that this formulation is still able to reproduce $\psi(\mathbf{x})$ exactly. But it should be mentioned, that in general along boundaries, the enrichment parts will be non-zero nevertheless.

3.2. Modelling of cracks

Now we will specialize in the modeling of cracks with the XFEM. Therefore special enrichment functions for the crack path and the crack tip have to be implemented.

3.2.1. Modelling the crack path

A crack is a strong discontinuity of displacements, crossing the crack all values of displacements will change abruptly. This behavior can be implemented by a jump function $\psi(\mathbf{x}) = \psi_{jump}(\mathbf{x})$ as enrichment function, suggested by [19, 23]. The jump function changes the value by crossing the crack. Both formulations of (3.4) span the same approximation space and therefore can be used. Only the values of the unknowns $\hat{\mathbf{a}}_i$ change (see (3.3)). One method to evaluate the values of the functions (3.4) will be described in Section 3.3.

$$\psi_{jump}(\mathbf{x}) = \begin{cases} 0: & \text{left from crack} \\ 1: & \text{right from crack} \end{cases} \quad \text{or} \quad \psi_{jump}(\mathbf{x}) = \begin{cases} -1: & \text{left from crack} \\ 0: & \text{on the crack} \\ 1: & \text{right from crack} \end{cases} \tag{3.4}$$

As these enrichment functions are constant outside elements, which are cut by a crack, the value $(\psi(\mathbf{x}) - \psi(\mathbf{x}_i))$ is only non-zero in these elements. This implies that there are no blending elements and that in all other elements standard FEM is applied.

Therefore, only nodes in elements cut by a crack, are added to the set of enriched nodes for the crack path $\breve{I}_c$ (see Figure 3.2). Also for not shifted enrichment functions only these nodes have to be enriched, because with a constant function $\psi(\mathbf{x})$ the enrichment would span the same space as the standard FEM.

3.2.2. Modelling the crack tip

Cracks end inside the domain with the crack tip. In general the tip is not aligned with an element edge. Therefore, additional enrichments are required to represent the tip in the element. In Section 2.2 the analytical solutions for the different

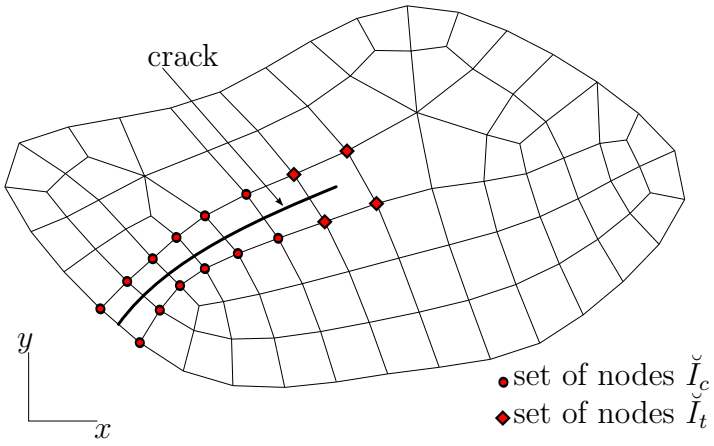

Figure 3.2. Enriched nodes for a crack

fracture modes have been shown. For the tip enrichment, enrichment functions, which span the whole solutions for Mode I and Mode II (see Section A.4), are used. The enrichment functions are shown in Figures 3.3, 3.4, 3.5 and 3.6.

$$\left\{\psi_{tip}^{(i)}(\mathbf{x})\right\} = \left\{\sqrt{r}\sin\left(\frac{\theta}{2}\right), \sqrt{r}\cos\left(\frac{\theta}{2}\right), \sqrt{r}\sin(\theta)\sin\left(\frac{\theta}{2}\right), \sqrt{r}\sin(\theta)\cos\left(\frac{\theta}{2}\right)\right\} \tag{3.5}$$

The local coordinate system for these enrichment functions can be seen in Figure 2.2. As the coordinate θ is in between $-\pi < \theta < \pi$, enrichment function $\psi_{tip}^{(1)}$ has a discontinuity for $\theta = \pm\pi$. The derivatives of all tip enrichment functions are singular for $r = 0$, because strains and stresses are singular there.

It should be mentioned that in normal cases, these enrichment functions have to be evaluated in global coordinates. Then, for each tip, the tip-coordinate $\mathbf{x}_t$ has to be stored, to be able to evaluate these functions.

In Figure 3.2 only nodes of the tip element are in the set of nodes $\breve{I}_t$, which get enriched. It can be observed that for cracks which are only slightly curved at the tip, a larger set of nodes $\breve{I}_t$ (e.g. inside a circle with enrichment radius r_e) provides better results (see Figure 3.7).

The resulting approximation for a crack with one tip is shown in the following:

$$\begin{aligned}\mathbf{u}(\mathbf{x}) = &\sum_{i\in I} N_i(\mathbf{x})\cdot\hat{\mathbf{u}}_i + \\ &\sum_{i\in\breve{I}_c} N_i(\mathbf{x})\cdot\left(\psi_{jump}(\mathbf{x}) - \psi_{jump}(\mathbf{x}_i)\right)\cdot\hat{\mathbf{a}}_i + \\ &\sum_{j=1}^{4}\sum_{i\in\breve{I}_t} N_i(\mathbf{x})\cdot\left(\psi_{tip}^{(j)}(\mathbf{x}) - \psi_{tip}^{(j)}(\mathbf{x}_i)\right)\cdot\hat{\mathbf{b}}_i^{(j)}\end{aligned} \tag{3.6}$$

For a second tip, the last part of this expression has to be implemented a second time.

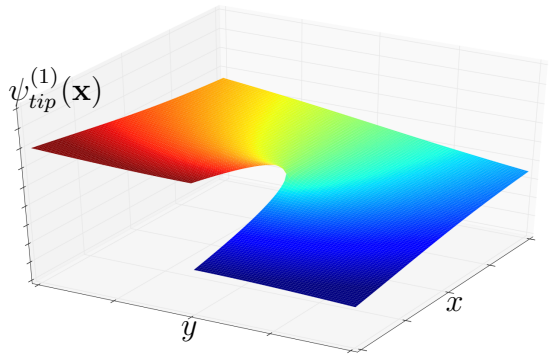

Figure 3.3. Enrichment function $\psi_{tip}^{(1)}(\mathbf{x})$

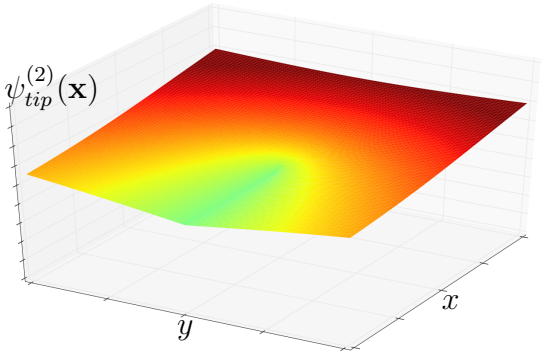

Figure 3.4. Enrichment function $\psi_{tip}^{(2)}(\mathbf{x})$

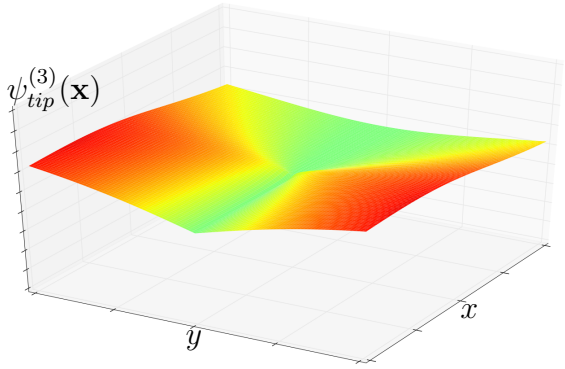

Figure 3.5. Enrichment function $\psi_{tip}^{(3)}(\mathbf{x})$

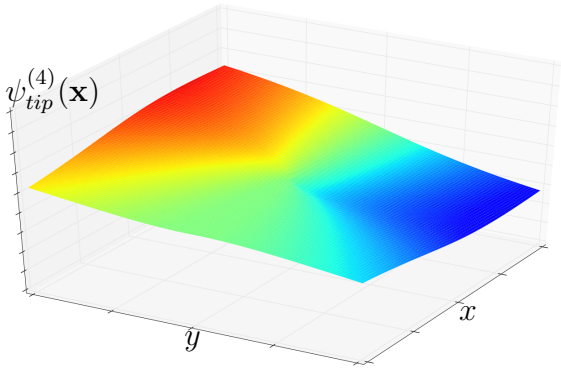

Figure 3.6. Enrichment function $\psi_{tip}^{(4)}(\mathbf{x})$

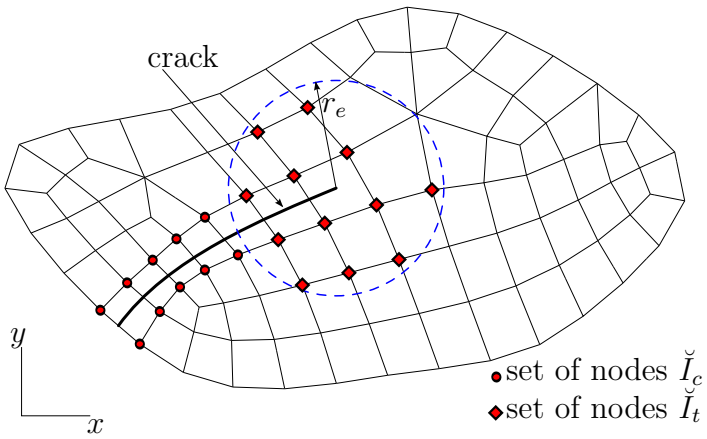

Figure 3.7. Enriched nodes for a crack with larger tip enrichment

3.3. Level set functions

In the previous sections, enrichment functions for cracks are shown. The description of the discontinuity or in general an interface is not mentioned there. This will be discussed now.

One possibility is to describe the crack path explicitly as a function in Cartesian coordinates. Then, a complex method which is able to evaluate $\psi_{jump}(\mathbf{x})$ as function of the explicit crack path would be required.

Looking at (3.4) it can be seen that $\psi_{jump}(\mathbf{x})$ can easily be evaluated, if a function describes the crack that changes the sign at the crack.

Therefore, the geometry of the crack will be given by a level set function $\tilde{\phi}(\mathbf{x})$, which is zero on the crack and has a different sign on each side of the discontinuity (see Figure 3.8 a)).

Then (3.4) can be evaluated with a sign function:

$$\psi_{jump}(\mathbf{x}) = \text{sign}(\tilde{\phi}(\mathbf{x})) \qquad \text{with} \qquad \text{sign}(\xi) = \begin{cases} -1 & : \xi < 0 \\ 0 & : \xi = 0 \\ 1 & : \xi > 0 \end{cases} \tag{3.7}$$

Only the values of the level set function in the nodes will be saved, and in between they are interpolated with the standard shape function:

$$\phi(\mathbf{x}) = \sum_{i \in I} N_i(\mathbf{x}) \cdot \phi_i \qquad \text{with} \qquad \phi_i = \tilde{\phi}(\mathbf{x}_i) \tag{3.8}$$

With these level set values ϕ_i in the nodes, it is very easy to find elements which are cut by a discontinuity. A detailed description, how this is done, is given in Section 4.3.

Additionally to the crack path description, there is still a second information about the crack tip(s) required. This is defined by a second level set function $\tilde{\phi}^t(\mathbf{x})$, which is positive in the area where the crack exists. By considering again only the values of this level set function in the nodes ϕ_i^t and ϕ_i, the crack tips can be found (see Section 4.4). Having the position of the tips, also (3.6) can be evaluated for every position $\mathbf{x}$ in the domain. In Figure 3.8, the full description of a crack with level set functions is shown.

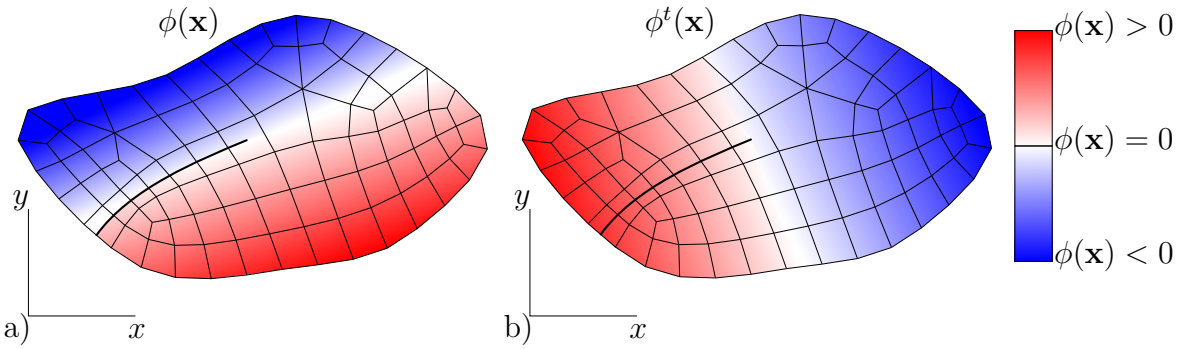

Figure 3.8. a) Description of crack path by $\phi(\mathbf{x})$ and b) crack tip by $\phi^t(\mathbf{x})$

Any function can be used as level set function, as long as the path where $\phi(\mathbf{x}) = 0$ is on the right position to describe the interface. Certainly, glancing intersections between $\phi(\mathbf{x}) = 0$ and $\phi^t(\mathbf{x}) = 0$ should be avoided to guarantee a reliable determination of the crack tips.

To describe the crack growth with this level set function, $\phi(\mathbf{x})$ and $\phi^t(\mathbf{x})$ have to be updated for every step. A method how to do this is presented in [22]. The approach which was used here, will be desribed in Section 4.9.5.

3.4. Numerical integration in the context of XFEM

In Section 1.8 the Gauss formulae, a method to calculate integrals numerically, are presented. It is shown that polynomials can be integrated exactly, by choosing enough sampling points. By using first-order Lagrange polynomials as shape functions (see (1.29)), integration of these can always be exactly performed.

As we added enrichment functions, which have discontinuities, to the FE approximation, this is not possible anymore. The integrands of interest are the resulting shape functions $N_i(\mathbf{x}) \cdot \psi_\star(\mathbf{x})$ and derivations of them ($\psi_\star(\mathbf{x})$ is any introduced enrichment function). As these functions cannot be represented by polynomials, there is no number of sampling points, which allows exact integration. Using a lot of sampling points to get acceptable accuracy, costs a lot of computing time. As we know the positions of the discontinuities in the integration domain, a much more elegant and efficient way is used.

The idea is to split the integration area into subareas, in which the integrands can be described more accurately by polynomials.

For elements cut by a crack, the element has to be split into two parts, which are integrated separately (see Figure 3.9). As the enrichment function $\psi_{jump}(\mathbf{x})$ is constant in each part, the resulting integrand will always be a polynomial and can be exactly integrated.

To integrate elements that are enriched by the crack tip enrichment functions $\psi_{tip}^{(i)}(\mathbf{x})$, they should be split at the crack to get a better solution (see discontinuity of $\psi_{tip}^{(1)}(\mathbf{x})$ for $\theta = \pm\pi$). In these elements attention should also be paid to the singularities of the derivatives at the crack tip ($r = 0$). By increasing the number of sampling points around this point, accuracy can be increased.

For the implementation in the computer code, only the calculation of new integration positions and weighting coefficients are necessary. These subelements are used for integration purposes only. Therefore, this method has no influence on the number of unknowns or the size of the resulting system of equations. The actually used method for decomposition of quadrilaterals is described in Section 4.6.

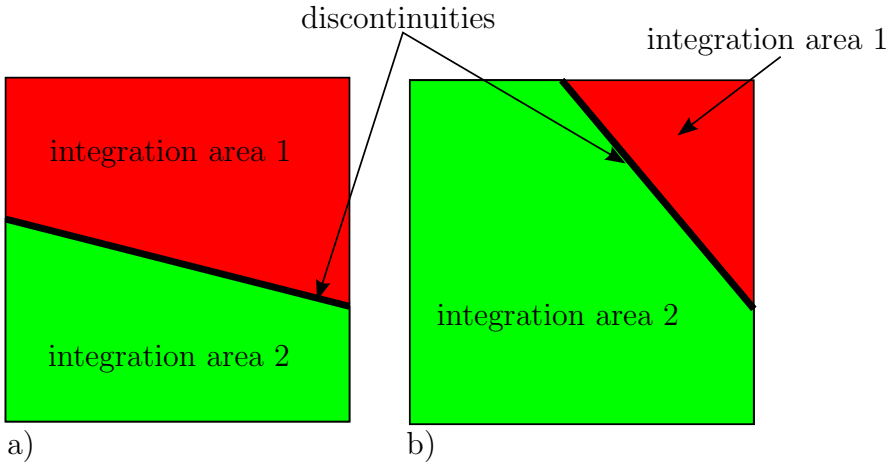

Figure 3.9. Integration areas for elements split by a discontinuity

4. Implementation

In the previous chapters, the theoretical background is given, which is necessary to implement the XFEM. Nevertheless for real implementations there are lots of different definitions and algorithms required.

In the following sections, the definitions and algorithms used in the actual implementation should be described, knowing that lots of other possibilities to realize an XFEM code exist.

The implementation of this linear XFEM code is done in the Python programming language, based on pySoofea (python software for object oriented finite element analysis), a computer code for the non-linear standard FEM , which has been written on the Institute for Strength of Materials at the Graz University of Technology [14].

To create meshes, the external tool Gmsh , a three-dimensional finite element mesh generator, is used [12].

All required problem specific informations are defined in a problem specific python file.

These informations are:

- Displacement constraints in boundary nodes
- Load situation
- Mesh file from Gmsh
- Element type and number of integration points in the element
- Height of the 2d problem
- Material type with material constants
- Number of time markers for crack growth calculation or for changing boundaries
- Level set functions $\phi(\mathbf{x})$ and $\phi^t(\mathbf{x})$ for each crack

This information describes a standard FEM model and in addition, the level set functions. Therefore, the calculation process (shown in Figure 4.1) starts with this information. All other informations, which are required to formulate the XFEM approximation (3.6) - like crack tip positions - have to be evaluated by the python code.

Finally, solving the occurring system of linear algebraic equations is done by the library LAPACK [1]. As a result, the displacements in the nodes ($\hat{\mathbf{u}}_i$), the unknowns of the crack path enrichment ($\hat{\mathbf{a}}_i$) and the unknowns of the crack tip enrichment ($\hat{\mathbf{b}}_i^{(j)}, j = 1...4$) are determined. Thus, with all these calculated quantities, the displacements in the whole domain can be evaluated with the help of (3.6).

Visualisations of the displacement field is done in ParaView (Open Source Scientific Visualization - www.paraview.org), and in the library Matplotlib [16].

To verify the results and to find bugs in the implementation, the free accessible XFEM codes in Matlab from the RWTH Aachen University were very helpful [9].

4.1. Calculation process

In Figure 4.1, the whole calculation process is shown. The details of the individual steps are presented in this chapter.

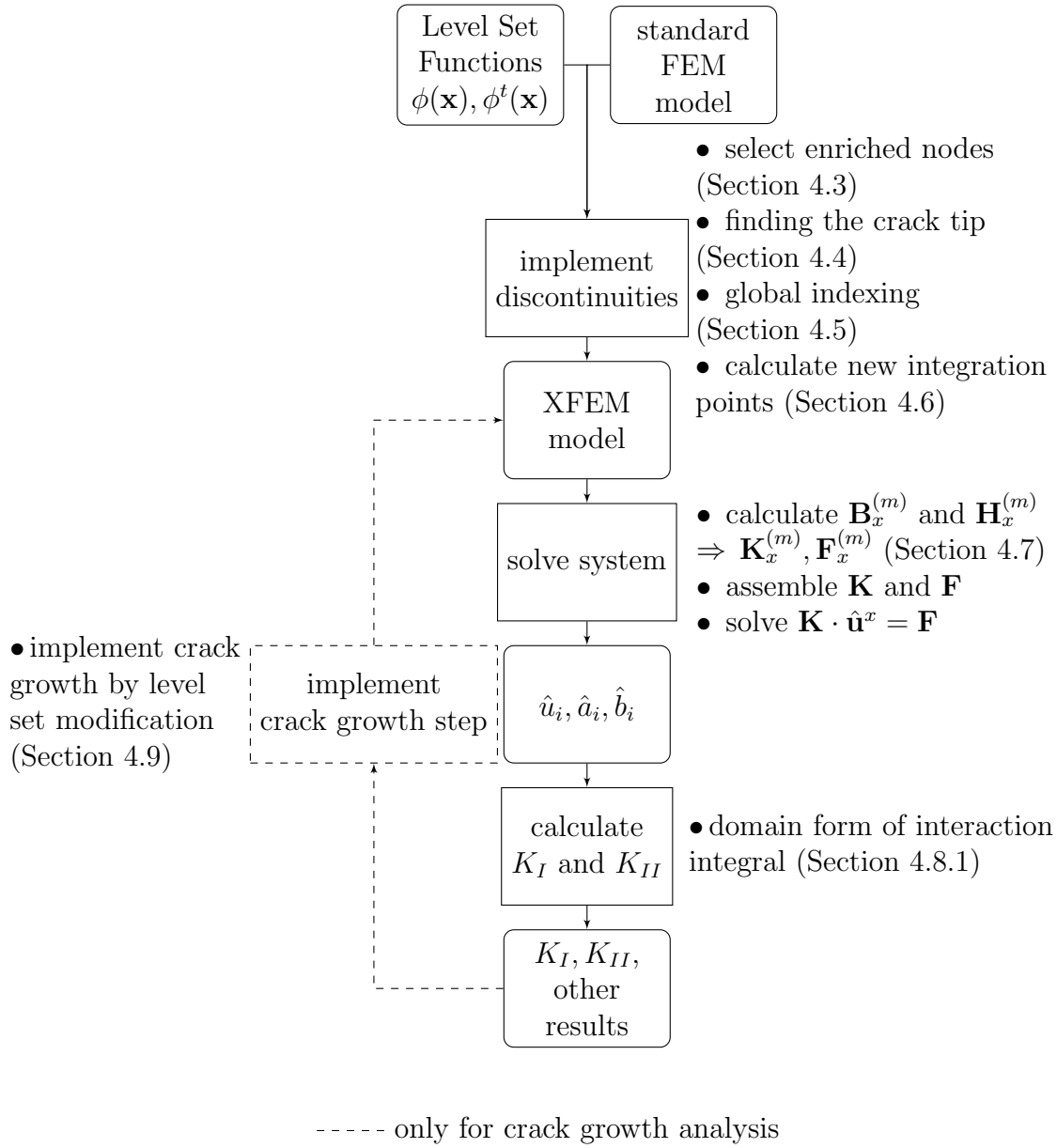

Figure 4.1. XFEM calculation process

4.2. Entry point and exit point of an interface in quadrilaterals

As the calculation of the entry and exit point of an interface in an element is required for several steps in the XFEM, the used approach will be described in this section. The condition for an existing entry or exit point $\mathbf{r}_P$ between node i and node $(i+1)$ is:

$$\text{sign}(\phi_i) \neq \text{sign}(\phi_{i+1}) \tag{4.1}$$

In Figure 4.2, the situation to calculate $\mathbf{r}_P$ between node 0 and node 1 is shown exemplarily. For this case $\mathbf{r}_P$ can be evaluated by:

$$\begin{aligned} r_P &= \frac{\phi_0}{\phi_1 - \phi_0} \cdot (r_0 - r_1) + r_0 \\ s_P &= -1 \end{aligned} \tag{4.2}$$

From this special case a general rule can be found:

$$\mathbf{r}_P = \frac{\phi_i}{\phi_{i+1} - \phi_i} \cdot (\mathbf{r}_i - \mathbf{r}_{i+1}) + \mathbf{r}_i \qquad \text{with} \qquad \phi_4 \mathrel{\hat{=}} \phi_0 \qquad \text{and} \qquad \mathbf{r}_4 \mathrel{\hat{=}} \mathbf{r}_0 \tag{4.3}$$

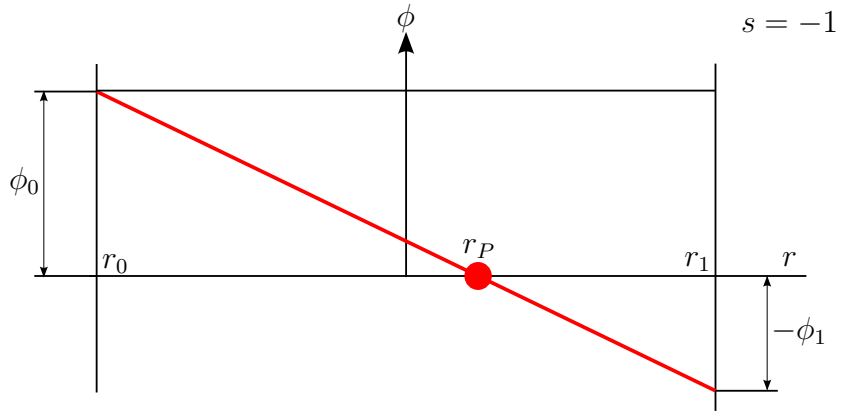

Figure 4.2. Evaluation of element entry point and exit point

4.3. Selection of enriched nodes

The first step to get an XFEM model is to find all nodes, which should be enriched. The required information is provided by the level set functions.

In Figure 4.3 a simple way to find elements which are cut by interfaces, is pointed out. By the use of the sign-function of the level set functions, it can be found that an interface in the element exists, if:

$$\left| \sum_{i=1}^{n_{el}} \text{sign}(\phi_i) \right| \neq \sum_{i=1}^{n_{el}} 1 \tag{4.4}$$

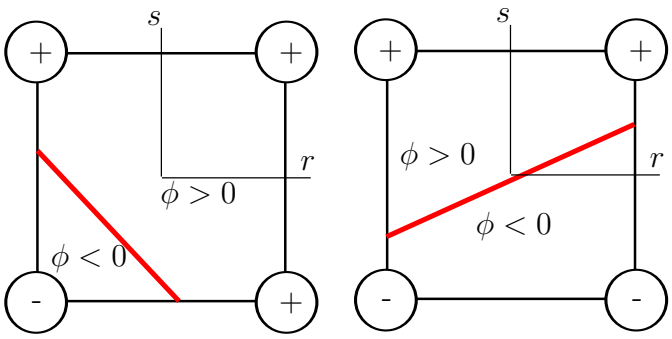

Figure 4.3. Possible interfaces described by level set function values ϕ_i

As can be seen in Figure 3.7, the selection of enriched nodes does not only depend on the defined interfaces, but also a larger area around the crack tip can be enriched with the tip enrichment function. Therefore, the positions of the tips (see Section 4.4) have to be evaluated for a final selection of the enriched nodes. This method to find the tips is used in every element that fulfills Condition (4.4) for ϕ_i and ϕ_i^t. As a result, we get the tip position and a statement, if there is a tip, a crack path or no discontinuity in the element (see Figure 4.4).

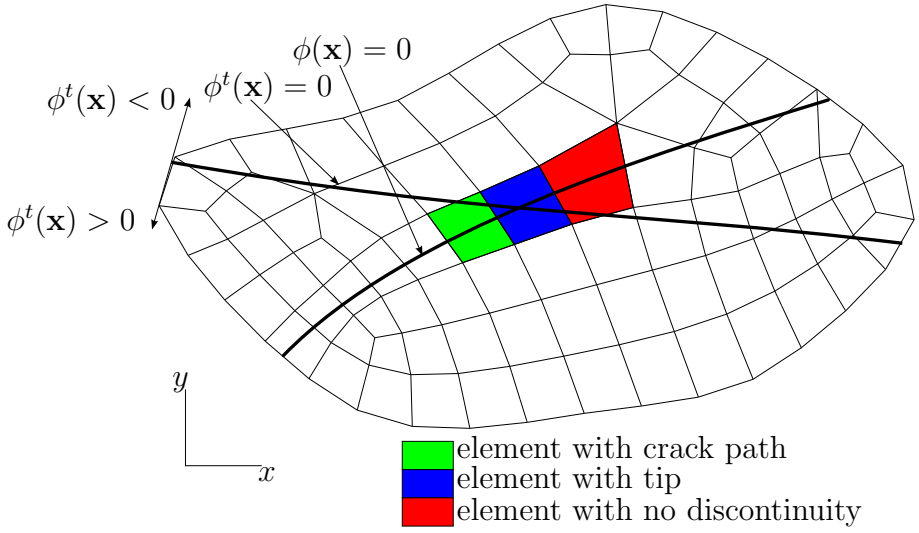

Figure 4.4. Types of elements that are cut by two interfaces

Then all nodes which are in a defined circle around the tip (Figure 3.7), or which belong to the tip element (Figure 3.2), get enriched by the tip enrichment function for the specific tip. 'Specific' means that an index which defines the tip, has to be set for every node, to allow a later calculation of the enrichment function (tip position is required).

If there are elements with a crack path inside (shown as green elements in Figure 4.4), the crack path enrichment is applied to all nodes in these elements.

Now, all nodes in elements which are cut by two interfaces, are enriched and all tip enrichments are set up. Other elements which are cut by the crack can be found

with the help of Condition (4.4) for ϕ_i only and:

$$\sum_{i=1}^{n_{el}} \text{sign}(\phi_i^t) = \sum_{i=1}^{n_{el}} 1 \tag{4.5}$$

By this condition, it can be ensured that elements on the crack interface $\phi(\mathbf{x}) = 0$ only on the side $\phi^t(\mathbf{x}) > 0$ get selected. The nodes which belong to these elements, get enriched with the crack path enrichment function.

As a last step, it is necessary to remove the crack path enrichment for all nodes which have a crack path enrichment and a crack tip enrichment. If crack growth should be simulated, the nodes, where the crack path enrichment gets deleted, should be stored, as the moving tip releases them again and they have to be added (see Section 4.9.3).

4.4. Finding the crack tip

For elements which are cut by two interfaces, the intersection point of these two curves should be evaluated. Here we focus on quadrilateral elements, cut by linear interfaces. Figure 4.5 shows the starting point for this derivation.

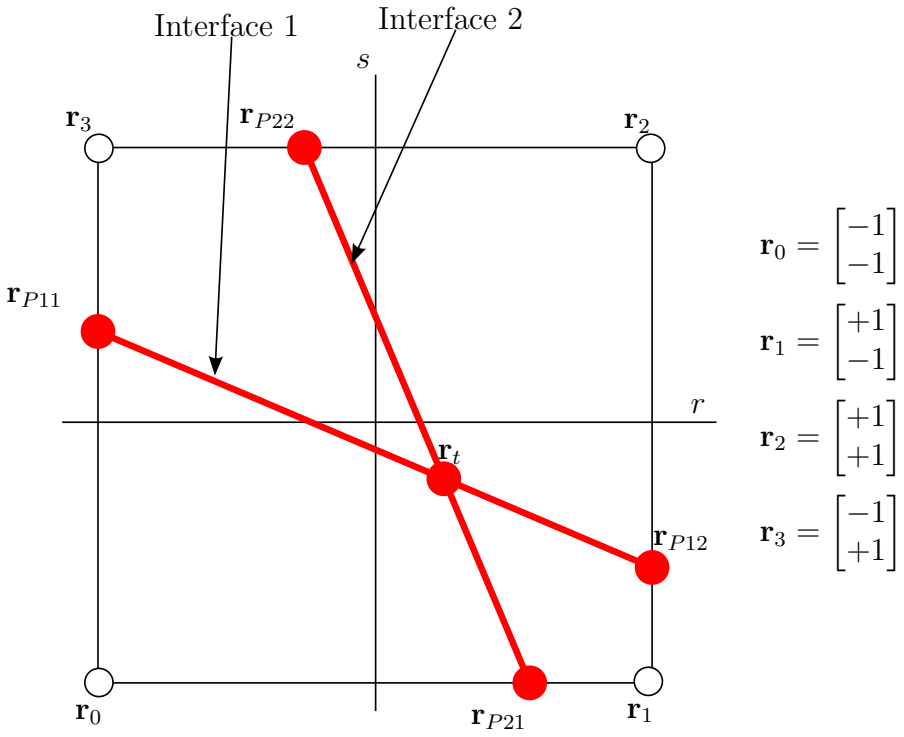

Figure 4.5. Quadrilateral cut by two interfaces

Since the shape functions for a quadrilateral are bilinear (see (1.31)), the interfaces are not linear in the (r, s)-system, in general. But on the boundaries of the element the shape functions are linear. This can be used to calculate the points $\mathbf{r}_{P11}$, $\mathbf{r}_{P12}$, $\mathbf{r}_{P21}$ and $\mathbf{r}_{P22}$. As a first step, all four points have to be evaluated by using the method shown in Section 4.2 four times.

As already mentioned before, the interfaces are not linear in the element because of the bilinear shape functions. Therefore, the intersection point will be evaluated in the (x, y)-system. By calculating the shape functions for these points $\mathbf{r}_P$ and using (1.33), the positions of these points $\mathbf{x}_P$ in the (x, y)-system can be evaluated. With these points $\mathbf{x}_P$, the linear equations of the interfaces are known and the intersection point can be calculated. Special treatment is requird for interfaces which are aligned with the y-axis.

$$\mathbf{x}_t = \begin{cases} \begin{bmatrix} x_{P11} \\ a \cdot (x_t - x_{P21}) + y_{P21} \end{bmatrix} & \text{for} \quad x_{P11} = x_{P12} \\ \begin{bmatrix} x_{P21} \\ b \cdot (x_t - x_{P11}) + y_{P11} \end{bmatrix} & \text{for} \quad x_{P21} = x_{P22} \\ \begin{bmatrix} (b \cdot x_{P11} - a \cdot x_{P21} + y_{P21} - y_{P11})/(b - a) \\ b \cdot (x_t - x_{P11}) + y_{P11} \end{bmatrix} & \text{otherwise} \end{cases}$$

$$\text{with} \quad a = \frac{y_{P22} - y_{P21}}{x_{P22} - x_{P21}} \quad \text{and} \quad b = \frac{y_{P12} - y_{P11}}{x_{P12} - x_{P11}} \tag{4.6}$$

To find out if the tip is inside the element, $\mathbf{r}_t$ is calculated from $\mathbf{x}_t$ (see A.3). The tip is inside the element if $|r_t| < 1$ and $|s_t| < 1$.

If the tip is inside the element, the entry point $\mathbf{x}_{te}$ ($\mathbf{x}_{P11}$ or $\mathbf{x}_{P12}$), which is on the crack, has to be evaluated for the calculation of the crack tip angle θ_t (see Figure A.1). $\mathbf{x}_{te}$ can be evaluated, with $\phi^t(\mathbf{x})$ from (3.8), by:

$$\mathbf{x}_{te} = \begin{cases} \mathbf{x}_{P11} & \text{for} \quad \phi^t(\mathbf{x}_{P11}) > 0 \\ \mathbf{x}_{P12} & \text{for} \quad \phi^t(\mathbf{x}_{P12}) > 0 \end{cases} \tag{4.7}$$

The crack tip angle can now be calculated:

$$\theta_t = \arctan\left(\frac{y_{te} - y_t}{x_{te} - x_t}\right) + \frac{[\text{sign}(x_{te} - x_t) + 1] \cdot \pi}{2} \tag{4.8}$$

If the tip isn't inside the element, it has to be verified if the crack goes across this element (see Figure 4.4). For $\phi^t(\mathbf{x}_{P11}) > 0$ and $\phi^t(\mathbf{x}_{P12}) > 0$ this is the case, as there is no change in the sign of $\phi^t(\mathbf{x})$.

4.5. Global indexing

To assemble a global stiffness matrix, it is necessary that every DOF ($\hat{u}_i$) has a unique index, which defines the position in the global matrix. In the standard FEM the number of DOFs per node are constant and for standard elements correspond to the dimension of the problem. Therefore, it is possible to calculate a global index for every DOF from the node index.

In the XFEM, the number of DOFs ($\hat{u}_i, \hat{a}_i, \hat{b}_i$) per node can change. As a result, indexing is an independent step after all DOFs are assigned. There are different ways to sort the existing DOFs. The method used is shown exemplarily for a mesh where

node 5 is enriched by the crack-path enrichment function and node 9 is enriched by the crack tip enrichment functions.

$$\hat{\mathbf{u}}_x = \Big[\hat{u}_1 \quad \hat{v}_1 \quad ... \quad \hat{u}_5 \quad \hat{v}_5 \quad \hat{a}_{51} \quad \hat{a}_{52} \quad \hat{u}_6 \quad \hat{v}_6 \quad ... \quad \hat{u}_8 \quad \hat{v}_8 \quad \hat{u}_9 \quad \hat{v}_9 \quad \hat{b}_{91}^{(1)} \quad \hat{b}_{92}^{(1)} \quad \hat{b}_{91}^{(2)} \quad \hat{b}_{92}^{(2)} \quad \hat{b}_{91}^{(3)} \quad \hat{b}_{92}^{(3)} \quad \hat{b}_{91}^{(4)} \quad \hat{b}_{92}^{(4)} \quad ... \Big]^T \tag{4.9}$$

To evaluate the global indices for each DOF, first all nodes which should be enriched have to be defined. Then, every vector group $\Big($like $[\hat{u}_i \quad \hat{v}_i]^T$, $[\hat{a}_{i1} \quad \hat{a}_{i2}]^T$ or $\left[\hat{b}_{i1}^{(j)} \quad \hat{b}_{i2}^{(j)}\right]^T \Big)$ gets assigned a continuous global index, by counting through all existing DOFs. The length of these vectors is constant and, therefore, it is possible to calculate every single index.

4.6. Integration points for elements with an interface

In Section 3.4, it is explained that for numerical integration in elements cut by a discontinuity, or which have a singularity, special treatment is required. For discontinuities, the integration area has to be split up, and near singularities an increased number of integration points should be used. Here, the evaluation of the positions and weights of these points for quadrilaterals will be shown.

4.6.1. Subelements for quadrilaterals cut by a discontinuity

We will use the integration points of quadrilateral subelements, to calculate the new integration points. There are two different possibilities how a quadrilateral can be cut by an interface (shown in Figure 3.9), which can be distinguished by:

$$\begin{aligned} \left| \sum_{i=1}^{n_{el}} \text{sign}(\phi_i) \right| = 0 \quad &\Longrightarrow \quad \text{case a)} \\ \left| \sum_{i=1}^{n_{el}} \text{sign}(\phi_i) \right| = 2 \quad &\Longrightarrow \quad \text{case b)} \end{aligned} \tag{4.10}$$

Case a)

In Figure 4.6, the quadrilateral subelements for case a) in all three occurring coordinate systems is shown. Here, a vertical interface in the (x, y)-system is shown. By (4.1) node i and node $(i+1)$ which belong to the edge, crossed by the interface, can be evaluated.

To get a more general method, which enables to handle all interfaces that split the element into two parts with two nodes on each side, the indices of the four edge points $\hat{\mathbf{r}}_l^{original} (l = 0...3)$ in the original occurring configuration get shifted by the index i evaluated before. The resulting point $\hat{\mathbf{r}}_k^{reference}$ belongs to the reference configuration, shown in Figure 4.6. As in all further steps only the reference

configuration will be used, the description '*reference*' for all points $\hat{\mathbf{r}}_k^{reference}$ is omitted.

$$\hat{\mathbf{r}}_k^{reference} = \begin{cases} \hat{\mathbf{r}}_{k+i}^{original} & \text{for} \quad k+i < 4 \\ \hat{\mathbf{r}}_{k+i-4}^{original} & \text{for} \quad k+i \geq 4 \end{cases} \qquad k = 0,1,2,3 \tag{4.11}$$

The next step is to calculate the node positions of the subelements in the (r,s)-system. As the position of nodes that are aligned with element edges are known, in case a) only the positions $\hat{\mathbf{r}}_4$ and $\hat{\mathbf{r}}_5$ have to be calculated. How $\hat{\mathbf{r}}_4$ and $\hat{\mathbf{r}}_5$ can be calculated is shown in Section 4.2.

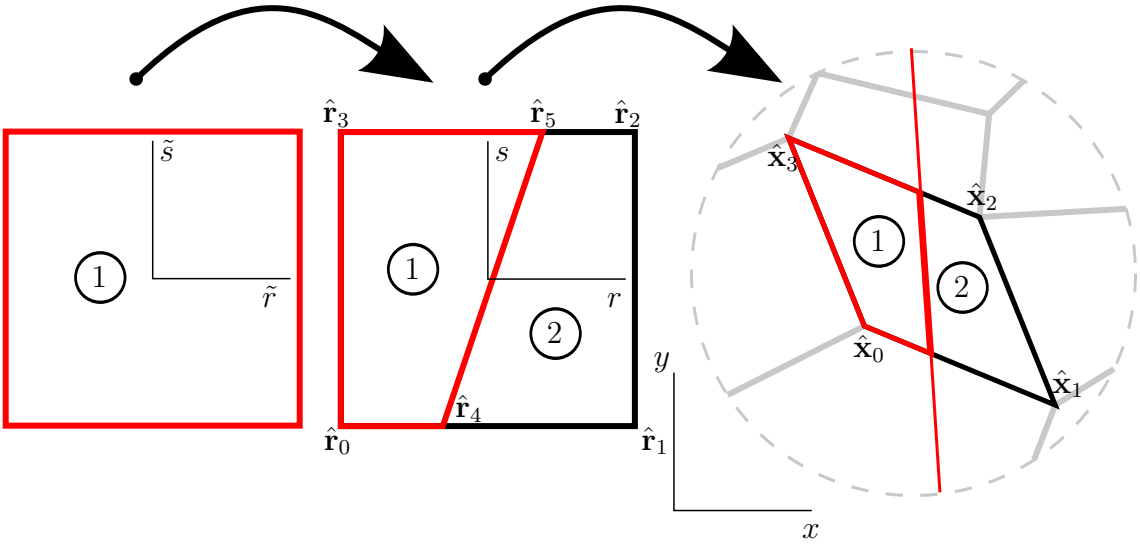

Figure 4.6. Quadrilateral subelements for the reference configuration of case a) in all three occurring coordinate systems

In the following, Table 4.1 shows the quadrilateral subelements with their node points $\hat{\mathbf{r}}_i$.

Table 4.1. Quadrilateral subelements with their node points for case a)

Subelement number	node pos. 0	node pos. 1	node pos. 2	node pos. 3
1	$\hat{\mathbf{r}}_0$	$\hat{\mathbf{r}}_4$	$\hat{\mathbf{r}}_5$	$\hat{\mathbf{r}}_3$
2	$\hat{\mathbf{r}}_4$	$\hat{\mathbf{r}}_1$	$\hat{\mathbf{r}}_2$	$\hat{\mathbf{r}}_5$

Case b)

In Figure 4.7 the quadrilateral subelements for case b) in all three occurring coordinate systems are shown. In this reference configuration, the interface separates node 1 from the rest of the element. With index i from condition (4.1), the separated node can be found. It is important that this rule is used counterclockwise and the

first index i found is used for the same shifting as in case a) (4.11). Then, the range of this approach can be enlarged to all quadrilaterals, split by an interface into one part with three nodes and the rest.

Again, points $\hat{\mathbf{r}}_4$ and $\hat{\mathbf{r}}_5$ in the (r, s)-system can be evaluated with the method shown in Section 4.2. All other points are expressed by the now known points. The positions can be chosen arbitrarily, because also other positions for these points would be possible.

$$\begin{aligned} \hat{\mathbf{r}}_6 &= \frac{\hat{\mathbf{r}}_4 + \hat{\mathbf{r}}_5}{2} & \hat{\mathbf{r}}_7 &= \frac{\hat{\mathbf{r}}_1 + \hat{\mathbf{r}}_4}{2} \\ \hat{\mathbf{r}}_8 &= \frac{\hat{\mathbf{r}}_1 + \hat{\mathbf{r}}_5}{2} & \hat{\mathbf{r}}_9 &= \frac{\hat{\mathbf{r}}_7 + \hat{\mathbf{r}}_8}{2} \end{aligned} \tag{4.12}$$

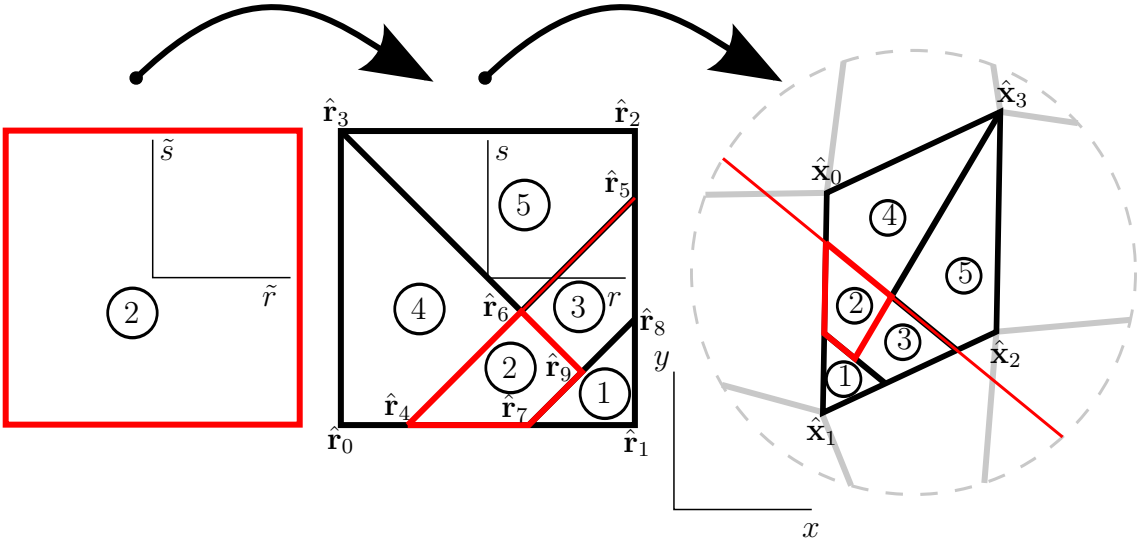

Figure 4.7. Quadrilateral subelements for the reference configuration of case b) in all three occurring coordinate systems

In the following, Table 4.2 shows the quadrilateral subelements with their node points $\hat{\mathbf{r}}_i$.

Table 4.2. Quadrilateral subelements with their node points for case b)

Subelement number	node pos. 0	node pos. 1	node pos. 2	node pos. 3
1	$\hat{\mathbf{r}}_1$	$\hat{\mathbf{r}}_8$	$\hat{\mathbf{r}}_9$	$\hat{\mathbf{r}}_7$
2	$\hat{\mathbf{r}}_4$	$\hat{\mathbf{r}}_7$	$\hat{\mathbf{r}}_9$	$\hat{\mathbf{r}}_6$
3	$\hat{\mathbf{r}}_9$	$\hat{\mathbf{r}}_8$	$\hat{\mathbf{r}}_5$	$\hat{\mathbf{r}}_6$
4	$\hat{\mathbf{r}}_4$	$\hat{\mathbf{r}}_6$	$\hat{\mathbf{r}}_3$	$\hat{\mathbf{r}}_0$
5	$\hat{\mathbf{r}}_6$	$\hat{\mathbf{r}}_5$	$\hat{\mathbf{r}}_2$	$\hat{\mathbf{r}}_3$

4.6.2. Subelements for quadrilaterals with a crack tip

In Figure 4.8, the subelements for the reference configuration are shown, which are used to calculate the integration points of an element with tip. To increase integration accuracy near the crack tip, where singular integrants occur, the density of integration points should be increased near the tip position. This can be achieved by using quadrilateral subelements with two nodes in the crack tip. As for the calculation of the crack tip (Section 4.4) the positions $\hat{\mathbf{r}}_4$ and $\hat{\mathbf{r}}_5$ are already known, it should be started from this point.

To get a method which is able to create subelements for all possible configuration of an element with crack tip, again the index of the node coordinates should be shifted by (4.11). The required shifting index i can be found as follows:

$$i = \begin{cases} \begin{cases} 1 & \text{for} \quad \hat{r}_4 > 0 \\ 3 & \text{for} \quad \hat{r}_4 < 0 \end{cases} & \text{and} \quad |\hat{r}_4| = 1 \\ \begin{cases} 2 & \text{for} \quad \hat{s}_4 > 0 \\ 0 & \text{for} \quad \hat{s}_4 < 0 \end{cases} & \text{and} \quad |\hat{r}_4| \neq 1 \end{cases} \tag{4.13}$$

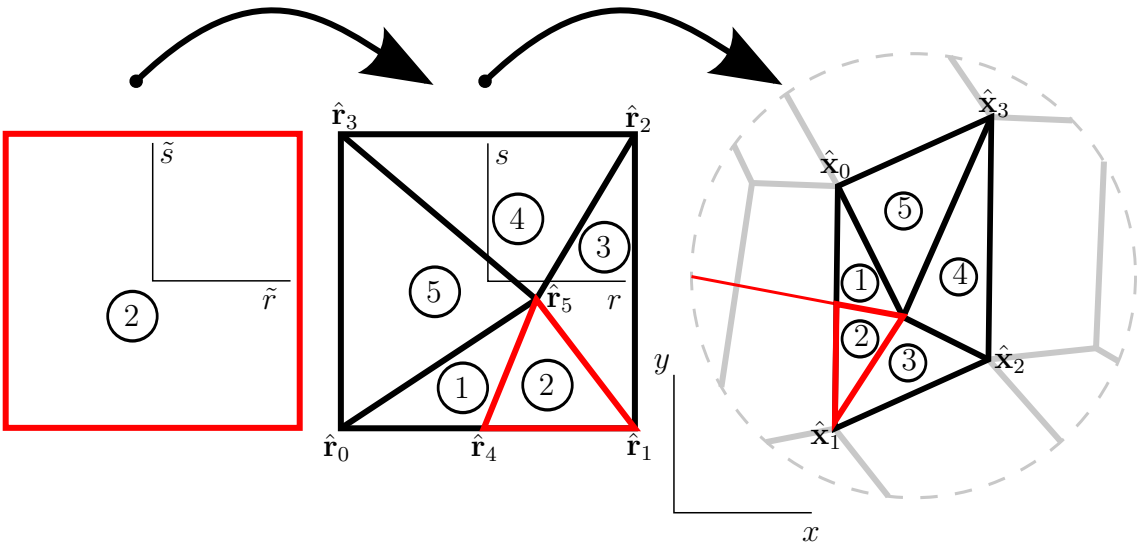

Figure 4.8. Quadrilateral subelements for the reference configuration of a crack tip interface in all three occurring coordinate systems

In the following, Table 4.3 shows the quadrilateral subelements for the treatment of crack tips with their node points $\hat{\mathbf{r}}_i$.

4.6.3. Positions and weights of integration points from subelements

Now the Positions of the integration points in the (r, s)-system should be evaluated. The positions $\tilde{\mathbf{r}}_{ip}$ of the integration points in the $(\tilde{r}, \tilde{s})$-system are known from the Gauss Formulas (see (1.44) II). Using the isoparametric concept, the positions $\mathbf{r}_{ip}$ for subelement $(\tilde{m})$ can be evaluated with the same interpolation matrix $(\mathbf{H}^{(\tilde{m})}(r, s) = \mathbf{H}^{(m)}(r, s))$ as used in (1.33).

Table 4.3. Quadrilateral subelements with their node points for elements with a crack tip

Subelement number	node pos. 0	node pos. 1	node pos. 2	node pos. 3
1	$\hat{\mathbf{r}}_0$	$\hat{\mathbf{r}}_4$	$\hat{\mathbf{r}}_5$	$\hat{\mathbf{r}}_5$
2	$\hat{\mathbf{r}}_4$	$\hat{\mathbf{r}}_1$	$\hat{\mathbf{r}}_5$	$\hat{\mathbf{r}}_5$
3	$\hat{\mathbf{r}}_1$	$\hat{\mathbf{r}}_2$	$\hat{\mathbf{r}}_5$	$\hat{\mathbf{r}}_5$
4	$\hat{\mathbf{r}}_2$	$\hat{\mathbf{r}}_3$	$\hat{\mathbf{r}}_5$	$\hat{\mathbf{r}}_5$
5	$\hat{\mathbf{r}}_3$	$\hat{\mathbf{r}}_0$	$\hat{\mathbf{r}}_5$	$\hat{\mathbf{r}}_5$

$$\mathbf{r}_{ip} = \mathbf{H}^{(\tilde{m})}(\tilde{r}_{ip}, \tilde{s}_{ip}) \cdot \hat{\mathbf{r}} \qquad \text{with} \qquad \hat{\mathbf{r}} = \begin{bmatrix} \hat{r}_0 \\ \hat{s}_0 \\ ... \\ \hat{r}_3 \\ \hat{s}_3 \end{bmatrix} \tag{4.14}$$

To calculate the positions $\mathbf{x}_{ip}$ of the integration points in the (x, y)-system (1.33) can be used:

$$\mathbf{x}_{ip} = \mathbf{H}^{(m)}(r_{ip}, s_{ip}) \cdot \hat{\mathbf{x}} \qquad \text{with} \qquad \hat{\mathbf{x}} = \begin{bmatrix} \hat{x}_0 \\ \hat{y}_0 \\ ... \\ \hat{x}_3 \\ \hat{y}_3 \end{bmatrix} \tag{4.15}$$

The known integration weights $\tilde{\alpha}_i$ from the Gauss formulae (see (1.45)) of the subelements have too big values, because they are evaluated in the natural interval of the subelements.

As the real domain of such a subelement is smaller than the natural interval in each axis, an approach similar to (1.38) is used. The integration weights α_i can be evaluated with $\mathbf{J}^r$.

$$\mathbf{J}^r(\tilde{r}, \tilde{s}) = \begin{bmatrix} \frac{\partial r}{\partial \tilde{r}} & \frac{\partial r}{\partial \tilde{s}} \\ \frac{\partial s}{\partial \tilde{r}} & \frac{\partial s}{\partial \tilde{s}} \end{bmatrix} \tag{4.16}$$

Similar to (1.37) $\mathbf{J}^r$ can be calculated by:

$$\mathbf{J}^r(\tilde{r}, \tilde{s}) = \left[\frac{\partial \mathbf{H}^{(\tilde{m})}(\tilde{r}, \tilde{s})}{\partial \tilde{r}} \cdot \hat{\mathbf{r}} \quad \frac{\partial \mathbf{H}^{(\tilde{m})}(\tilde{r}, \tilde{s})}{\partial \tilde{s}} \cdot \hat{\mathbf{r}} \right] \tag{4.17}$$

Analogous to (1.38) the finite Volume $\mathrm{d}V^{\tilde{r}}$ of the subelement in the $(\tilde{r}, \tilde{s})$-system can be expressed by the finite Volume $\mathrm{d}V^{r}$ in the (r, s)-system.

$$\mathrm{d}V^{r} = \det(\mathbf{J}^{r}(\tilde{r}, \tilde{s})) \cdot \mathrm{d}\tilde{r} \cdot \mathrm{d}\tilde{s} = \det(\mathbf{J}^{r}(\tilde{r}, \tilde{s})) \cdot \mathrm{d}V^{\tilde{r}} \tag{4.18}$$

Using (1.46) with already multiplied weighting factors $\tilde{\alpha}_{ip}$ for the 2d case, finally α_{ip} can be evaluated :

$$\int_{V^{\tilde{r}}} F(\tilde{r}, \tilde{s})\, \mathrm{d}V^{\tilde{r}} \approx \sum_{ip} \tilde{\alpha}_{ip} \cdot F(\tilde{r}_{ip}, \tilde{s}_{ip})$$

$$\int_{V^{r}} F(r, s)\, \mathrm{d}V^{r} = \int_{V^{\tilde{r}}} F(\tilde{r}, \tilde{s}) \cdot \det\big(\mathbf{J}^{r}(\tilde{r}, \tilde{s})\big)\, \mathrm{d}V^{\tilde{r}} \approx \sum_{ip} \alpha_{ip} \cdot F(r_{ip}, s_{ip})$$

$$\Longrightarrow \alpha_{ip} = \det\big(\mathbf{J}^{r}(\tilde{r_{ip}}, \tilde{s_{ip}})\big) \cdot \tilde{\alpha}_{ip} \tag{4.19}$$

In Figure 4.9, a structured XFEM grid of quadrilaterals with a crack inside is shown. The positions of the integration points are illustrated by the blue points. The weighting factor of each one relative to the others is given by the size of the point.

To improve clarity of the figure, only two integration points in each direction of the quadrilateral (subelement) were used. By increasing the number of integration points in each direction, the integration accuracy in the crack tip element can be enhanced.

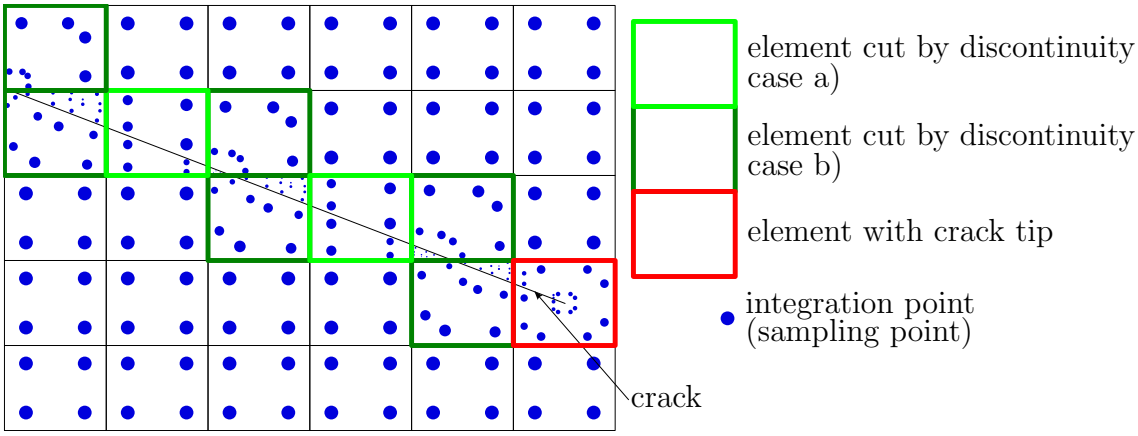

Figure 4.9. Integration points for a structured grid of quadrilaterals with a crack discontinuity

4.7. Formulation of matrices in the FE equilibrium

The FE formulation of the equilibrium equation in form (1.26) should be used. Therefore attention has to be paid to the occurring matrices. As already mentioned

in Section 1.6.2, it is not effective to use the same global indexing scheme, because the element matrices would get very big. Therefore, only DOFs which belong to this element will be considered. Additionally, it is not necessary to use the same order of DOFs. To enable simple standard- and enrichment-matrices, the following order is used:

$$\hat{\mathbf{u}}_x^{(m)} = \Big[\hat{u}_1 \quad \hat{v}_1 ... \quad \hat{u}_{n_{el}} \quad \hat{v}_{n_{el}} \quad \hat{a}_{11} \quad \hat{a}_{12} \quad ... \quad \hat{a}_{n_{el}1} \quad \hat{a}_{n_{el}2} \quad \hat{b}_{11}^{(1)} \quad \hat{b}_{12}^{(1)} \quad ... \quad \hat{b}_{n_{el}1}^{(1)} \quad \hat{b}_{n_{el}2}^{(1)} \quad \hat{b}_{11}^{(2)} \quad \hat{b}_{12}^{(2)} \quad ... \quad \hat{b}_{n_{el}1}^{(2)} \quad \hat{b}_{n_{el}2}^{(2)} \quad ... \quad \Big]^T \tag{4.20}$$

It should be pointed out that only existing enrichment DOFs are put into this vector. Therefore, the length of this local 'displacement'- vector is varying, even for elements with the same number of standard degrees of freedom.

4.7.1. Evaluation of the strain-displacement matrix

The strain-displacement matrix (see (1.24)) for standard Finite Element Analysis (FEA) has to be enlarged, to capture all parts of (3.6). For every enrichement an extra strain-displacement matrix is constructed and afterwards they are combinded. The first part is the standard **B**-matrix for the 2d case (row 3, 5, 6 and every third column are removed from (1.24)).

To build the matrix for the enrichment parts, the derivatives of the resulting shape functions $N_i(\mathbf{x}) \cdot \psi_\star(\mathbf{x})$ have to be evaluated by the chain rule ($\psi_\star(\mathbf{x})$ stands for any enrichment function). The derivatives of all specific enrichment functions ($\psi_{jump}(\mathbf{x})$ and $\psi_{tip}^{(i)}(\mathbf{x})$) for the crack problem are given in Appendix A.2.

$$\frac{\partial \left[N_i(\mathbf{x}) \cdot \psi_\star(\mathbf{x}) \right]}{\partial x_i} = \frac{\partial N_i(\mathbf{x})}{\partial x_i} \cdot \psi_\star(\mathbf{x}) + \frac{\partial \psi_\star(\mathbf{x})}{\partial x_i} \cdot N_i(\mathbf{x}) \tag{4.21}$$

By using these derivatives, the $\mathbf{B}_\star^{(m)}(\mathbf{x})$-matrices for the enrichment parts of the approximation can be denoted. Here an example for an element, where node 2 and node 4 are enriched, is given:

$$\mathbf{B}_\star^{(m)}(\mathbf{x}) = \begin{bmatrix} \frac{\partial [N_2(\mathbf{x}) \cdot \psi_\star(\mathbf{x})]}{\partial x} & 0 & \frac{\partial [N_4(\mathbf{x}) \cdot \psi_\star(\mathbf{x})]}{\partial x} & 0 \\ 0 & \frac{\partial [N_2(\mathbf{x}) \cdot \psi_\star(\mathbf{x})]}{\partial y} & 0 & \frac{\partial [N_4(\mathbf{x}) \cdot \psi_\star(\mathbf{x})]}{\partial y} \\ \frac{\partial [N_2(\mathbf{x}) \cdot \psi_\star(\mathbf{x})]}{\partial y} & \frac{\partial [N_2(\mathbf{x}) \cdot \psi_\star(\mathbf{x})]}{\partial x} & \frac{\partial [N_4(\mathbf{x}) \cdot \psi_\star(\mathbf{x})]}{\partial y} & \frac{\partial [N_4(\mathbf{x}) \cdot \psi_\star(\mathbf{x})]}{\partial x} \end{bmatrix} \tag{4.22}$$

It should be pointed out that the size of this matrix changes, depending on the number of enriched nodes. Only for full enriched elements, it has the same size as the standard **B**-matrix. To get the extended **B**-matrix ($\mathbf{B}_x^{(m)}$), which fits to the local DOF order (see (4.20)), the 2d form of the standard- (1.24) and enrichment- (4.22) matrix have to be combined as shown in the following.

$$\mathbf{B}_x^{(m)} = \begin{bmatrix} \mathbf{B}^{(m)} & \mathbf{B}_{jump}^{(m)} & \mathbf{B}_{tip(1)}^{(m)} & \mathbf{B}_{tip(2)}^{(m)} & \mathbf{B}_{tip(3)}^{(m)} & \mathbf{B}_{tip(4)}^{(m)} \end{bmatrix} \tag{4.23}$$

4.7.2. Evaluation of the interpolation matrix

Also the interpolation matrix (1.22) for the standard FEA has to be enlarged, to get an equivalent equation to (3.6) in matrix-form. For every enrichment, an extra interpolation matrix is built before all matrices are assembled to the extended interpolation matrix $\mathbf{H}_x^{(m)}$. The first part is the standard interpolation matrix as shown in (1.22) for the 2d case (last row and every third column are removed).

For the interpolation matrix the 'effective' shape functions are required:

$$N_i^{eff}(\mathbf{x}) = N_i(\mathbf{x}) \cdot (\psi_\star(\mathbf{x}) - \psi_\star(\mathbf{x}_i)) \tag{4.24}$$

By using these 'effective' shape functions the extra interpolation matrices $\mathbf{H}_\star^{(m)}(\mathbf{x})$ for the enrichment parts can be found. Here, an example for an element where node 2 and node 4 are enriched is given:

$$\mathbf{H}_\star^{(m)}(\mathbf{x}) = \begin{bmatrix} N_2^{eff}(\mathbf{x}) & 0 & N_4^{eff}(\mathbf{x}) & 0 & \\ 0 & N_2^{eff}(\mathbf{x}) & 0 & & N_4^{eff}(\mathbf{x}) \end{bmatrix} \tag{4.25}$$

The size of this matrix is changing depending on the number of enriched nodes for the specific enrichment $\psi_\star(\mathbf{x})$.

To get the extended interpolation matrix $\mathbf{H}_x^{(m)}$, all interpolation matrices are assembled as shown in the following:

$$\mathbf{H}_x^{(m)} = \begin{bmatrix} \mathbf{H}^{(m)} & \mathbf{H}_{jump}^{(m)} & \mathbf{H}_{tip(1)}^{(m)} & \mathbf{H}_{tip(2)}^{(m)} & \mathbf{H}_{tip(3)}^{(m)} & \mathbf{H}_{tip(4)}^{(m)} \end{bmatrix} \tag{4.26}$$

4.8. Evaluation of stress intensity factors

With the SIFs (K_I and K_{II}) an 'amplitude' for the displacements and stresses in the crack tip field is defined (see Section 2.2). In the XFEM, these quantities can be the result of the calculation, or they are required in the formulation of crack growth criteria. There are different methods to evaluate the SIFs.

Results aquired by the XFEM would allow a direct evaluation of the SIFs, as linear combination of the calculated crack tip enrichment coefficients $\hat{b}_i^{(j)}$[24]. This approach has been implemented and analyzed for K_I on several simple test cases. The evaluated (K_I)s differed significantly from the exact solutions, and therefore, another method was used, which is standard in the XFEM.

The domain form of the interaction integral is a very accurate approach and for this reason was used in the implementation. The interaction integral as path integral is shown in [26], the domain form is given in [20].

4.8.1. Domain form of the interaction integral

Starting at the local tip (x_1, x_2)-coordinate system (see Figure 4.10), the J-integral (see (2.8)) for the sum of two states should be evaluated for $k = 1$. State (1) with stresses $\sigma_{ij}^{(1)}$, strains $\epsilon_{ij}^{(1)}$, displacements $u_i^{(1)}$ and state (2) with stresses $\sigma_{ij}^{(2)}$, strains $\epsilon_{ij}^{(2)}$, displacements $u_i^{(2)}$.

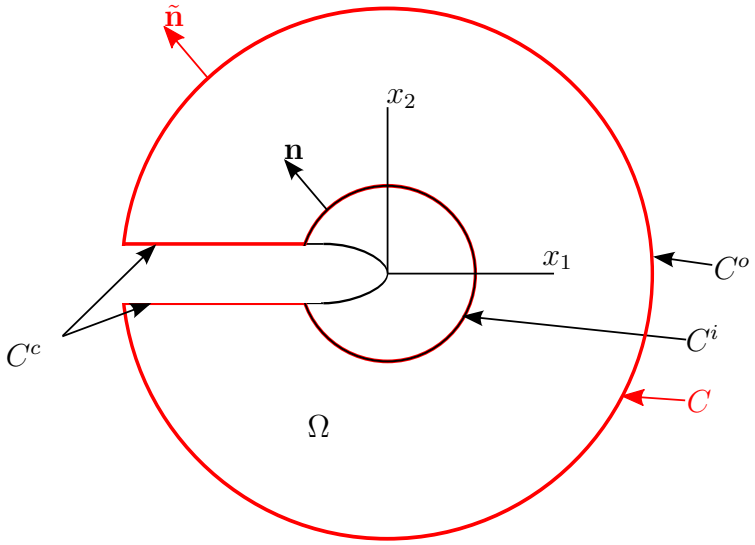

Figure 4.10. Paths around crack tip and coordinate system

$$
\begin{aligned}
J_1^{(1)} &= \int_{C^i} \left[\frac{1}{2}\sigma_{mn}^{(1)}\epsilon_{mn}^{(1)}\delta_{j1} - \sigma_{ij}^{(1)}\frac{\partial u_i^{(1)}}{\partial x_1} \right] n_j \, \mathrm{d}C^i \\
J_1^{(2)} &= \int_{C^i} \left[\frac{1}{2}\sigma_{mn}^{(2)}\epsilon_{mn}^{(2)}\delta_{j1} - \sigma_{ij}^{(2)}\frac{\partial u_i^{(2)}}{\partial x_1} \right] n_j \, \mathrm{d}C^i \\
J_1^{(1+2)} &= \int_{C^i} \left[\frac{1}{2}(\sigma_{mn}^{(1)} + \sigma_{mn}^{(2)})(\epsilon_{mn}^{(1)} + \epsilon_{mn}^{(2)})\delta_{j1} - (\sigma_{ij}^{(1)} + \sigma_{ij}^{(2)})\frac{\partial (u_i^{(1)} + u_i^{(2)})}{\partial x_1} \right] n_j \, \mathrm{d}C^i
\end{aligned}
\tag{4.27}
$$

The interaction integral for state (1) and (2) is shown in the following:

$$
I_1^{(1,2)} = J_1^{(1+2)} - J_1^{(1)} - J_1^{(2)} \tag{4.28}
$$

$$
I_1^{(1,2)} = \int_{C^i} \left[\frac{1}{2}(\sigma_{mn}^{(1)}\epsilon_{mn}^{(2)} + \sigma_{mn}^{(2)}\epsilon_{mn}^{(1)})\delta_{j1} - \sigma_{ij}^{(1)}\frac{\partial u_i^{(2)}}{\partial x_1} - \sigma_{ij}^{(2)}\frac{\partial u_i^{(1)}}{\partial x_1} \right] n_j \, \mathrm{d}C^i \tag{4.29}
$$

Using the symmetry of the elasticity tensor (see (1.11)), the following simplification can be demonstrated:

$$
\begin{aligned}
\sigma_{mn}^{(1)}\epsilon_{mn}^{(2)} &= \mathbb{C}_{mnop}\epsilon_{op}^{(1)}\epsilon_{mn}^{(2)} \\
\sigma_{mn}^{(2)}\epsilon_{mn}^{(1)} &= \mathbb{C}_{mnop}\epsilon_{op}^{(2)}\epsilon_{mn}^{(1)} = \mathbb{C}_{opmn}\epsilon_{mn}^{(2)}\epsilon_{op}^{(1)} = \mathbb{C}_{mnop}\epsilon_{mn}^{(2)}\epsilon_{op}^{(1)}
\end{aligned}
\tag{4.30}
$$

$$
I_1^{(1,2)} = \int_{C^i} \left[\sigma_{mn}^{(2)}\epsilon_{mn}^{(1)}\delta_{j1} - \sigma_{ij}^{(1)}\frac{\partial u_i^{(2)}}{\partial x_1} - \sigma_{ij}^{(2)}\frac{\partial u_i^{(1)}}{\partial x_1} \right] n_j \, \mathrm{d}C^i \tag{4.31}
$$

With Equation (2.11) for a 2d case ($K_{III} = 0$) and (4.28) a relation between the interaction integral and the SIFs can be found.

$$I_1^{(1,2)} = \frac{2}{E'}\left(K_I^{(1)}K_I^{(2)} + K_{II}^{(1)}K_{II}^{(2)}\right) \tag{4.32}$$

By setting state (1) to be the actual calculated result and state (2) to be a reference state, it is possible to evaluate K_I and K_{II}.

If state (2) is chosen to be the crack tip field for Mode 1 ($K_I = 1$ and $K_{II} = 0$), K_I can be evaluated.

$$K_I^{(1)} = \frac{E'}{2} I_1^{(1,\text{Mode 1})} \tag{4.33}$$

Analogously to this, K_{II} can be evaluated by choosing state (2) to be the crack tip field for Mode 2 ($K_I = 0$ and $K_{II} = 1$).

$$K_{II}^{(1)} = \frac{E'}{2} I_1^{(1,\text{Mode 2})} \tag{4.34}$$

As the contour integral (4.31) is not in a proper form to be evaluated from FEM results, a domain form of the interaction integral is preferred. Therefore the integrand is multiplied with a smooth weighting function $q(\mathbf{x})$, which is 1 on C^i and 0 on C^o(see Figure 4.11).

Assuming traction free and straight crack surfaces, the interaction integral can also be evaluated by integration along the path C shown on Figure 4.10, which consists of $C^i + C^c + C^o$. By implementing the normal vector components $\tilde{n}_j$ of the enclosed domain Ω which is $-n_j$ on C^i, the formulation (4.35) can be obtained.

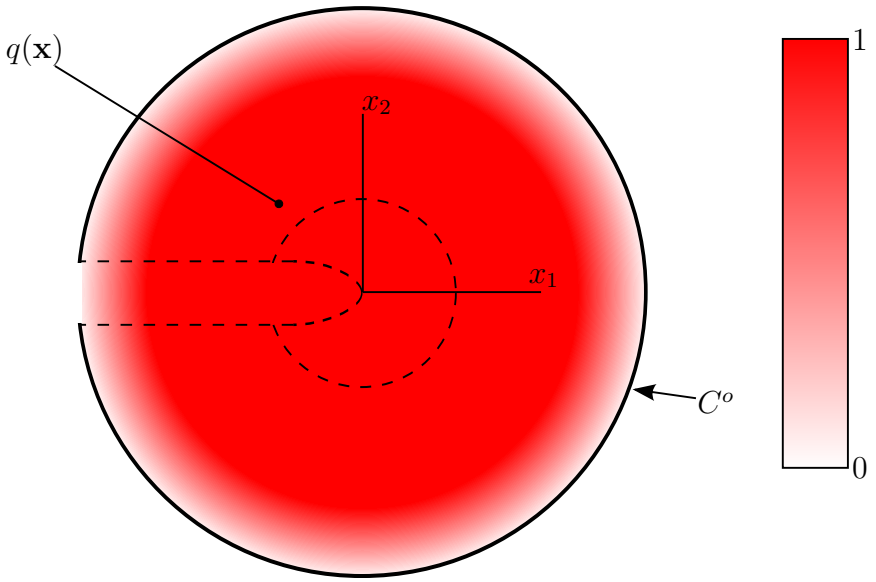

Figure 4.11. Weighting function $q(\mathbf{x})$ around the crack tip

$$I_1^{(1,2)} = -\int_C \left[\sigma_{mn}^{(2)}\epsilon_{mn}^{(1)}\delta_{j1} - \sigma_{ij}^{(1)}\frac{\partial u_i^{(2)}}{\partial x_1} - \sigma_{ij}^{(2)}\frac{\partial u_i^{(1)}}{\partial x_1}\right] q\tilde{n}_j \,\mathrm{d}C \tag{4.35}$$

Applying Gauss' theorem on this contour integral, an integral in domain Ω can be created. As these integrals are valid for any arbitrary contour C^i, it can be reduced to the crack tip, whereby Ω is the whole domain inside C^o. Using the fact, that the derivative of the terms between the brackets with respect to x_j is zero (see Appendix A.5), the following form can be found:

$$I_1^{(1,2)} = -\int_\Omega \left[\underbrace{\sigma_{mn}^{(2)}\epsilon_{mn}^{(1)}\delta_{j1}}_{I} - \underbrace{\sigma_{ij}^{(1)}\frac{\partial u_i^{(2)}}{\partial x_1}}_{II} - \underbrace{\sigma_{ij}^{(2)}\frac{\partial u_i^{(1)}}{\partial x_1}}_{III} \right] \frac{\partial q}{\partial x_j}\,\mathrm{d}\Omega \tag{4.36}$$

4.8.2. Implementation of the interaction integral

To evaluate the interaction integral with the FEM, the weighting function $q(\mathbf{x})$ is created from values $\hat{q}_i$ in the element nodes and interpolated with the standard shape functions (see (4.37)). Then $q(\mathbf{x})$ can easily be found by setting $\hat{q}_i = 1$ inside C^o and $\hat{q}_i = 0$ outside (shown in Figure 4.12). Using the derivatives of the standard shape functions and the inverse Jacobian matrix (1.35), the gradient of the weighting function can be evaluated.

$$q(\mathbf{x}) = \mathbf{H}^{(m)}(r,s)\cdot\hat{\mathbf{q}} \qquad \text{with} \qquad \hat{\mathbf{q}} = \begin{bmatrix} \hat{q}_1 \\ ... \\ \hat{q}_{n_{el}} \end{bmatrix} \tag{4.37}$$

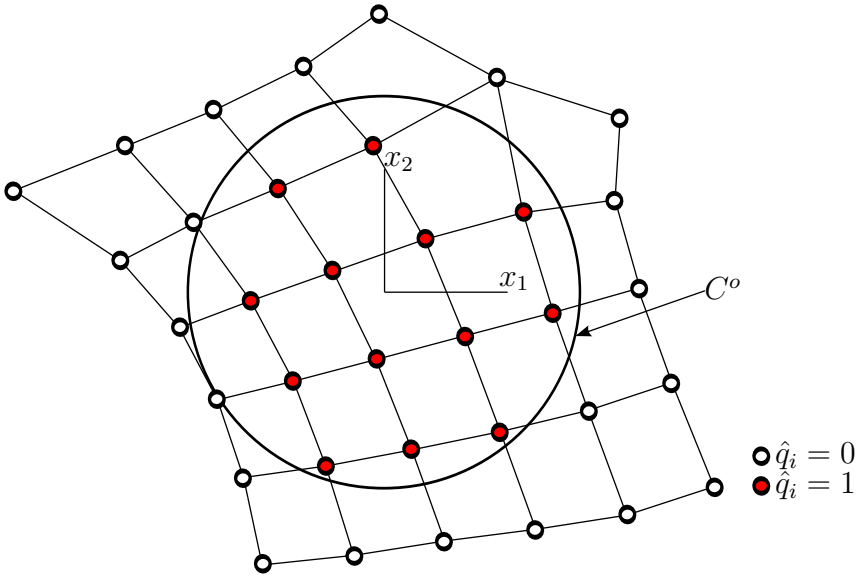

Figure 4.12. Weighting function $q(\mathbf{x})$ created from nodal values $\hat{q}_i$, for a grid around the crack tip

To calculate the first part of (4.36)-I, the stress from the reference state (2) and the strain from the actual results are required.

The stress of the reference state (2) can be evaluated from the solutions of the crack tip field ((2.1) or (2.4)). As these stresses are given in x_1, y_1-system ($\mathbf{S}_{x_1,y_1}$),

the stresses in the x, y-system ($\mathbf{S}_{x,y}$) can be evaluated with with the rotation matrix $\mathbf{A}$ (see Figure 4.13).

$$\begin{aligned} & \mathbf{S}_{x,y} = \mathbf{A} \cdot \mathbf{S}_{x_1,y_1} \cdot \mathbf{A}^T \\ \text{with} \qquad & \mathbf{S}_{x,y} = \begin{bmatrix} \sigma_{xx} & \sigma_{xy} \\ \sigma_{xy} & \sigma_{yy} \end{bmatrix}, \qquad \mathbf{S}_{x_1,y_1} = \begin{bmatrix} \sigma_{x_1x_1} & \sigma_{x_1y_1} \\ \sigma_{x_1y_1} & \sigma_{y_1y_1} \end{bmatrix} \\ \text{and} \qquad & \mathbf{A} = \begin{bmatrix} \cos\left(\theta_{t(i)}\right) & -\sin\left(\theta_{t(i)}\right) \\ \sin\left(\theta_{t(i)}\right) & \cos\left(\theta_{t(i)}\right) \end{bmatrix} \end{aligned} \tag{4.38}$$

To get the strain in actual state (1), the 2d form of Equation (1.23), with the matrix $\mathbf{B}_x^{(m)}$, can be used. The Kronecker symbol δ_{j1} in the (x_1, y_1)-system can be considered as shown in the following. In matrix notation, δ_{j1} in the (x_1, y_1)-system can be written as $\delta_{1j} \hat{=} \begin{bmatrix} 1 \\ 0 \end{bmatrix}$. For the transformation into the (x, y)-system, the rotational matrix $\mathbf{A}$ has to be applied.

$$\mathbf{A} \cdot \begin{bmatrix} 1 \\ 0 \end{bmatrix} = \begin{bmatrix} \cos(\theta_{t(i)}) \\ \sin(\theta_{t(i)}) \end{bmatrix} \tag{4.39}$$

$$\Longrightarrow \sigma_{mn}^{(2)} \epsilon_{mn}^{(1)} \delta_{j1} \hat{=} \left(\sigma_{mn}^{(2)} \epsilon_{mn}^{(1)}\right) \cdot \begin{bmatrix} \cos\left(\theta_{t(i)}\right) \\ \sin\left(\theta_{t(i)}\right) \end{bmatrix} \tag{4.40}$$

For II in (4.36), the derivatives of the displacements $\frac{\partial u_i^{(2)}}{\partial x_1}$ from the reference state (2) are shown in Appendix A.6. As these displacements are given in the directions of the local crack tip coordinate system (x_1, y_1), they have to be transformed by the rotation matrix $\mathbf{A}$.

$$\begin{bmatrix} \frac{\partial u}{\partial x_1} \\ \frac{\partial v}{\partial x_1} \end{bmatrix} = \mathbf{A} \cdot \begin{bmatrix} \frac{\partial u_1}{\partial x_1} \\ \frac{\partial v_1}{\partial x_1} \end{bmatrix} \tag{4.41}$$

The stress $\sigma_{ij}^{(1)}$ can be evaluated by the 2d equivalent of Equations (1.23) and (1.25) with the matrix $\mathbf{B}_x^{(m)}$.

The derivatives of the displacements that are required in (4.36) - III can be found by manipulation of the $\mathbf{B}_x^{(m)}$ - matrix (see (4.23)). With $(\mathbf{B}_x^{(m)})_i$ as the i-th row of the $\mathbf{B}_x^{(m)}$ - matrix, with $(\mathbf{B}_x^{(m)})_{3\,odd}$ where every second element of $(\mathbf{B}_x^{(m)})_3$ is set to zero and with $(\mathbf{B}_x^{(m)})_{3\,even}$ where all other elements of $(\mathbf{B}_x^{(m)})_3$ are changed to zero, the derivatives can be evaluated as shown in the following.

$$\frac{\partial u^{(1)}}{\partial x} = \epsilon_{xx} = (\mathbf{B}_x^{(m)})_1 \cdot \hat{\mathbf{u}}_x^{(m)} \tag{4.42}$$

$$\frac{\partial v^{(1)}}{\partial y} = \epsilon_{yy} = (\mathbf{B}_x^{(m)})_2 \cdot \hat{\mathbf{u}}_x^{(m)} \tag{4.43}$$

$$\frac{\partial u^{(1)}}{\partial y} = (\mathbf{B}_x^{(m)})_{3\,odd} \cdot \hat{\mathbf{u}}_x^{(m)} \tag{4.44}$$

$$\frac{\partial v^{(1)}}{\partial x} = (\mathbf{B}_x^{(m)})_{3\,even} \cdot \hat{\mathbf{u}}_x^{(m)} \tag{4.45}$$

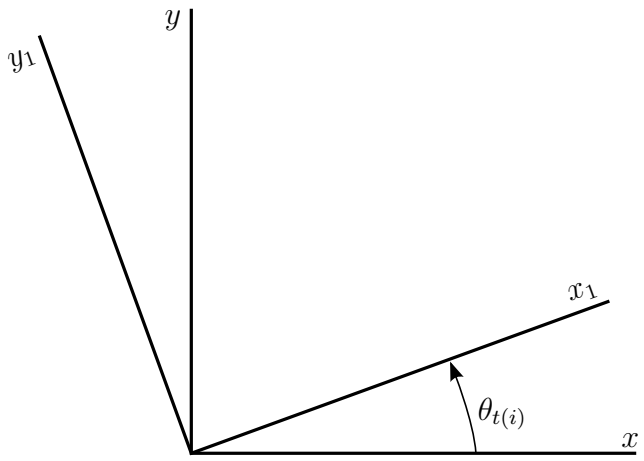

Figure 4.13. Local crack coordinate system

From Figure 4.13 the following derivatives can be found:

$$\frac{\partial x}{\partial x_1} = \cos\left(\theta_{t(i)}\right) \qquad \text{and} \qquad \frac{\partial y}{\partial x_1} = \sin\left(\theta_{t(i)}\right) \tag{4.46}$$

Using the chain rule, finally the required derivatives can be evaluated:

$$\frac{\partial u^{(1)}}{\partial x_1} = \frac{\partial u^{(1)}}{\partial x} \cdot \cos\left(\theta_{t(i)}\right) + \frac{\partial u^{(1)}}{\partial y} \cdot \sin\left(\theta_{t(i)}\right) \tag{4.47}$$

$$\frac{\partial v^{(1)}}{\partial x_1} = \frac{\partial v^{(1)}}{\partial x} \cdot \cos\left(\theta_{t(i)}\right) + \frac{\partial v^{(1)}}{\partial y} \cdot \sin\left(\theta_{t(i)}\right) \tag{4.48}$$

The stress in reference state (2) has already been evaluated for part I.

4.9. Crack growth by modification of level set functions

With quasi-static crack growth simulation, the crack path, which results from the load situation, should be calculated. Here no dynamic effects will be considered and the crack path will be created step by step. The equilibrium, given in Equation (1.1) without inertial forces, is satisfied for every step.

A method to evaluate the enrichment functions for the crack path ($\psi_{jump}(\mathbf{x})$) and the crack tip ($\psi_{tip}^{(i)}(\mathbf{x})$) in the new crack path segment is required. As the crack growth enrichment function gets evaluated by the value of the level set function for the crack path, this level set function should be modified for every crack growth step. To calculate the crack tip enrichment functions, simply the new crack tip position and crack tip angle have to be evaluated.

4.9.1. Crack growth process

In the following Figure 4.14, the whole process which is used to generate the XFEM model for the next step of a crack growth analysis is shown.

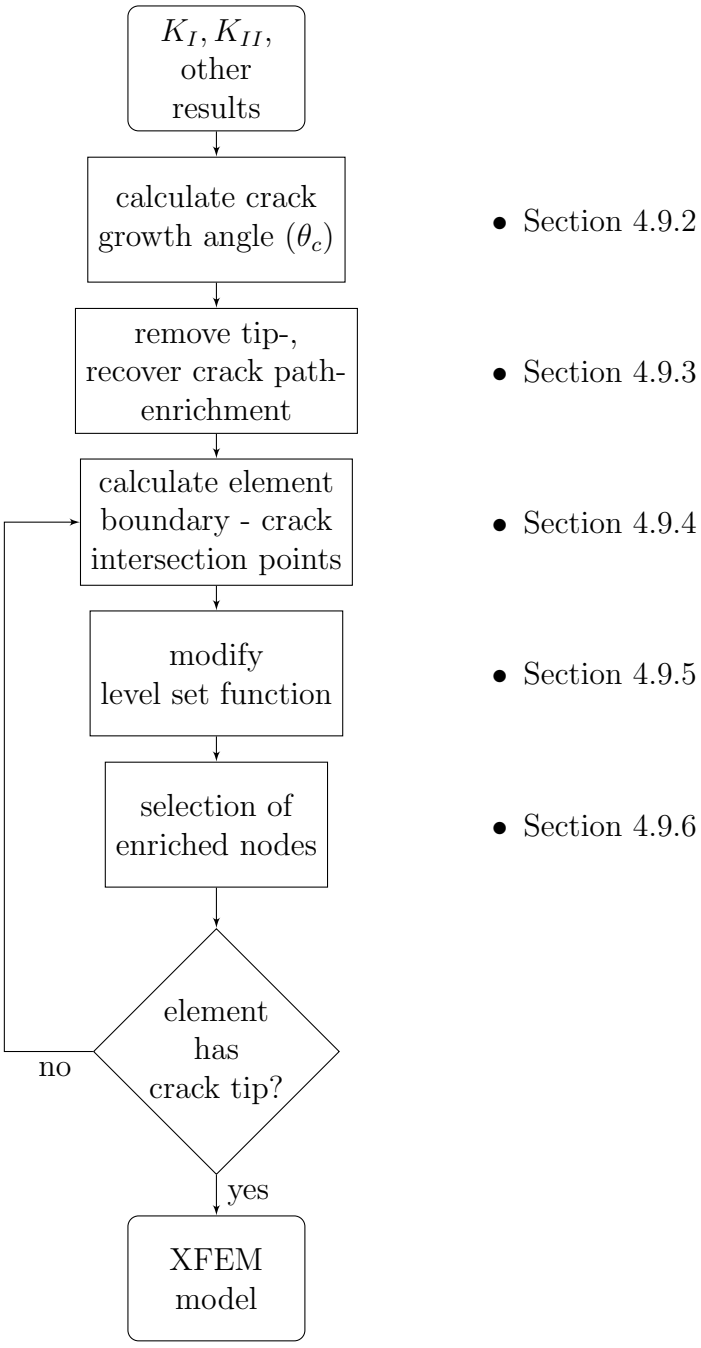

Figure 4.14. XFEM crack growth process

4.9.2. Calculate crack growth angle

In this calculation, a growth length l_c in which the growth angle does not change, is set (see Figure 4.15). Therefore, a criterion for the direction of growth is required. Here, the maximal circumferential stress criterion, which has already been described in Section 2.4.1 should be used. Equation (2.14) gives the angle for the next crack growth segment.

An equal formulation, which is easier to implement (proposed in [24]) is used. Here $\theta_c > 0$ for $K_{II} < 0$ and $\theta_c < 0$ for $K_{II} > 0$. A detailed derivation is given in Appendix A.1.

$$\theta_c = 2 \arctan \left[\frac{-2K_{II}/K_I}{1 + \sqrt{1 + 8(K_{II}/K_I)^2}} \right] \tag{4.49}$$

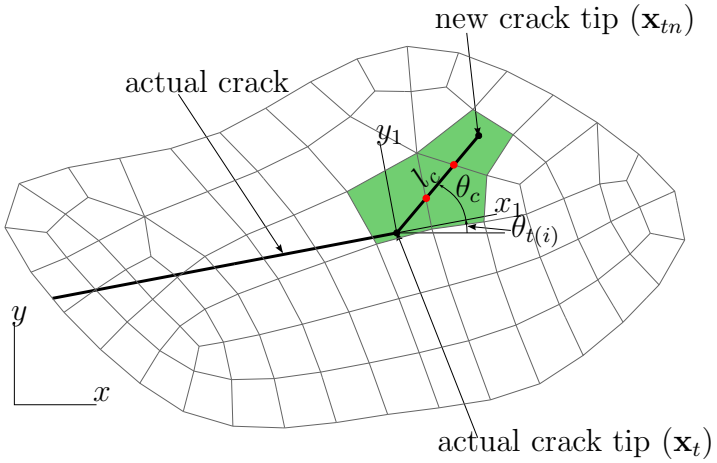

Figure 4.15. Crack growth

4.9.3. Remove tip enrichment, recover crack path enrichment

For tip enrichments which are applied inside a radius around the crack tip, these tip enrichments have to be removed and the path enrichments in this area have to be recovered (see Figure 4.16). As this is the inverse procedure which is done to select the tip enrichment nodes, it is advantageous to store all crack path enriched nodes, which were removed before (see Section 4.3).

The following steps will be applied on all elements along the new crack segment (green elements in Figure 4.15), starting with the element which has the actual crack tip inside.

4.9.4. Calculate element boundary - crack intersection points

In this section, the two points, where the new crack segment cuts the boundaries of a specific element should be evaluated. Therefore, the linear functions, which describe the element boundary and the crack segment, are defined (see Figure 4.17)

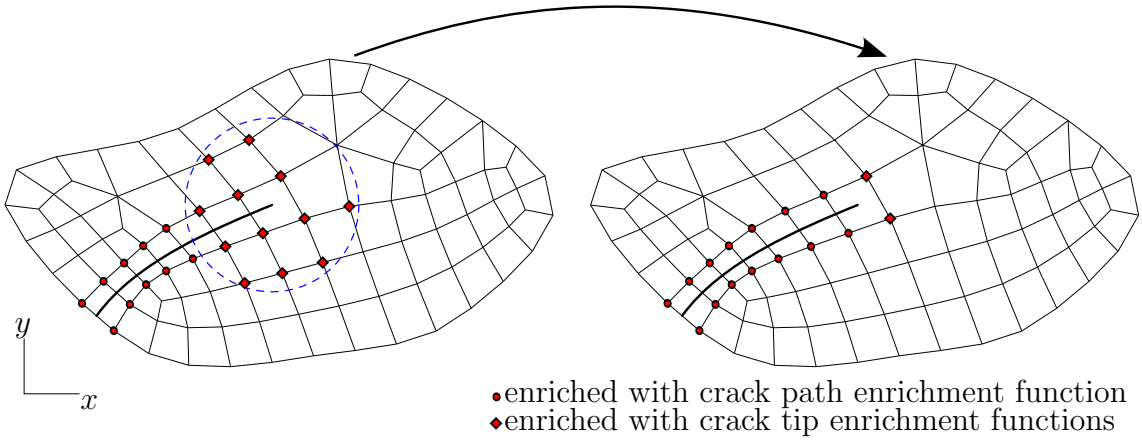

Figure 4.16. Recover crack path enrichment

in Equation (4.50) and (4.51), with $\mathbf{x}_t$ as previous crack tip position and $\mathbf{x}_i$ as the position of the element edges. Evaluating the free parameter α from this system of equations, the intersection point $x_c^{(j)}$ can be calculated.

If the calculated point is between x_{i+1} and x_i, an intersection point is found. This case can be proved by the condition $0 \leq \alpha \leq 1$. In the following step, we will use the angle $\theta = \theta_c + \theta_{t(i)}$.

$$\text{for the crack segment} \qquad y = \tan(\theta) \cdot (x - x_t) + y_t \tag{4.50}$$

$$\text{for the element boundary} \qquad \mathbf{x} = \alpha \cdot (\mathbf{x}_{i+1} - \mathbf{x}_i) + \mathbf{x}_i \tag{4.51}$$

$$\Longrightarrow \alpha = \frac{(y_i - y_t) - \tan(\theta) \cdot (x_i - x_t)}{\tan(\theta) \cdot (x_{i+1} - x_i) - (y_{i+1} - y_i)} \tag{4.52}$$

Applying this method for $i = 0, 1, ..., (n_{el} - 1)$ two points $\mathbf{x}_c^{(\alpha 1)}$ and $\mathbf{x}_c^{(\alpha 2)}$ should be found. To find the entry ($\mathbf{x}_c^{(1)}$) and exit ($\mathbf{x}_c^{(2)}$) point of the crack segment, the following approach can be used:

$$\begin{aligned}
\mathbf{x}_c^{(1)} &= \begin{cases} \mathbf{x}_c^{(\alpha 1)} & \text{for} \quad \operatorname{sign}\big(\cos(\theta)\big) \cdot \mathbf{x}_c^{(\alpha 1)} < \operatorname{sign}\big(\cos(\theta)\big) \cdot \mathbf{x}_c^{(\alpha 2)} \\ \mathbf{x}_c^{(\alpha 2)} & \text{for} \quad \operatorname{sign}\big(\cos(\theta)\big) \cdot \mathbf{x}_c^{(\alpha 1)} > \operatorname{sign}\big(\cos(\theta)\big) \cdot \mathbf{x}_c^{(\alpha 2)} \end{cases} \\
\mathbf{x}_c^{(2)} &= \begin{cases} \mathbf{x}_c^{(\alpha 1)} & \text{for} \quad \operatorname{sign}\big(\cos(\theta)\big) \cdot \mathbf{x}_c^{(\alpha 1)} > \operatorname{sign}\big(\cos(\theta)\big) \cdot \mathbf{x}_c^{(\alpha 2)} \\ \mathbf{x}_c^{(\alpha 2)} & \text{for} \quad \operatorname{sign}\big(\cos(\theta)\big) \cdot \mathbf{x}_c^{(\alpha 1)} < \operatorname{sign}\big(\cos(\theta)\big) \cdot \mathbf{x}_c^{(\alpha 2)} \end{cases}
\end{aligned} \tag{4.53}$$

4.9.5. Modify level set function

In order to describe the crack, two level set functions were used. As $\phi^t(\mathbf{x})$ only describes the position of the crack tips, this level set function will not be used in the crack growth process, since the position of the crack tip can be calculated easily.

The function $\phi(\mathbf{x})$ will be updated by a local modification. Hereby, local means that the level set function will only be modified in elements, which are cut by the new crack segment. To modify the level set function, the form which interpolates level set values on the nodes (ϕ_i) will be used (see (3.8)). This reduces the problem to a modification of nodal values.

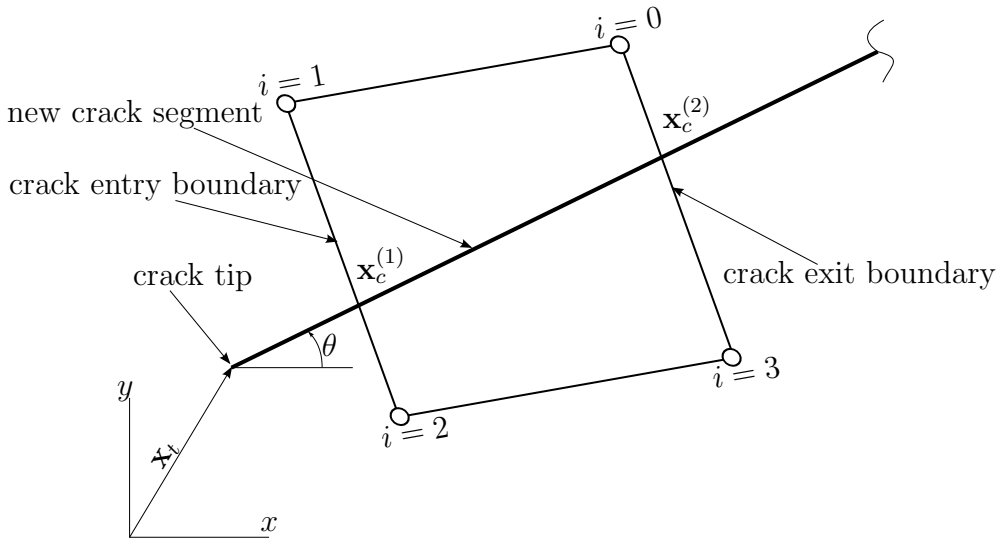

Figure 4.17. Element cut by a new crack segment

As a result of this local approach, the crack path enrichment function $\psi_{jump}(\mathbf{x})$ has to be evaluated in elements which are cut by a crack only. Evaluating the crack path enrichment function outside these elements, is not required anyway, as the shifted enrichment is always zero in these elements.

The level set function values ϕ_i, which belong to the boundary where the crack enters the element, already describe the interface correctly on the boundary. Therefore, these values should remain untouched. To evaluate the level set value in the other nodes, two possible configurations, of how a quadrilateral can be cut by a crack interface, have to be distinguished.

configuration a)

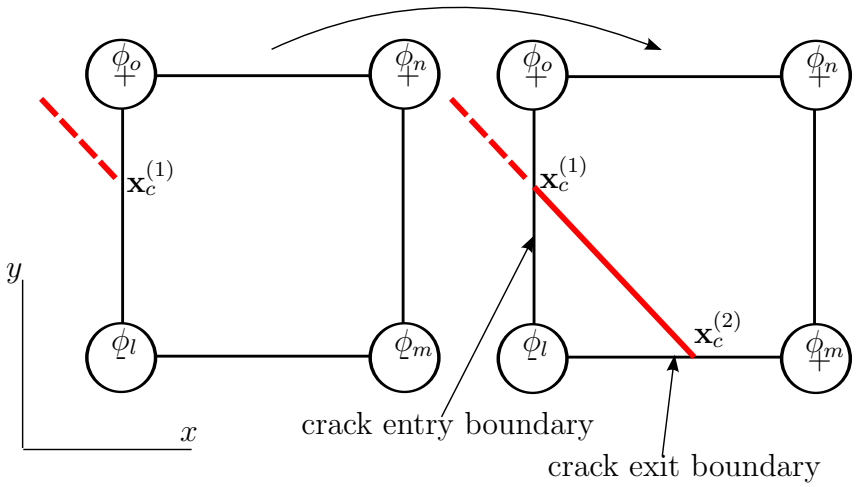

Figure 4.18. Modification of the level set function $\phi(\mathbf{x})$ for crack growth in a quadrilateral; configuration a)

In configuration a), shown in Figure 4.18, one node gets separated by the crack.

For this configuration, there is only one level set value on the crack exit boundary left, which has to be evaluated. The value ϕ_m is defined by the other level set value on the crack exit boundary and the position of the crack on this boundary, expressed by the evaluated parameter α (from (4.52)). Here, ϕ_i is the value which should be evaluated and the neighbouring values ϕ_{i+1} (counterclockwise) or ϕ_{i-1} (clockwise) on the exit boundary.

$$\phi_i = \begin{cases} \frac{\alpha}{(\alpha-1)} \cdot \phi_{i+1} & \text{for node i and node } (i+1) \text{ on the exit boundary} \\ \frac{(\alpha-1)}{\alpha} \cdot \phi_{i-1} & \text{for node i and node } (i-1) \text{ on the exit boundary} \end{cases} \tag{4.54}$$

With the three just evaluated level set values, the interface is defined on the element boundary. The last level set value ϕ_n defines, if there is a second interface in the element (not wanted) and the shape of the interface. By defining the interface to be a straight line, the level set value on the remaining node can be evaluated from a plane, which gives the level set values inside the quadrilateral. A plane can be set up by:

$$\phi(x, y) = \beta_1 x + \beta_2 y + \beta_3 \qquad \text{or} \tag{4.55}$$

$$\phi(\mathbf{x}^\star) = \boldsymbol{\beta} \cdot \mathbf{x}^\star \qquad \text{with} \qquad \mathbf{x}^\star = \begin{bmatrix} x \\ y \\ 1 \end{bmatrix} \qquad \text{and} \qquad \boldsymbol{\beta} = \begin{bmatrix} \beta_1 \\ \beta_2 \\ \beta_3 \end{bmatrix} \tag{4.56}$$

To evaluate the unknown parameter vector $\boldsymbol{\beta}$, the level set values which are known can be used (ϕ_l, ϕ_m, ϕ_o should be known on the positions $\mathbf{x}_l^\star, \mathbf{x}_m^\star, \mathbf{x}_o^\star$).

$$\boldsymbol{\phi} = \mathbf{A} \cdot \boldsymbol{\beta} \qquad \text{with} \qquad \boldsymbol{\phi} = \begin{bmatrix} \phi_l \\ \phi_m \\ \phi_o \end{bmatrix} \qquad \text{and} \qquad \mathbf{A} = \begin{bmatrix} \mathbf{x}_l^{\star T} \\ \mathbf{x}_m^{\star T} \\ \mathbf{x}_o^{\star T} \end{bmatrix} \tag{4.57}$$

$$\Longrightarrow \boldsymbol{\beta} = \mathbf{A}^{-1} \cdot \boldsymbol{\phi} \tag{4.58}$$

With this formulation for the plane, finally, the level set value ϕ_n, on the last node position $\mathbf{x}_n^\star$, can be calculated with help of (4.56). However, by using this exact approach, big oscillations of the level set values occur after some crack growth steps. To avoid this effect, only the sign of the resulting level set value is used (with $\phi_{n(old)}$ to be the previous value and $\phi_{n(new)}$ to be the exact value on the plane).

$$\phi_{n(corr)} = \text{sign}\left(\phi_{n(new)}\right) \cdot \left|\phi_{n(old)}\right| \tag{4.59}$$

This approach causes a non-linear crack interface (shown in Figure 4.19), but as long as this curved interface does not exceed any integration point, it has no effect on the approximation and, therefore, on the results. The crack entry position and exit position remains untouched, because of the bilinear shape functions of the quadrilateral.

configuration b)

In configuration b) (shown in Figure 4.20), the crack interface splits the element into two parts with two nodes. The two level set values on the crack exit boundary

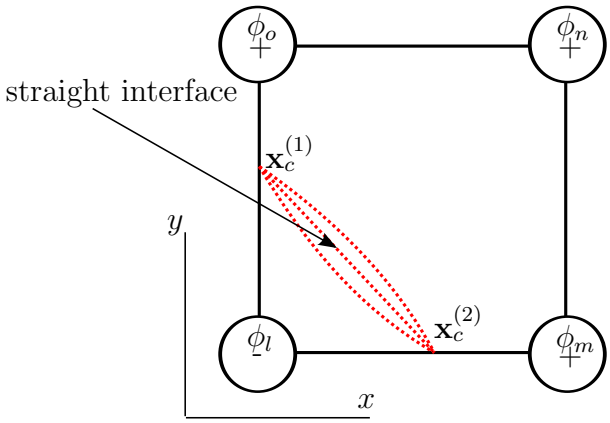

Figure 4.19. Effect of varying the level set value ϕ_n on the crack interface

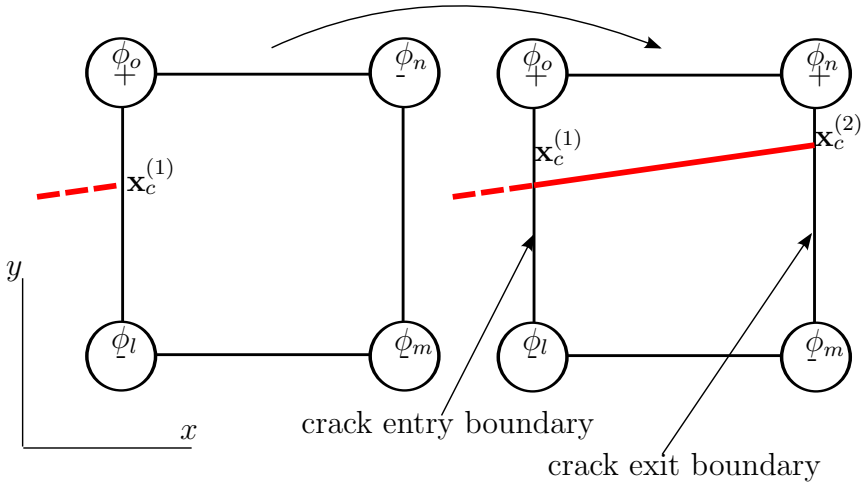

Figure 4.20. Modification of the level set function $\phi(\mathbf{x})$ for crack growth in a quadrilateral; configuration b)

should have the required sign and should define the position of the crack on the boundary. Therefore, the value of ϕ_m is evaluated by:

$$\phi_m = \text{sign}(\phi_l) \cdot abs(\phi_m) \tag{4.60}$$

Then the value of ϕ_n can be evaluated equally to configuration a) by Equation (4.54).

In Figure 4.21 the modification of the level set function $\phi(\mathbf{x})$ for a calculated example is shown.

4.9.6. Selection of enriched nodes

To select the enriched nodes, it has first to be tested, if the crack tip is in the investigated element. This can be proved by the crack growth length l_c, the position of the previous crack tip $\mathbf{x}_t$ and an assumed crack point on the crack exit boundary $\mathbf{x}_c^{(2)}$ of the actual element. The tip is not inside this element if:

$$l_c^2 > \left(x_t - x_c^{(2)}\right)^2 + \left(y_t - y_c^{(2)}\right)^2 \tag{4.61}$$

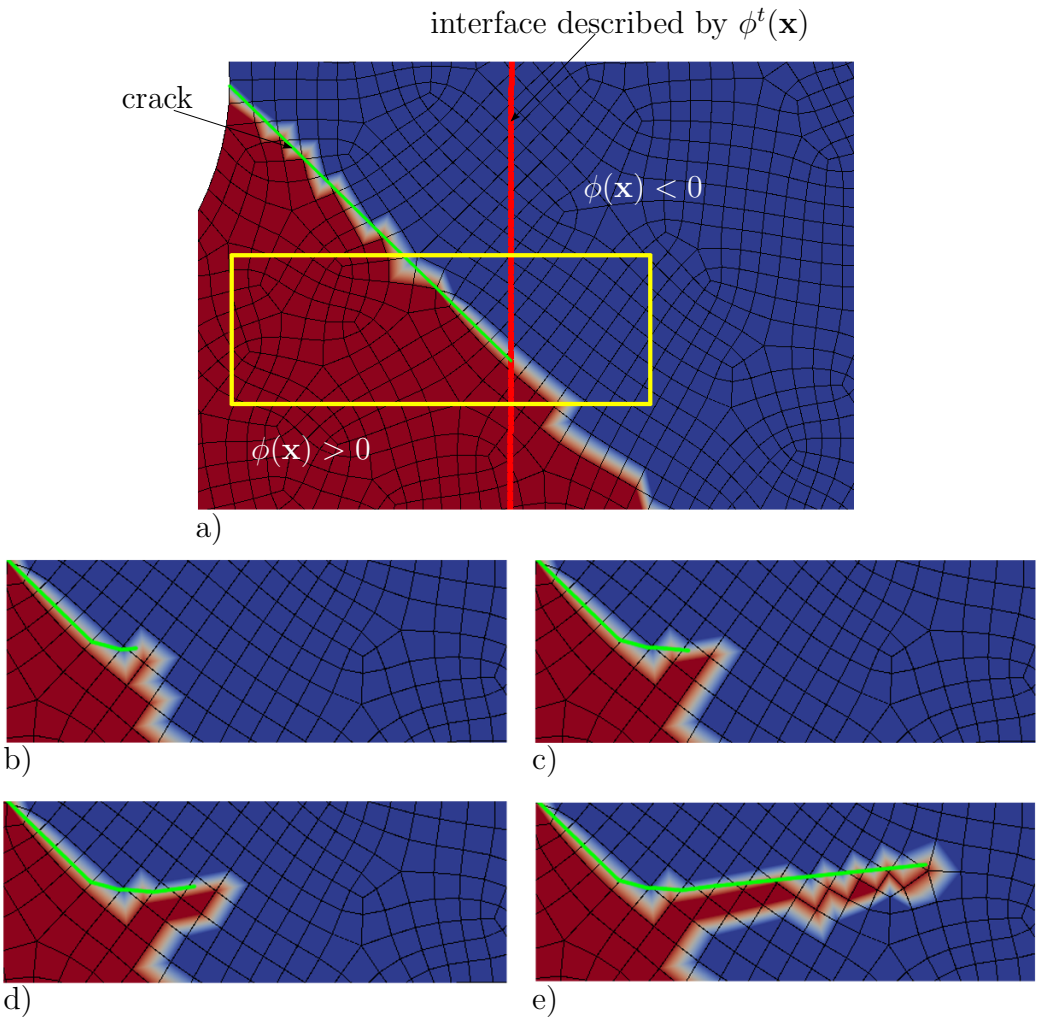

Figure 4.21. Modification of the level set function $\phi(\mathbf{x})$ (illustrated by color) with actual crack for a crack growth example; a) 1st step (inital state), b) 2nd step, c) 3rd step, d) 4th step), e) 10th step

All nodes which belong to elements fulfilling this condition, are enriched with the crack path enrichment. If there are nodes which are enriched by the tip enrichment function, this tip enrichment function will be removed, as it stems from the old crack tip position.

If condition (4.61) is not true, the crack tip is in the element. Then, the new crack tip coordinate $\mathbf{x}_{tn}$ has to be calculated. Figure 4.15 shows the situation for one crack growth segment.
The crack tip position can be calculated from the old crack tip position $\mathbf{x}_t$.

$$\mathbf{x}_{tn} = \mathbf{x}_t + l_c \cdot \begin{bmatrix} \cos(\theta) \\ \sin(\theta) \end{bmatrix} \tag{4.62}$$

With this point, the new crack tip is defined and the nodes of this element will be enriched by the crack tip enrichment function. Again it is possible to enrich all nodes inside a circle around the tip to increase accuracy. Then, all crack path enrichments inside the circle have to be removed. These removed enrichments should be stored in a list to be able to recover them for the next crack growth step (see Section 4.9.3).

The new crack tip position $\mathbf{x}_{tn}$ should now be used to calculate the value for the crack tip enrichment function $\psi_{tip}(\mathbf{x})$.

As Figure 4.14 shows, the last three steps of the crack growth process have to be repeated for every element in the new crack segment. As criterion to find the next element along the crack, the fact that the two nodes on the crack exit boundary of the actually investigated element belong to the next element, can be used.

5. Numerical examples

In the previous chapters the essential background was given. In this section numerical examples calculated in the created python code are shown.

5.1. Edge crack under tensile stress in a stretched plate

As first case an edge crack under tensile stress (the red line in Figure 5.1 illustrates the crack) in a plate should be analyzed. The 2d stress-strain situation should be a plane strain case.

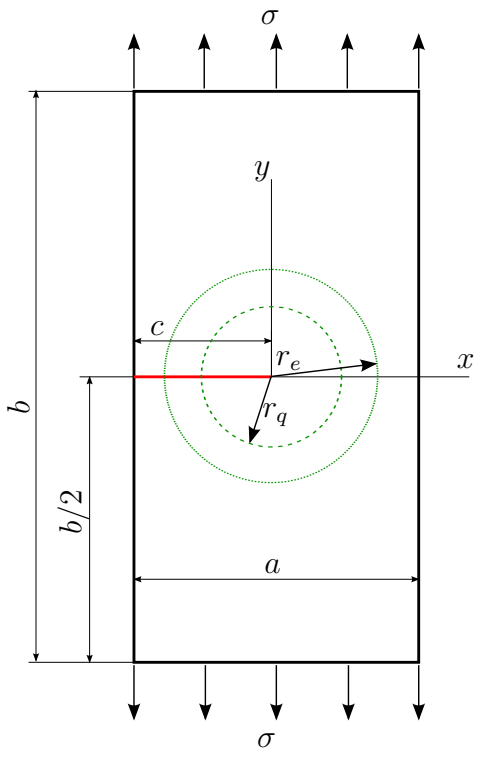

$a = 1\,mm$

$b = 2\,mm$

$c = 0.5\,mm$

$E = 210000\,N/mm^2$

$\nu = 0.3$

$\sigma = 1\,N/mm^2$

Figure 5.1. Edge crack under tensile stress in a stretched plate

5.1.1. Analytical solution

The analytical solution for an infinite plate with a crack inside is $K_I = \sigma\sqrt{\pi c}$ [13]. As the analyzed plate has an edge crack with a traction free left edge, a stress raising effect can be noticed. This effect and the finite dimensions of the plate

can be described most accurately by the following formulation (0.5% deviation for $c/a < 0.6$) [8].

$$K_I = C\left(\frac{c}{a}\right) \cdot \sigma \cdot \sqrt{\pi \cdot c} \qquad \text{with}$$
$$C\left(\frac{c}{a}\right) = 1.12 - 0.231\left(\frac{c}{a}\right) + 10.55\left(\frac{c}{a}\right)^2 - 21.72\left(\frac{c}{a}\right)^3 + 30.39\left(\frac{c}{a}\right)^4 \tag{5.1}$$

Noticing that this symmetric case has no mode II components, both SIFs can be evaluated:

$$K_I = 3.542336\, N/mm^{3/2} \qquad \text{and} \qquad K_{II} = 0\, N/mm^{3/2}$$

5.1.2. Numerical solution

The SIFs should be calculated by the domain form of the interacton integral and compared to the analytical solution. Different weighting functions $q(\mathbf{x})$ should be applied. The area, where $q(\mathbf{x}) = 1$, is defined by a circle with radius r_q.

To investigate the influence of different crack tip enrichment zones, the size of the circle (defined by r_e, see Figure 3.7), which defines this zone, is changed too. Therefore, the number of unknowns in the linear system of equations changes.

Furthermore, three different meshes should be used, a coarse structured grid, a fine structured grid and an unstructured grid. Figure 5.2 shows these meshes with the crack.

To describe the crack, the following level set functions were used:

$$\phi(x, y) = y \qquad \text{and} \qquad \phi^t(x, y) = -x \tag{5.2}$$

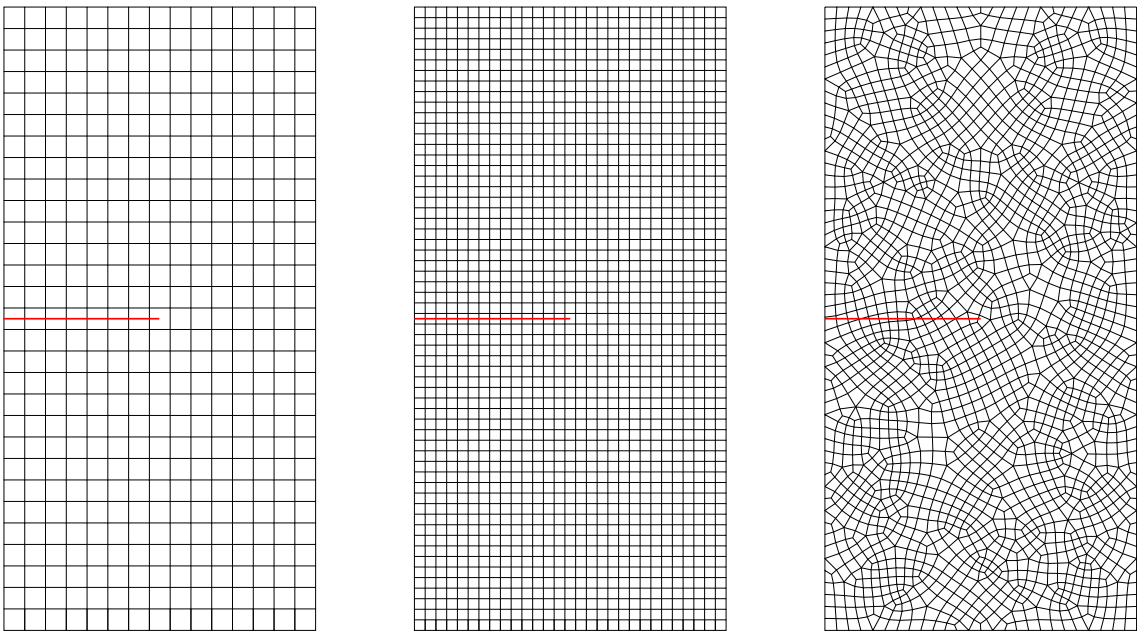

a) b) c)

Figure 5.2. Meshes for the calculation of the edge crack (marked) - a) coarse structured; b) fine structured; c) unstructured

In Figure 5.3, the deformed plate as a result of the calculation is shown. To visualize the deformed figure, on each side of the crack, the displacements were evaluated with the complete displacement approximation.

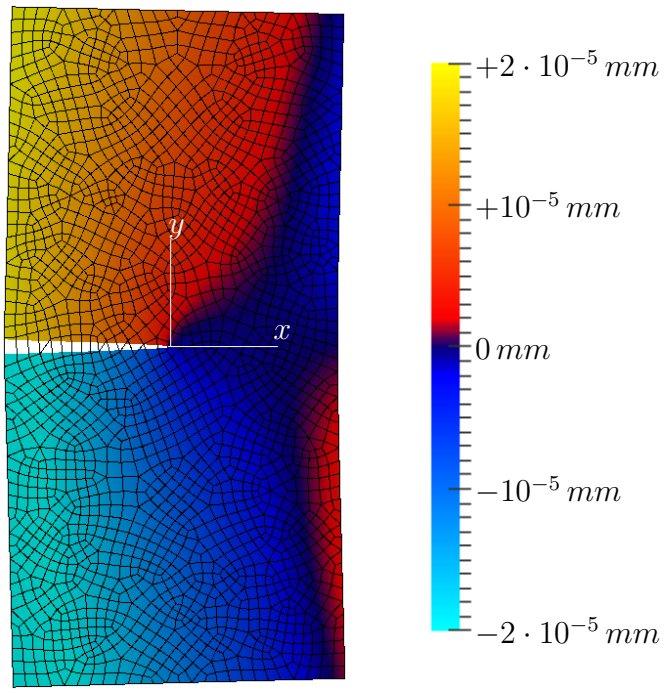

Figure 5.3. Deformed plate with an edge crack under tensile stress (displacements multiplied by factor 10^3); color shading shows y - displacement

In Table 5.1, 5.2 and 5.3 the calculated values of K_I for the different meshes are shown. For the coarse mesh, the weight function with $r_q = 0.1\,mm$ and the enrichment zone $r_e = 0.1\,mm$ would only select the tip element and therefore was not calculated. The maximal occurring K_{II} value was approximately $10^{-10}\,N/mm^{3/2}$ for the structured meshes and $0.003331\,N/mm^{3/2}$ for the unstructured mesh, which is a good result.

The coarse mesh shows already good agreement with the analytical solution. As expected, the fine mesh leads to more accurate results. It is remarkable that the unstructured mesh can provide approximately the same accuracy as the fine mesh for this symmetric case.

It can be seen that the variation of K_I for different weight functions of the interaction integral (defined by r_q) is very small for all meshes and enrichment zones. This shows, that there is a good represention of the mode I crack tip field in the whole plate. For general cases, where the global displacement is not similar to a crack tip field, the weight function should select a small region around the crack tip, to avoid other influences. The accuracy also for small regions is very good in this case, as can be seen from the results.

For this stretched plate with edge crack under tensile stress, the accuracy of the results explicitly depends on the tip enrichment area. The more nodes around the crack tip are enriched, the more accurate results can be calculated. It should be mentioned that this behavior is not expected for curved cracks, as the crack tip field only describes a straight crack.

Table 5.1. Calculated K_I for structured coarse mesh, for different enrichment zone and weight functions of the interaction integral

norm. K_I $[-]$	K_I $[N/mm^{3/2}]$	r_q $[mm]$	r_e $[mm]$	number of unknowns
0.959397	3.398507	0.2	only tip element	1020
0.959284	3.398106	0.3		
0.959202	3.397817	0.4		
0.985415	3.490669	0.2	0.2	1236
0.980728	3.474067	0.3		
0.980572	3.473514	0.4		
0.982719	3.481122	0.2	0.3	1456
0.987635	3.498534	0.3		
0.984588	3.487740	0.4		
0.988071	3.500079	0.2	0.4	1864
0.988008	3.499856	0.3		
0.990457	3.508530	0.4		

Table 5.2. Calculated K_I for structured fine mesh, for different enrichment zone and weight functions of the interaction integral

norm. K_I $[-]$	K_I $[N/mm^{3/2}]$	r_q $[mm]$	r_e $[mm]$	number of unknowns
0.979974	3.471397	0.1	only tip element	3688
0.980449	3.473079	0.2		
0.980398	3.472897	0.3		
0.980380	3.472834	0.4		
0.995483	3.526337	0.1	0.1	3872
0.990848	3.509917	0.2		
0.990786	3.509695	0.3		
0.990766	3.509626	0.4		
0.994006	3.521101	0.1	0.2	4532
0.996062	3.528387	0.2		
0.994779	3.523840	0.3		
0.994756	3.523761	0.4		
0.995933	3.527929	0.1	0.3	5576
0.995850	3.527636	0.2		
0.996829	3.531102	0.3		
0.996190	3.528840	0.4		
0.996899	3.531350	0.1	0.4	7100
0.996850	3.531176	0.2		
0.996832	3.531114	0.3		
0.997410	3.533161	0.4		

Table 5.3. Calculated K_I for unstructured mesh, for different enrichment zone and weight functions of the interaction integral

norm. K_I $[-]$	K_I $\left[N/mm^{3/2}\right]$	r_q $[mm]$	r_e $[mm]$	number of unknowns
0.982228	3.479380	0.1	only tip element	4338
0.982528	3.480443	0.2		
0.982534	3.480465	0.3		
0.982474	3.480253	0.4		
0.995533	3.526511	0.1	0.1	4546
0.990632	3.509150	0.2		
0.990637	3.509168	0.3		
0.990574	3.508945	0.4		
0.994636	3.523334	0.1	0.2	5230
0.996233	3.528992	0.2		
0.995094	3.524957	0.3		
0.995030	3.524732	0.4		
0.996391	3.529551	0.1	0.3	6458
0.996464	3.529811	0.2		
0.997227	3.532513	0.3		
0.996722	3.530724	0.4		
0.997832	3.534655	0.1	0.4	8306
0.997829	3.534647	0.2		
0.997830	3.534649	0.3		
0.998129	3.535708	0.4		

5.2. Rotated, centered crack under tensile stress in a stretched plate (mixed mode crack problem)

The first example was a pure mode I case. To analyze the performance of the XFEM also in mixed mode crack problems, as second example, a rotated, centered crack under tensile stress in a stretched plate should be investigated (case shown in Figure 5.4).

To allow comparison of the calculated solution to an analytical solution, an infinite plate with uniaxial stress would be required. The large dimensions of the mesh in comparison to the crack create a nearly uniaxial stress situation and therefore, the difference between an infinite plate and this example around the crack tips is very small. Also for this example plane strain should be assumed.

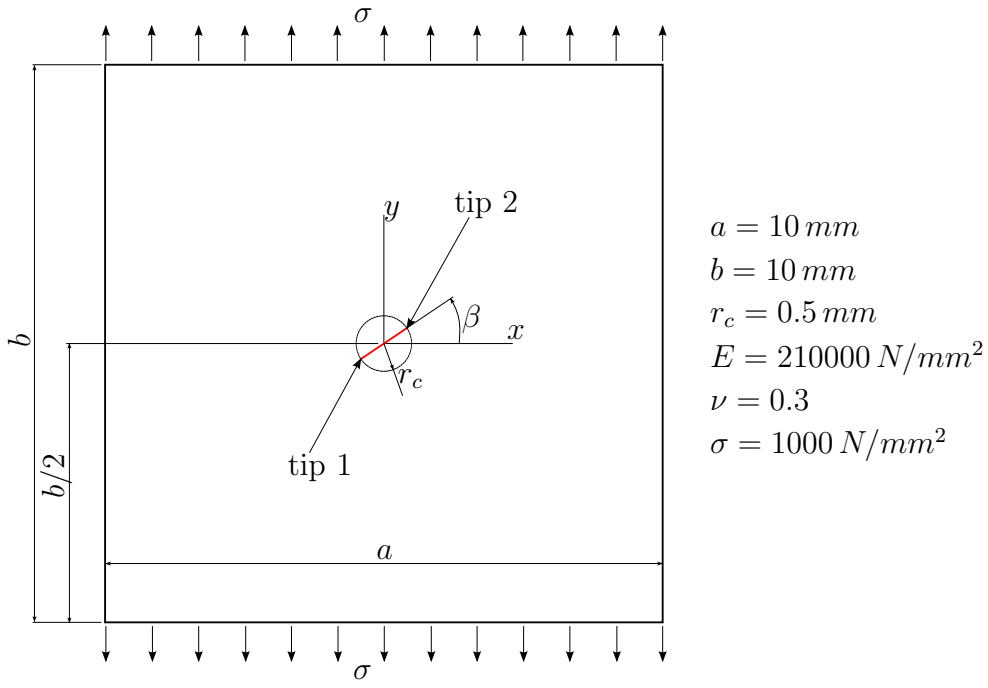

Figure 5.4. Rotated, centered crack under tensile stress in a stretched plate

5.2.1. Analytical solution

As reference solution, the solution for an rotated, centered crack under uniaxial stress for an infinite plate will be used [21]:

$$K_I = \sigma \cdot \sqrt{\pi \cdot r_c} \cdot \cos^2(\beta) \tag{5.3}$$

$$K_{II} = \sigma \cdot \sqrt{\pi \cdot r_c} \cdot \sin(\beta) \cdot \cos(\beta) \tag{5.4}$$

5.2.2. Numerical solution

To obtain a numerical solution, an unstructured mesh with 4529 quadrilaterals, shown in Figure 5.5, is used. For this centered crack two crack tips exist. The

tip enrichment zones, defined by r_e, which should not overlap are chosen to be $r_e = 0.3\,mm$. For the evaluation of the SIFs, r_q which defines the weighting function in the interaction integral is set to $0.3\,mm$. The case should be calculated for $\beta = 0°$, 15°, 30°, 45°, 60°, 75°, 90°, 105°, 120°, 135°, 150°, 165°, 180°.

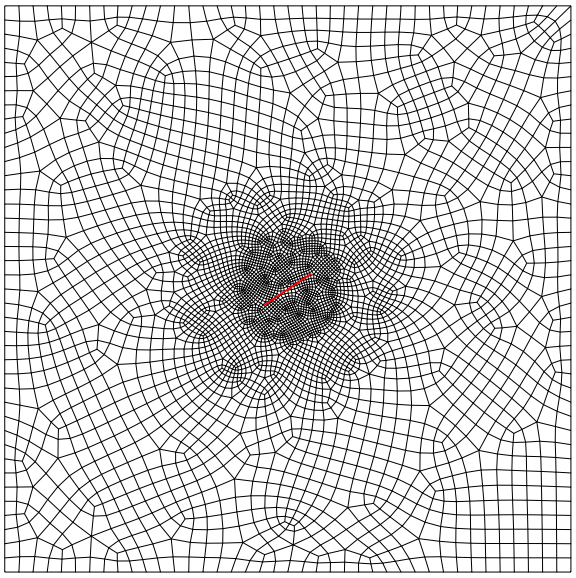

Figure 5.5. Unstructured mesh for the calculation of the rotated, centered crack (marked) under tensile stress with refined zone in the crack area

The crack is defined by the following two level set functions:

$$\phi(x, y) = \tan(\beta) \cdot x - y \qquad \text{and} \qquad \phi^t(x, y) = r_c^2 - x^2 - y^2 \tag{5.5}$$

Figure 5.6 shows the deformation of the plate with rotated, centered crack for three different angles β. In Figure 5.7 the calculated results for K_I and K_{II} are shown. The calculated values agree excellently with the analytical ones. Therefore, it is not possible to differ between the calculated SIFs for each tip in this diagram, as they are aligned. To show the very small deviation, the normalized SIFs are shown in Figure 5.8. Here it can be seen that the error is smaller than 1.5%.

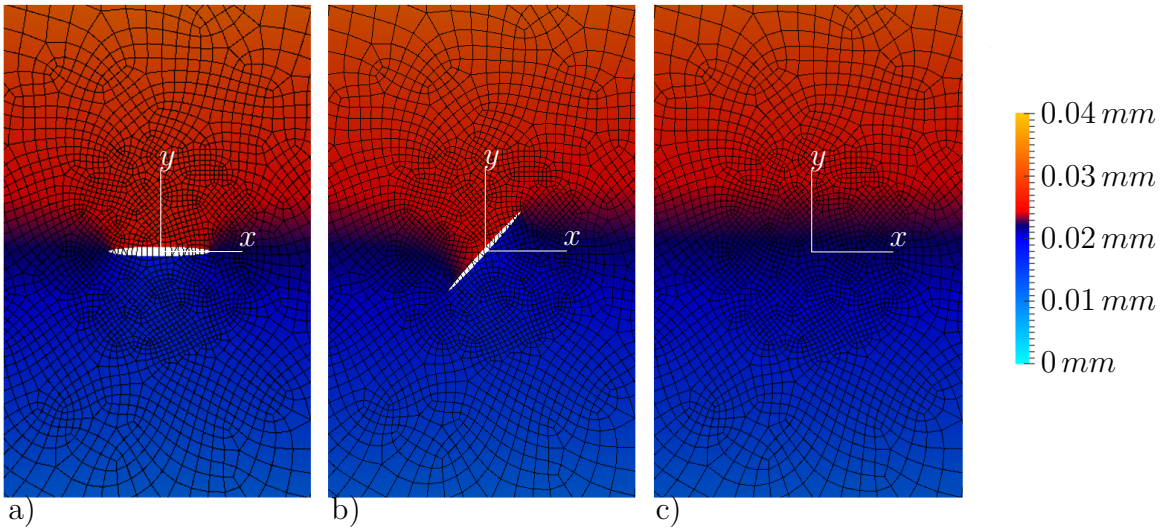

Figure 5.6. Detail of the deformed plate with a rotated, centered crack under tensile stress (displacements multiplied by factor 5); color shading shows y - displacement; a) $\beta = 0°$, b) $\beta = 45°$, c) $\beta = 90°$

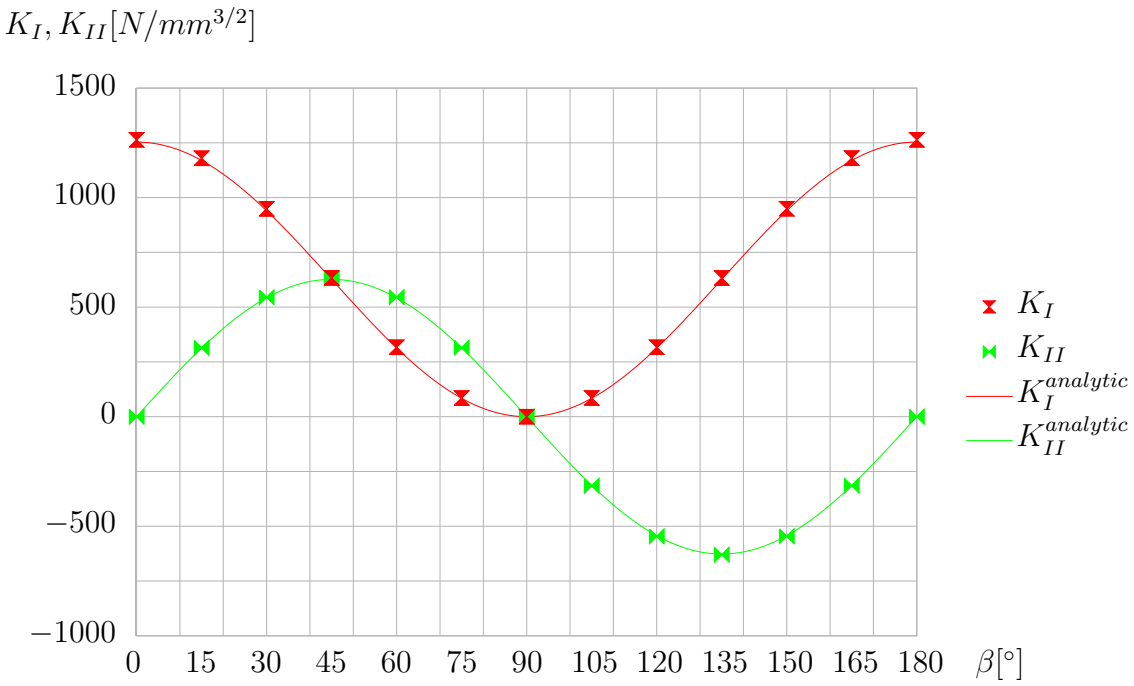

Figure 5.7. K_I and K_{II} - numerical solution compared to analytical solution for rotated, centered crack under tensile stress

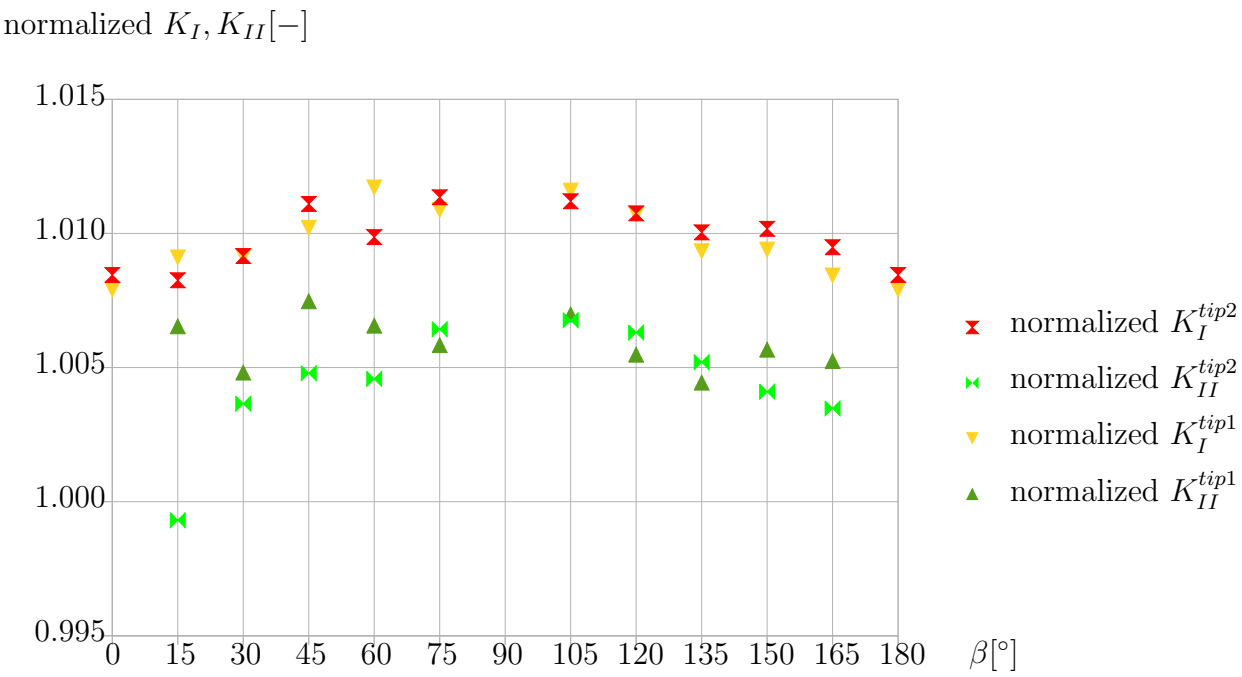

Figure 5.8. Normalized K_I and K_{II} with reference to the analytical solution for both crack tips, for rotated, centered crack under tensile stress

5.3. Centered, circular crack under biaxial stress in a stretched plate

All cracks investigated before were straight. To analyze the influence of curves in a crack, a circular crack should be analyzed. With respect to available analytical solutions, the load should be a biaxial stress. Again plane strain case for this plate should be assumed. The whole problem is shown in Figure 5.9.

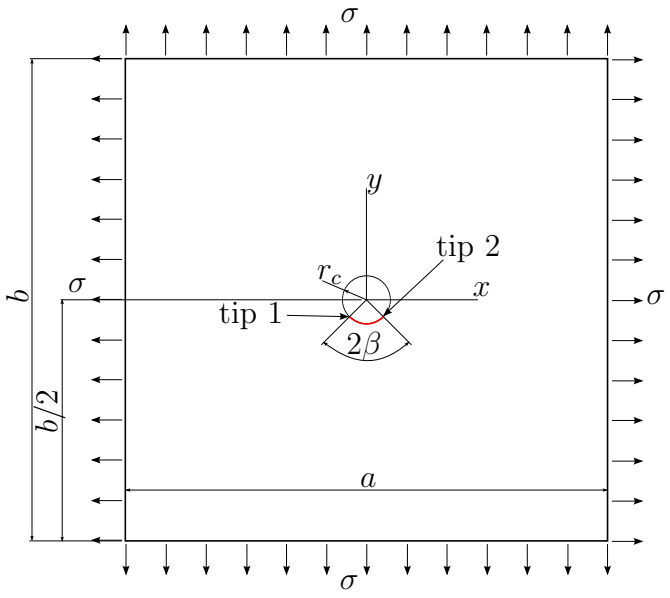

$a = 10\,mm$
$b = 10\,mm$
$r_c = 0.5\,mm$
$E = 210000\,N/mm^2$
$\nu = 0.3$
$\sigma = 1000\,N/mm^2$

Figure 5.9. Centered, circular crack under biaxial stress in a stretched plate

5.3.1. Analytical solution

For an infinite plate a solution of this circular crack under biaxial stress for different angles β and radii r_c can be given (for tip 2) [21]:

$$K_I = \frac{\sigma}{1+\sin^2\left(\frac{\beta}{2}\right)}\sqrt{\frac{\pi r_c \sin(\beta)\big(1+\cos(\beta)\big)}{2}} \tag{5.6}$$

$$K_{II} = \frac{\sigma}{1+\sin^2\left(\frac{\beta}{2}\right)}\sqrt{\frac{\pi r_c \sin(\beta)\big(1-\cos(\beta)\big)}{2}} \tag{5.7}$$

By inserting the values of the actual case, the following analytic solutions for different angles β can be evaluated (see Table 5.4). Taking the symmetry of the circular crack into account, it can be found that K_{II}^{tip1} for tip 1 is $-K_{II}^{tip2}$ and that the (K_I)s are equal for both tips.

5.3.2. Numerical solution

Again it is necessary that the mesh has a big area around the crack to get conditions close to the biaxial stress state. In contrast to the straight cracks, there are some points which require a finer grid, because

- the crack path in elements is linear, more elements should be used to get a good representation of a curved crack.
- the J-integral is only path independent for a straight crack. To get acceptable accuracy for the calculation of the SIFs, the interaction integral should be evaluated very close to the crack tip.
- the tip enrichment function describes the displacement for a straight crack and therefore, a small element with the crack tip inside is advantageous.

Table 5.4. Analytic solutions of K_I and K_{II} for the centered, circular crack

β [°]	K_I $[N/mm^{3/2}]$	K_{II} $[N/mm^{3/2}]$
45	849.305529	351.793869
60	808.064212	466.536090
75	713.002039	547.105707
90	590.817950	590.817950

Therefore, a mesh with very small elements in the middle of the domain and coarse elements outside is used (26652 elements), see Figure 5.10.

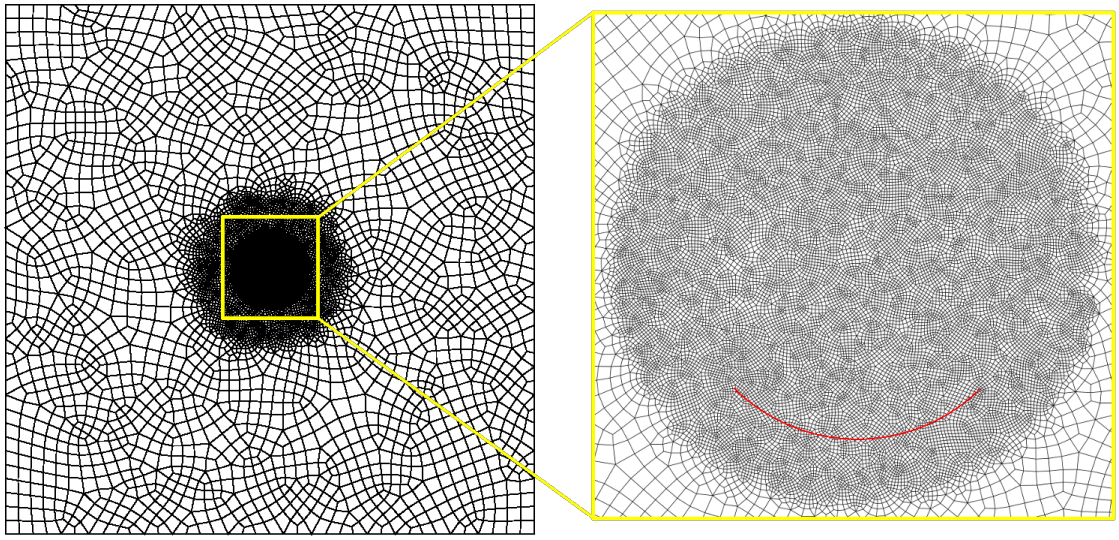

Figure 5.10. Unstructured mesh for the calculation of the centered, circular crack under biaxial stress with refined zone in the crack area

To describe the circular crack, the following level set functions where used:

$$\phi(x,y) = x^2 + y^2 - r_c^2 \qquad \text{and} \qquad \phi^t(x,y) = -\left[|x| \cdot \tan\left(\frac{\pi}{2} - \beta\right) + y\right] \tag{5.8}$$

As first case of this configuration the solution for $\beta = 45°$ was evaluated. The solution for different enrichment zones, defined by the radius of the enrichment zone r_e is given in Table 5.5 ($r_q = 0.025mm$).

Table 5.5. Calculated K_I and K_{II} for different enrichment zones of the circular crack with $\beta = 45°$

Tip	norm. K_I $[-]$	norm. K_{II} $[-]$	K_I $\left[N/mm^{3/2}\right]$	K_{II} $\left[N/mm^{3/2}\right]$	r_e $[mm]$	number of unknowns
1	1.004304	0.978770	852.961287	−344.325441	tip elem.	53690
1	1.004072	0.978355	852.764076	−344.179343	0.0125	53736
1	0.964658	0.876850	819.289741	−308.470541	0.025	54158
2	1.002081	0.974663	851.073131	342.880292	tip elem.	53690
2	1.002013	0.975060	851.015033	343.020226	0.0125	53736
2	0.945025	0.808187	802.615152	284.315062	0.025	54158

In contrast to the straight edge crack, where the accuracy of the calculation was increased by bigger enrichment zones, here the inverse effect can be observed. This effect could be expected, as the crack tip enrichment functions describe the crack tip field of a straight crack. Enlarging the crack tip enrichment zone, implies a straight crack near the tip. As this is not correct for curved cracks the accuracy decreases. Therefore, for all further examples with crack growth only, the tip element will be enriched with the crack tip enrichment function, to avoid this error.

In Table 5.6, the results of the calculation for different angles β are shown. Here already the results for crack tip enrichment only in the tip element are given. For all three angles the results agree very well with the analytical results. With these results it can be argued that also for curved cracks this method to calculate the SIFs is very accurate as long as the tip enrichment zone and also the zone of the weighting function in the interaction integral (defined by r_q) are small around the crack tip.

In Figure 5.11, the displacements of the plate with circular crack are shown.

Table 5.6. Calculated K_I and K_{II} for different angles β of the circular crack. Thereby, only the crack tip element is enriched by the crack tip enrichment functions

Tip	β $[°]$	norm. K_I $[-]$	norm. K_{II} $[-]$	K_I $\left[N/mm^{3/2}\right]$	K_{II} $\left[N/mm^{3/2}\right]$	number of unknowns
1	45	1.004304	0.978770	852.961287	−344.325441	53690
1	60	1.002949	0.984365	810.447359	−459.241936	53842
1	90	1.007333	0.986883	595.150592	−583.068228	54172
2	45	1.002081	0.974663	851.073131	342.880292	53690
2	60	1.007204	0.981420	813.885188	457.8679829	53842
2	90	0.993311	0.986706	586.865680	582.963491	54172

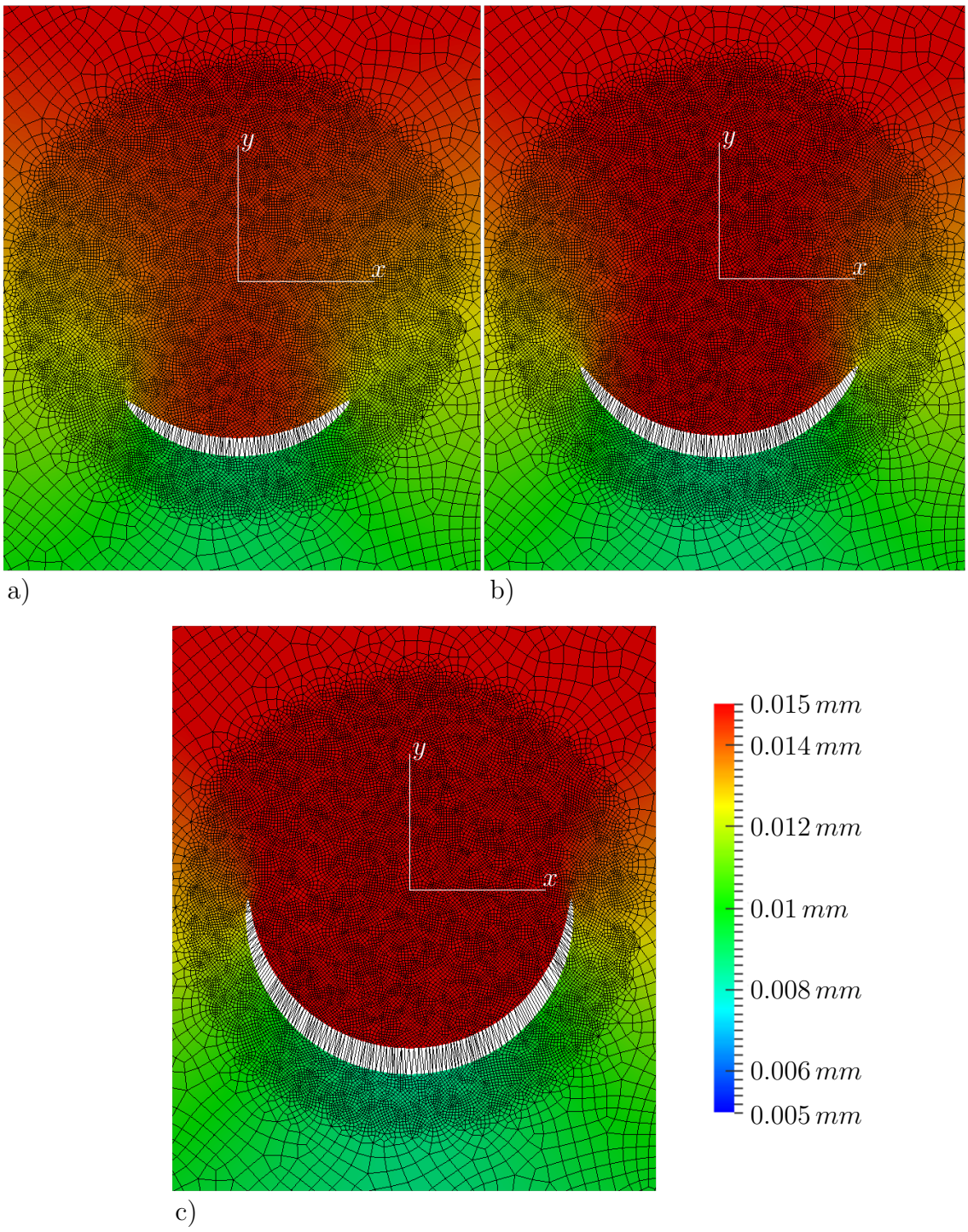

Figure 5.11. Detail of the deformed plate with a centered, circular crack under biaxial stress (displacements multiplied by factor 10); color shading shows y - displacement; a) $\beta = 45°$, b) $\beta = 60°$, c) $\beta = 90°$

5.4. Crack growth under point force load in a beam

In this example, the crack growth in a beam under force load should be investigated. The case with the inital crack of length c is shown in Figure 5.12.

For the symmetric configuration an unstable straight crack path in the middle of the beam would be expected [15]. To get stable crack growth in positive x - direction, symmetry is disturbed by setting the initial crack at $x = 0.01\,mm$. Again the plane strain case should be assumed.

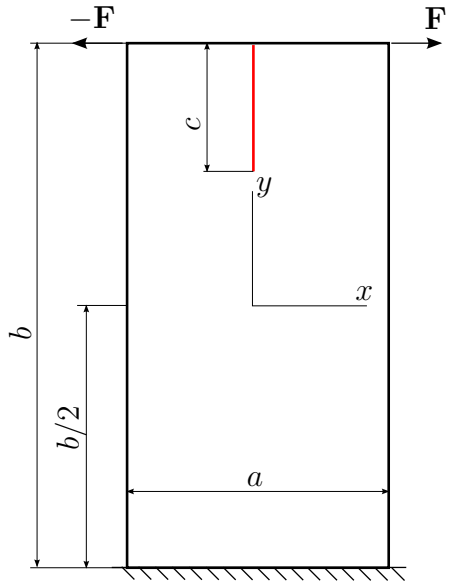

$a = 1\,mm$

$b = 2\,mm$

$c = 0.5\,mm$

$E = 210000\,N/mm^2$

$\nu = 0.3$

$\mathbf{F} = \begin{bmatrix} 100 \\ 0 \\ 0 \end{bmatrix} N$

Figure 5.12. Initial configuration for crack growth analysis under point force load in a beam

5.4.1. Numerical solution

For this calculation an unstructured mesh with 11446 elements is used, which is shown in Figure 5.13.

The crack is described by following level set functions:

$$\phi(x, y) = x - 0.01 \qquad \text{and} \qquad \phi^t(x, y) = y - 0.5 \tag{5.9}$$

The crack growth will be analyzed in a quasi-static manner with a constant crack growth length and by the maximal circumferential stress criterion as already described in Section 4.9. Only the tip element will be enriched by the tip enrichment function and for the radius r_q of the weight function in the interaction integral $r_q = 0.1\,mm$ is chosen. To analyze the influence of the crack growth length l_c, three calculations with different (l_c)s where made.

In Figure 5.14, the crack tip positions for every crack growth step are shown for different crack growth lengths l_c. These crack paths agree very well with the calculated results for a similar test case in [3] and [15].

It can be seen that for these crack growth steps the crack path depends significantly on l_c. This behavior is expected as the real crack path would be a

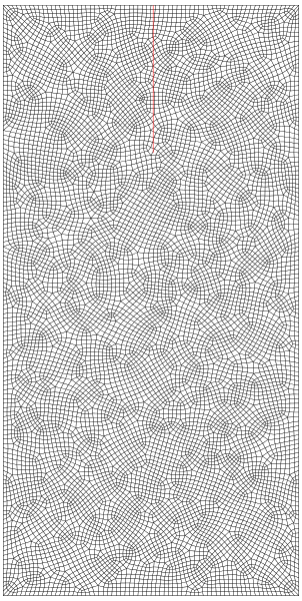

Figure 5.13. Unstructured mesh for the crack growth analysis under point force load in a beam

smooth curve and is approximated by linear segments. A further reduction of the crack growth step for this mesh would be useless, as the steps would be smaller than the elements. To improve the accuracy of the calculated crack, a mesh with more elements and a reduction of l_c would be required. In Figure 5.15 the deformed beam for different crack growth steps with growth length $l_c = 0.025\,mm$ is shown.

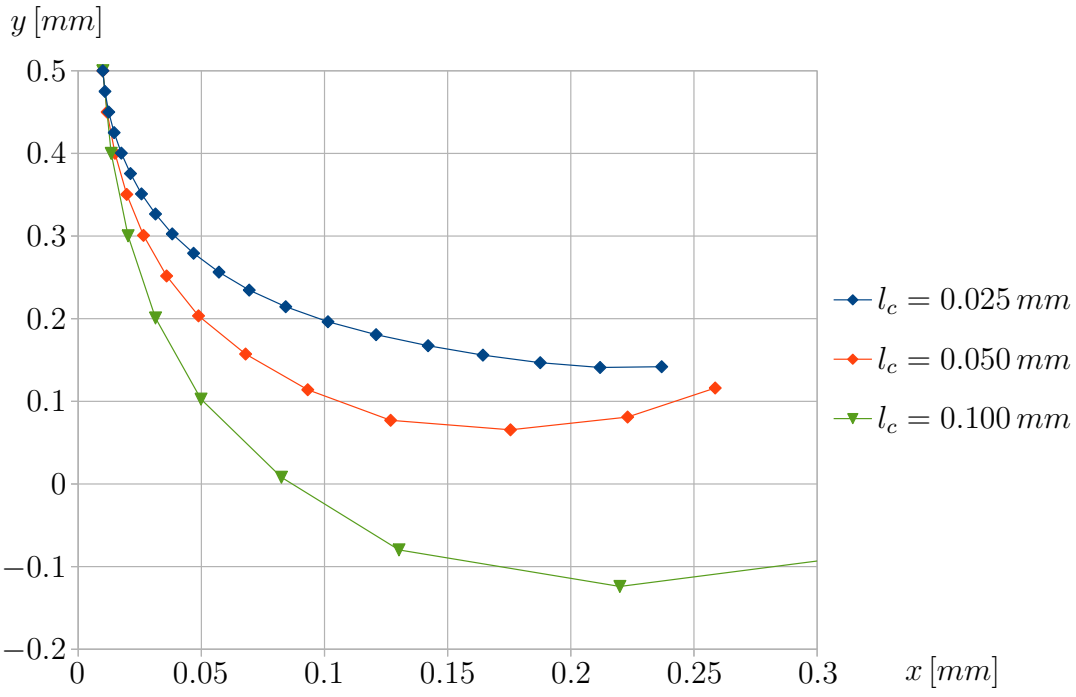

Figure 5.14. Position of the crack tip for the different crack growth lengths l_c

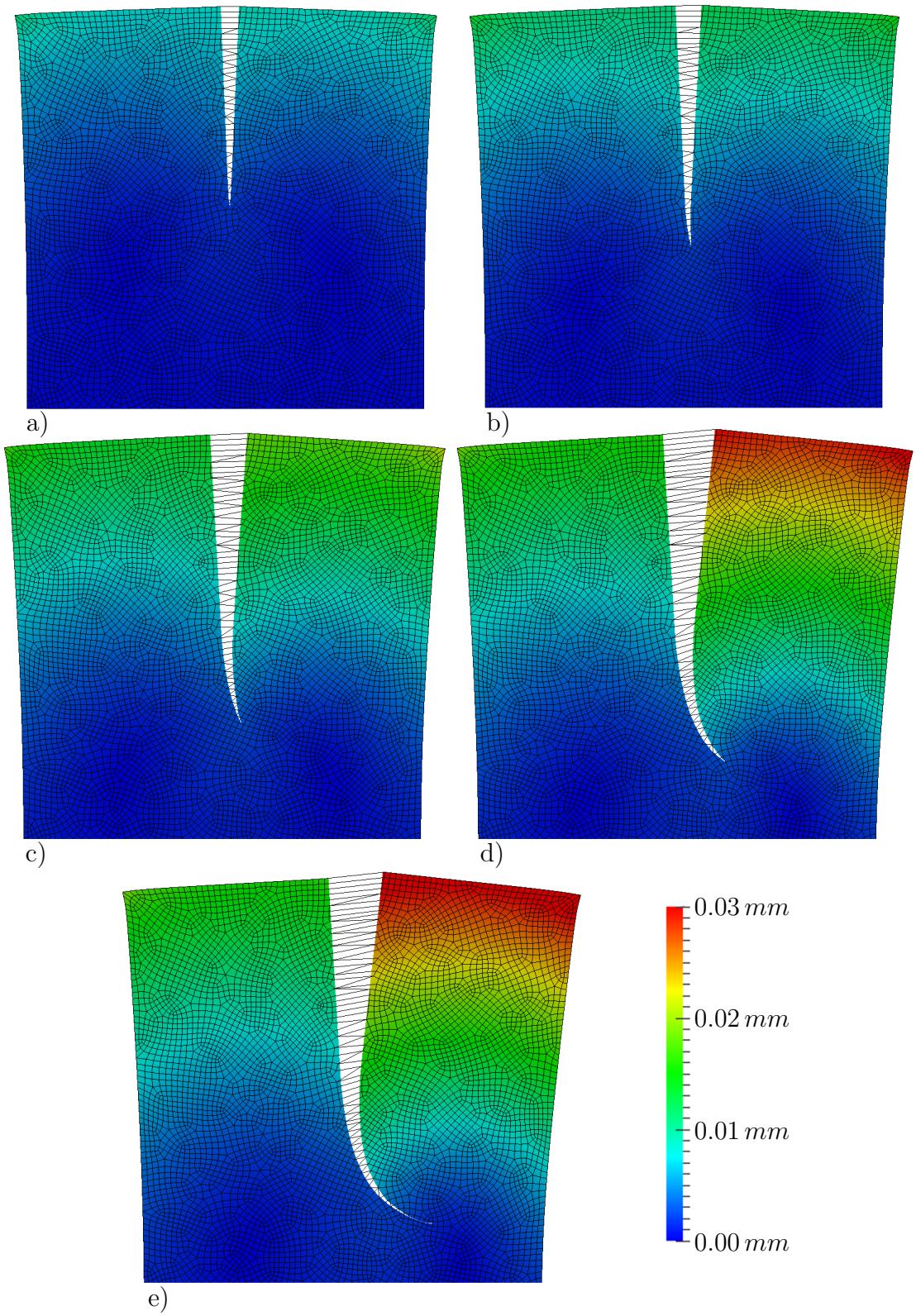

Figure 5.15. Detail of deformed beam under point force load for different crack growth steps with growth length $l_c = 0.025\,mm$ (displacements multiplied by factor 3); color shading shows the magnitude of the displacement ; a) Step 1 (inital configuration), b) Step 5, c) Step 10, d) Step 15, e) Step 20

5.5. Crack growth from two holes in a plate under tensile stress

In this example, the crack growth from two holes with an inital crack should be analyzed. Again, a plate under tensile stress with plane strain assumption is considered. In Figure 5.16, the initial configuration for this case is shown.

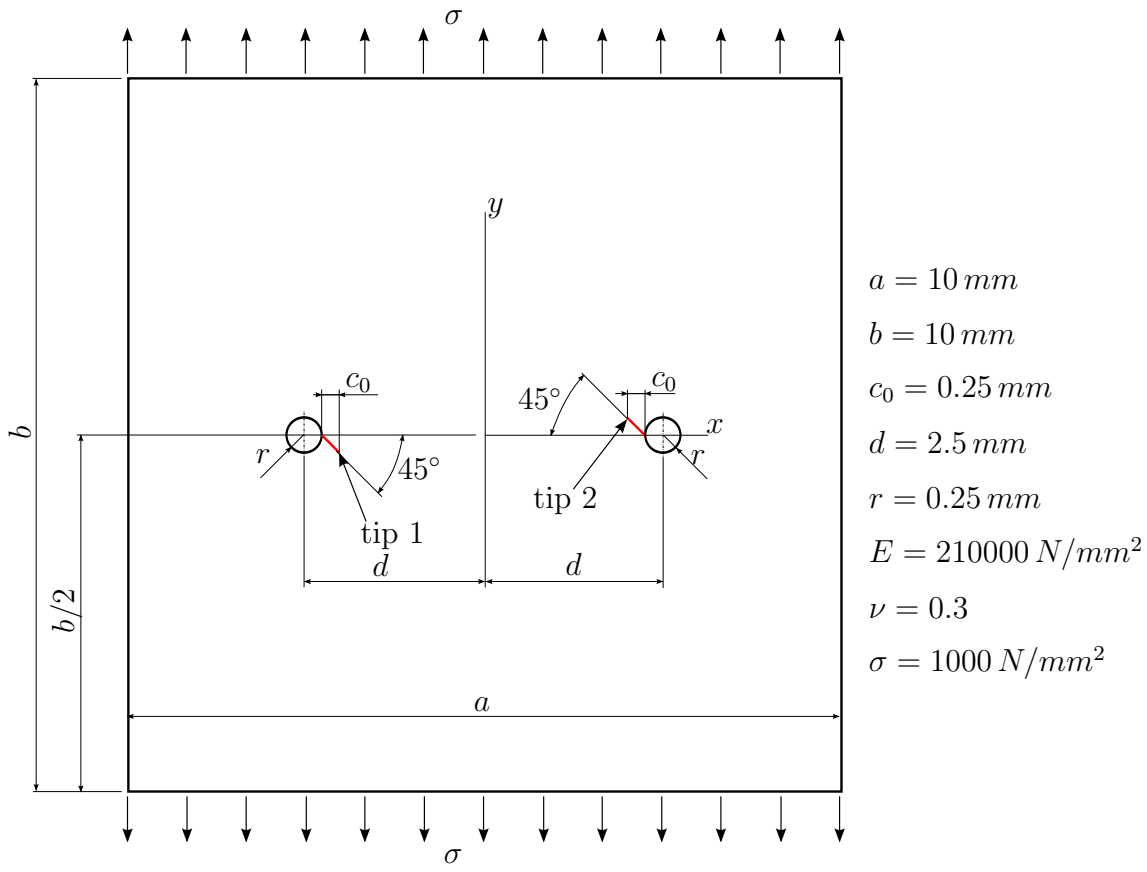

Figure 5.16. Initial configuration for crack growth analysis from two holes in a plate under tensile stress

5.5.1. Numerical solution

For this calculation two unstructured meshes were used. A coarse one with 4874 elements (shown in Figure 5.17), and a mesh with refinement in the crack area with 28726 elements (shown in Figure 5.18).

To describe the two inital cracks the level set functions in (5.10) were used. Hereby, $\phi^t(x,y)$ is a polynomial which fulfills the conditions $\phi^t(0,y) = -1$, $\phi^t(\pm 2, y) = 0$ and $\phi^t(\pm 2.4, y) = 0$.

$$\begin{aligned} \phi(x,y) &= -x + 2.25 \cdot \text{sign}(x) - y \qquad \text{and} \\ \phi^t(x,y) &= -\frac{25}{576} \cdot x^4 + \frac{61}{144} \cdot x^2 - 1 \end{aligned} \tag{5.10}$$

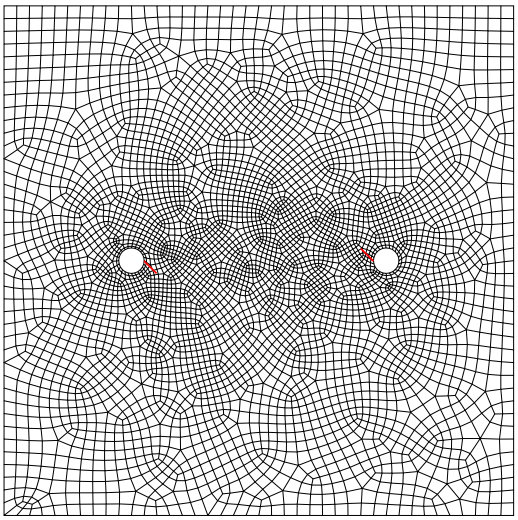

Figure 5.17. Unstructured coarse mesh with 4874 quadrilaterals for crack growth analysis from two holes in a plate under tensile stress

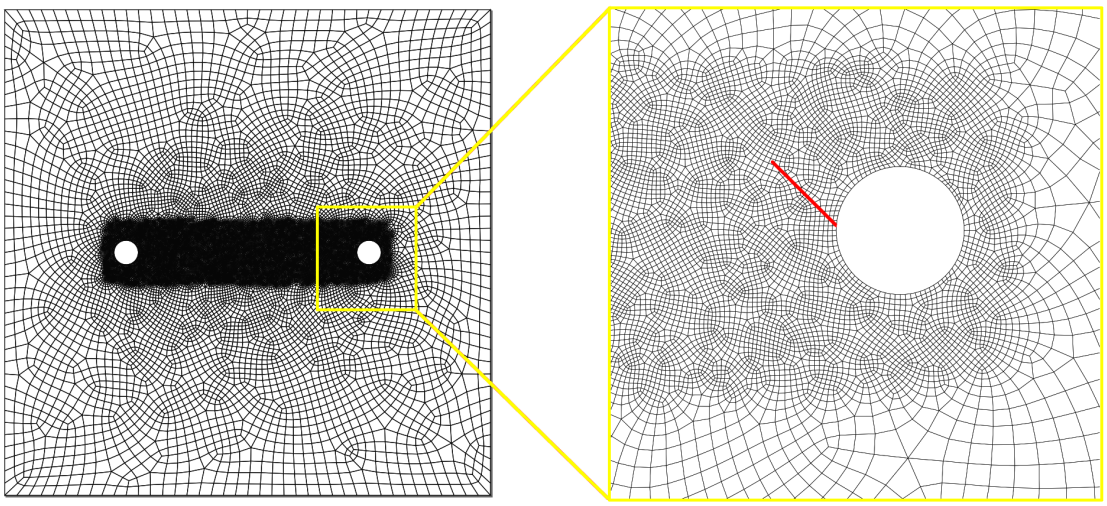

Figure 5.18. Unstructured, refined mesh with 28726 quadrilaterals for crack growth analysis from two holes in a plate under tensile stress

The crack growth should be analyzed quasi-statically, with constant crack growth length l_c. Evaluation of the crack growth direction will be done by the maximal circumferential stress criterion. Only the quadrilateral with the crack tip inside should be enriched by the crack tip enrichment functions. For the two meshes different crack growth lengths l_c and radii r_q of the weighting function in the interaction integral should be applied.

In Figure 5.19 the calculated crack paths with different crack growth lengths l_c for both meshes are shown. The result for $l_c = 0.1\,mm$ is calculated on the coarse mesh, the results for $l_c = 0.05\,mm$ and $l_c = 0.025\,mm$ are evaluated on the mesh with refinement in the crack area.

It can be seen that the propagation is in the same horizonal direction, as calculated for a simular test case in [19]. Analysing the calculated different crack paths, a

significant difference between the single solutions can be found. Nevertheless, for a reduction of the crack growth length l_c, the solutions seem to converge to a single path. From these results it can be concluded that very fine meshes are requird, to get reproduceable crack paths.

In Figure 5.20 the deformed plate for different crack growth steps is shown.

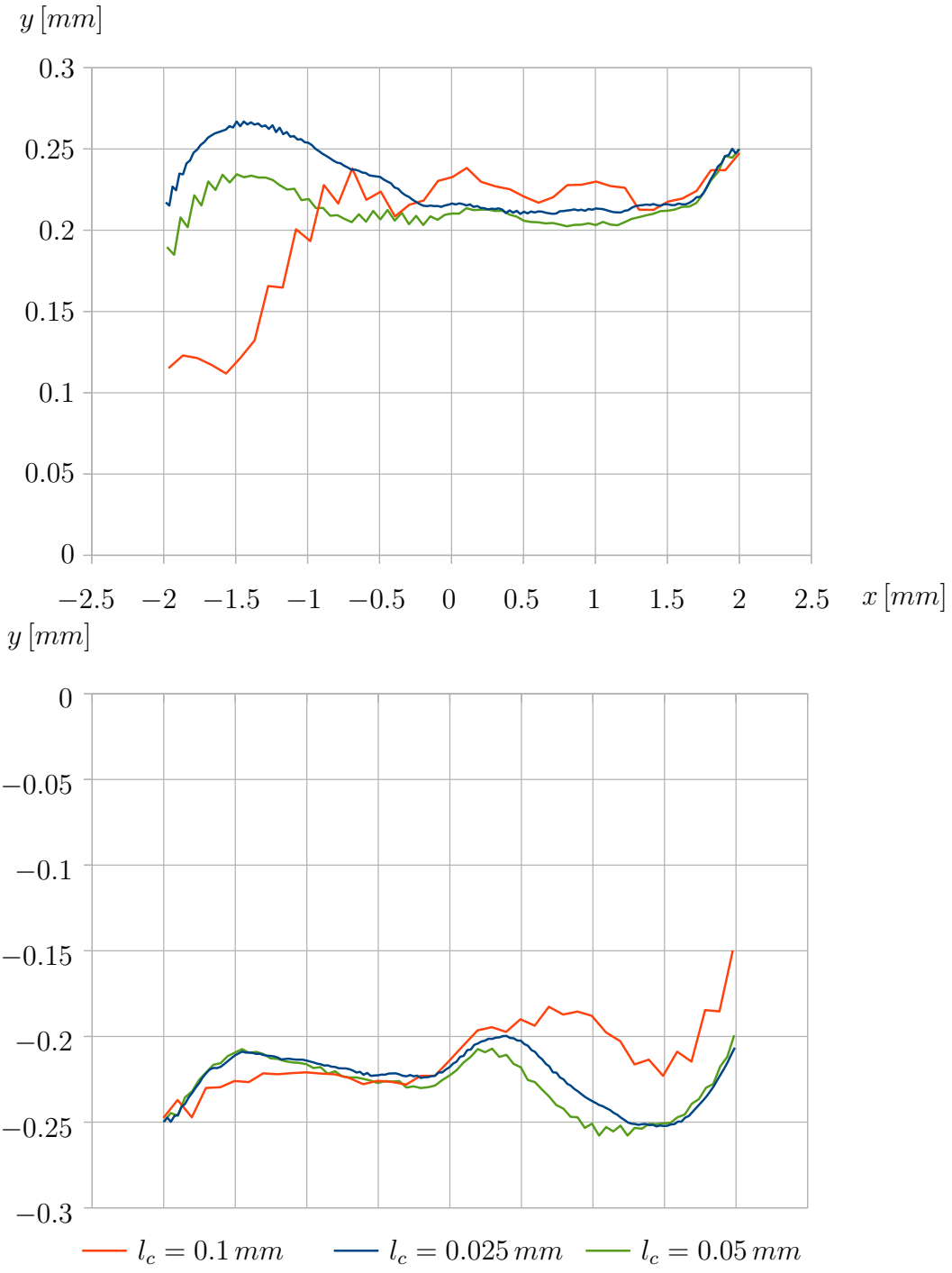

Figure 5.19. Positions of the crack tip for the different crack growth lengths l_c and varying meshes; top: tip 2, bottom: tip 1

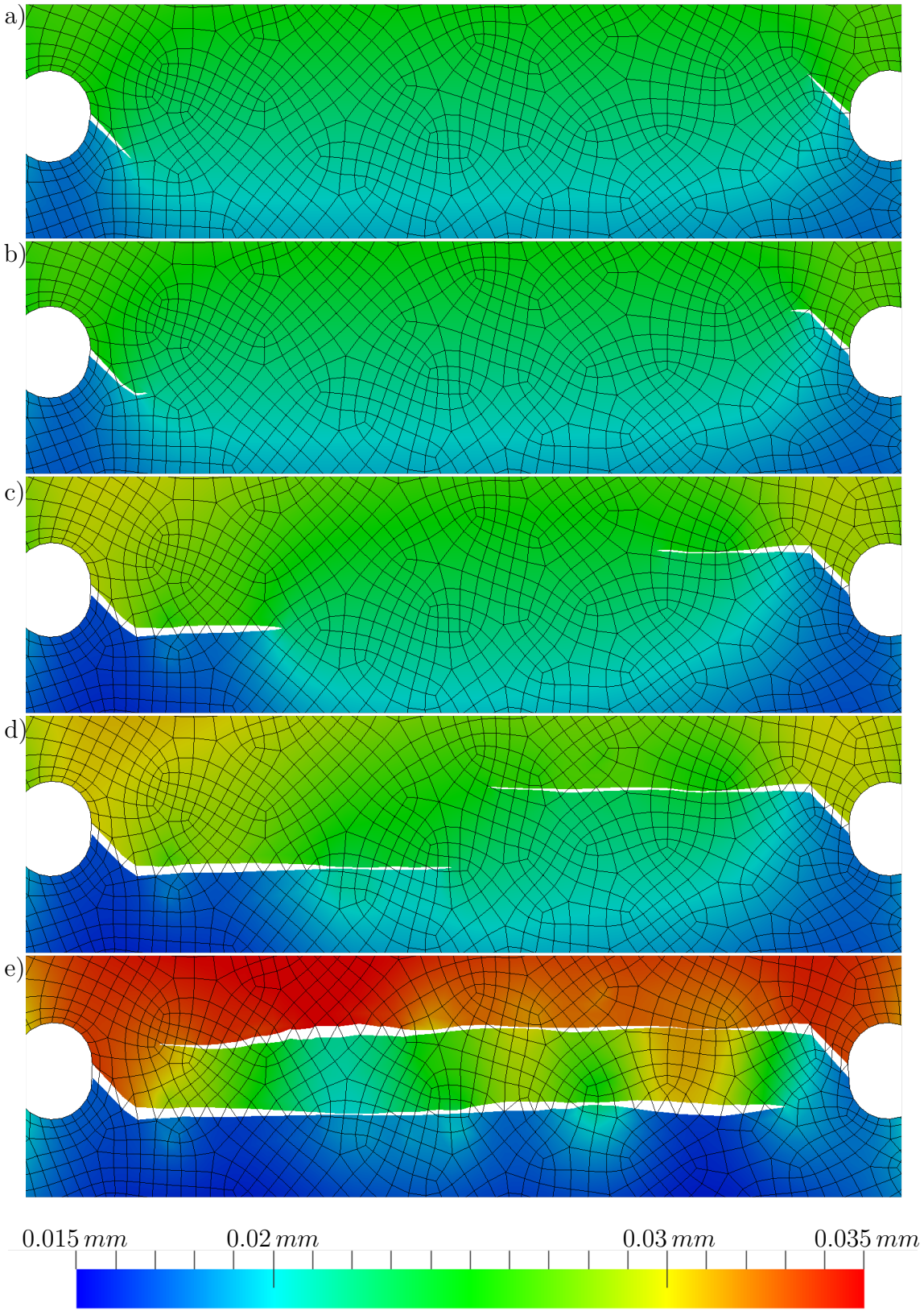

Figure 5.20. Detail of deformed plate with two holes for different crack growth steps with growth length $l_c = 0.1\,mm$ (displacements multiplied by factor 5); color shading shows y - displacement; a) Step 1(inital configuration), b) Step 2, c) Step 10, d) Step 20, e) Step 40

6. Conclusion

The application of the XFEM for quasi-static crack growth made it possible to gain insight into this method. Here some points of the gathered experience should be discussed.

Differences to the classical FEM in the implementation

The differences to the classical FEM in the implementation are: varying number of degrees of freedom per node, varying size of the element stiffness matrices, implementation of the level set functions, algorithms for the detection of the crack tips, selection of enriched nodes, evaluation of new integration points and the calculation of enrichment functions.

Additionally, for crack calculations the SIFs and a crack growth method (here modification of the level set function) have to be evaluated.

Level set method

Defining the interface of the crack path by level set functions, and storing the values in the nodes of the mesh, makes it very easy and efficient to evaluate the enrichment function for the crack path, as it can be calculated simply from these values. For crack growth analysis this level set function $\phi(\mathbf{x})$ has to be modified in each step, to provide the simple evaluation of the enrichment function of the crack path. In a discrete formulation of the crack path, this additional effort could be avoided, but it would cause a more complex evaluation of the crack path enrichment function.

The description of the crack tips by a second level set function $\phi^t(\mathbf{x})$ is straight forward. For static crack cases it ensures that the crack tip is on the crack path, as the intersection of both interfaces defines the crack tip. For the evaluation of the crack tip enrichement functions, $\phi^t(\mathbf{x})$ cannot be used, because the local tip coordinates r, θ are required. For crack growth simulations a modification of $\phi^t(\mathbf{x})$ for each step is not necessary, as the crack tip positions for each step are known from the crack growth critera.

Integration in elements cut by a crack

To perform an accurate integration in elements that are cut by a crack, new integration points and integration weights are calculated. This is done, by a division of the elements into subelements and using the integration points of these subelements. This is the standard approach in the XFEM, because of the high accuracy of the integration. For implementation in a computer code, this approach has the big disadvantage that for every element type new rules for spliting the element into subelements have to be implemented.

Elements

In this implementation first-order quadrilateral elements were used. For such elements it has always to be considered that the shape functions of these elements are bilinear. Therefore, a straight interface in the global coordinate system is not a straight interface in the local element coordinate system. This fact has to be considered in some points of the implementation, like the evaluation of the crack tip position.

For the implementation of any other elements, especially the calculation of the integration points with subelements would have to be adopted. For higher-order elements the interface inside the element could be a higher-order polynom and therefore, more subelements for the calculation of the integration points would be required. On the other hand, higher-order polynoms would lead to a better representation of the crack path than polygons.

Domain form of the interaction integral

The evaluation of the SIFs by the domain form of the interaction integral can be performed very accurately. A disadvantage of this method is that the radius r_q for the weighting function is a new free parameter which influences the result significantly. Here, an automated evaluaton of r_q from the element size is advantageous.

Crack tip enrichment zone

For simple test cases with straight cracks it has been found that a big tip enrichment area around the crack tip, defined by the radius r_e, leads to higher accuracy. Once curved cracks have to be considered, a big crack tip enrichment zone leads to failures in the results. As a result of that, for crack growth simulations, where always curved cracks should be considered, the enrichment of the crack tip element only leads to better results.

Quasi-static crack growth

The calculation of the crack path by quasi-static crack growth, using the maximal circumferential stress criterion, is very sensitive to the chosen growth length l_c. To get reproduceable crack paths for quasi-static crack growth, in general, very small steps l_c and therefore very fine meshes are required.

The XFEM is a very good method to consider cracks and other possible interfaces without creating a specific mesh for that case. In particular, for moving interfaces or the comparison of results for different interfaces this method is very efficient.

Appendix A.

Derivations

A.1. Derivation of crack growth direction

In Section 2.4.1 the evaluation of the crack growth direction is shown. Here the derivation in detail, starting from (2.12), is given.

For $\theta_c \neq \pm\pi$ and ,thus, $\cos\left(\frac{\theta_c}{2}\right) \neq 0$, the following expression can be gathered:

$$K_I \sin\left(\frac{\theta_c}{2}\right)\cos\left(\frac{\theta_c}{2}\right) + K_{II}\left[1 - 3\sin^2\left(\frac{\theta_c}{2}\right)\right] = 0 \tag{A.1}$$

Using $\sin(\theta_c) = 2\sin\left(\frac{\theta_c}{2}\right)\cos\left(\frac{\theta_c}{2}\right)$ and $\cos(\theta_c) = 1 - 2\sin^2\left(\frac{\theta_c}{2}\right)$ leads to:

$$K_I \frac{\sin(\theta_c)}{2} + K_{II}\left[1 + 3\,\frac{\cos(\theta_c) - 1}{2}\right] = 0 \tag{A.2}$$

Multiplication by factor 2, gives Equation (2.13). To derive the crack growth direction, Equation (A.1) is used as inital point. Using $\sin^2\left(\frac{\theta_c}{2}\right) = 1 - \cos^2\left(\frac{\theta_c}{2}\right)$ gives:

$$\frac{K_I}{K_{II}}\sin\left(\frac{\theta_c}{2}\right)\cos\left(\frac{\theta_c}{2}\right) + \left[3\cos^2\left(\frac{\theta_c}{2}\right) - 2\right] = 0 \tag{A.3}$$

$$\frac{K_I}{K_{II}}\tan\left(\frac{\theta_c}{2}\right) + \left[3 - \frac{2}{\cos^2\left(\frac{\theta_c}{2}\right)}\right] = 0 \tag{A.4}$$

Finally, with $\frac{1}{\cos^2\left(\frac{\theta_c}{2}\right)} = 1 + \tan^2\left(\frac{\theta_c}{2}\right)$ the following expressions can be found:

$$\tan^2\left(\frac{\theta_c}{2}\right) - \frac{1}{2}\frac{K_I}{K_{II}}\tan\left(\frac{\theta_c}{2}\right) - \frac{1}{2} = 0 \tag{A.5}$$

$$\tan\left(\frac{\theta_c}{2}\right) = \frac{1}{4}\frac{K_I}{K_{II}} \pm \sqrt{\frac{1}{16}\left(\frac{K_I}{K_{II}}\right)^2 + \frac{1}{2}} \tag{A.6}$$

$$\Longrightarrow \theta_c = 2\arctan\left\{\frac{1}{4}\left[\frac{K_I}{K_{II}} \pm \sqrt{\left(\frac{K_I}{K_{II}}\right)^2 + 8}\right]\right\} \tag{A.7}$$

By the proof $\left.\frac{\partial^2 \sigma_{\theta\theta}}{\partial \theta^2}\right|_{\theta_c} < 0$ for a maximum, it can be found that for $K_{II} < 0$ the '+'-sign and for $K_{II} > 0$ the '−'-sign has to be used. Here '±' can be replaced by

$-\text{sign}(K_{II})$ for the case $K_{II} \neq 0$.
For this special case $K_{II} \neq 0$, it will be shown that (4.49) is equal to (A.7). First of all, some transformations on the expression between the curly brackets in (A.7) should be applied.

$$\begin{aligned}
&\frac{1}{4}\left[\frac{K_I}{K_{II}} - \text{sign}(K_{II})\sqrt{\left(\frac{K_I}{K_{II}}\right)^2 + 8}\right] \\
=&\frac{1}{4}\left[\frac{K_I}{K_{II}} - \underbrace{\text{sign}(K_{II}) \cdot \text{sign}(K_{II})}_{=1}\frac{K_I}{K_{II}}\sqrt{1 + 8\left(\frac{K_{II}}{K_I}\right)^2}\right] \\
=&\frac{1}{4}\frac{K_I}{K_{II}}\left[1 - \sqrt{1 + 8\left(\frac{K_{II}}{K_I}\right)^2}\right] \\
=&\frac{1}{4}\frac{K_I}{K_{II}}\frac{\left[1 - \sqrt{1 + 8\left(\frac{K_{II}}{K_I}\right)^2}\right] \cdot \left[1 + \sqrt{1 + 8\left(\frac{K_{II}}{K_I}\right)^2}\right]}{\left[1 + \sqrt{1 + 8\left(\frac{K_{II}}{K_I}\right)^2}\right]} \\
=&\frac{1}{4}\frac{K_I}{K_{II}}\frac{1 - \left[1 + 8\left(\frac{K_{II}}{K_I}\right)^2\right]}{1 + \sqrt{1 + 8\left(\frac{K_{II}}{K_I}\right)^2}} = \frac{-2\,\frac{K_{II}}{K_I}}{1 + \sqrt{1 + 8\left(\frac{K_{II}}{K_I}\right)^2}}
\end{aligned} \tag{A.8}$$

Finally, by inserting this expression in (A.7), θ_c can be evaluated.

$$\Longrightarrow \theta_c = 2\arctan\left\{\frac{-2\,\frac{K_{II}}{K_I}}{1 + \sqrt{1 + 8\left(\frac{K_{II}}{K_I}\right)^2}}\right\} \tag{A.9}$$

From (A.2) it can be seen that for $K_{II} = 0$, $\sin\left(\frac{\theta_c}{2}\right) = 0$ and therefore $\theta_c = 0$. Equation (A.9) fulfills this condition too and is - thus - valid for all (K_{II})s.

A.2. Derivatives of enrichment functions

In this section the required derivatives for the different enrichment functions $\psi_\star(\mathbf{x})$ will be shown.

Derivatives of the crack path enrichment function

With the method shown in Section 4.6, there are no integration points on the discontinuity of the function, therefore, $\psi_{jump}(\mathbf{x})$ is constant in all considered regions. Thus the derivatives are:

$$\frac{\partial \psi_{jump}(\mathbf{x})}{\partial x} = \frac{\partial \psi_{jump}(\mathbf{x})}{\partial y} = 0 \tag{A.10}$$

Derivatives of the tip enrichment functions

The functions $\psi_{tip}^{(i)}(r,\theta)$ are given in (3.5). The derivatives should be evaluated on a specific point $\mathbf{x}$, with $\mathbf{x}_{t(i)}$ as tip position and $\theta_{t(i)}$ the tip angle from tip i (shown in Figure A.1).

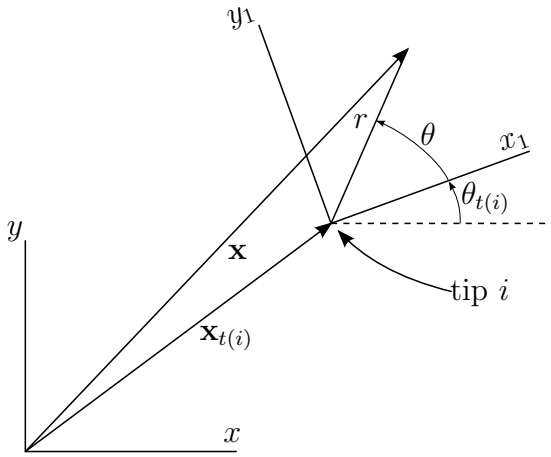

Figure A.1. Tip coordinate systems

The local polar coordinates (r,θ) for any point $\mathbf{x}$ can be evaluated by:

$$r(x,y) = \sqrt{(x-x_{t(i)})^2 + (y-y_{t(i)})^2} \tag{A.11}$$

$$\theta(x,y) = \arctan\left(\frac{y-y_{t(i)}}{x-x_{t(i)}}\right) - \theta_{t(i)} \tag{A.12}$$

As the derivatives with respect to $\mathbf{x}$ for a specific position $\mathbf{x}$ are required, the chain rule is used.

$$\begin{aligned}
\frac{\partial \psi_{tip}^{(i)}(\mathbf{x})}{\partial x} &= \frac{\partial \psi_{tip}^{(i)}(r,\theta)}{\partial r}\cdot\frac{\partial r}{\partial x} + \frac{\partial \psi_{tip}^{(i)}(r,\theta)}{\partial \theta}\cdot\frac{\partial \theta}{\partial x} \\
\frac{\partial \psi_{tip}^{(i)}(\mathbf{x})}{\partial y} &= \frac{\partial \psi_{tip}^{(i)}(r,\theta)}{\partial r}\cdot\frac{\partial r}{\partial y} + \frac{\partial \psi_{tip}^{(i)}(r,\theta)}{\partial \theta}\cdot\frac{\partial \theta}{\partial y}
\end{aligned} \tag{A.13}$$

The derivatives of r and θ can be evaluated from (A.11) and (A.12):

$$\begin{aligned}
\frac{\partial r}{\partial x} &= \frac{x-x_{t(i)}}{\sqrt{(x-x_{t(i)})^2 + (y-y_{t(i)})^2}} = \frac{x-x_{t(i)}}{r(x,y)} \\
\frac{\partial r}{\partial y} &= \frac{y-y_{t(i)}}{\sqrt{(x-x_{t(i)})^2 + (y-y_{t(i)})^2}} = \frac{y-y_{t(i)}}{r(x,y)}
\end{aligned} \tag{A.14}$$

$$\begin{aligned}
\frac{\partial \theta}{\partial x} &= -\frac{(y-y_{t(i)})}{(x-x_{t(i)})^2 + (y-y_{t(i)})^2} = -\frac{(y-y_{t(i)})}{r^2(x,y)} \\
\frac{\partial \theta}{\partial y} &= \frac{(x-x_{t(i)})}{(x-x_{t(i)})^2 + (y-y_{t(i)})^2} = \frac{(x-x_{t(i)})}{r^2(x,y)}
\end{aligned} \tag{A.15}$$

The derivatives of $\psi_{tip}^{(i)}$ can be determined in a straight forward way from (3.5):

$$\begin{aligned}\frac{\partial \psi_{tip}^{(1)}}{\partial r} &= \frac{1}{2\sqrt{r}} \cdot \sin\left(\frac{\theta}{2}\right) \\ \frac{\partial \psi_{tip}^{(1)}}{\partial \theta} &= \frac{\sqrt{r}}{2} \cdot \cos\left(\frac{\theta}{2}\right)\end{aligned} \tag{A.16}$$

$$\begin{aligned}\frac{\partial \psi_{tip}^{(2)}}{\partial r} &= \frac{1}{2\sqrt{r}} \cdot \cos\left(\frac{\theta}{2}\right) \\ \frac{\partial \psi_{tip}^{(2)}}{\partial \theta} &= -\frac{\sqrt{r}}{2} \cdot \sin\left(\frac{\theta}{2}\right)\end{aligned} \tag{A.17}$$

$$\begin{aligned}\frac{\partial \psi_{tip}^{(3)}}{\partial r} &= \frac{1}{2\sqrt{r}} \cdot \sin(\theta) \cdot \sin\left(\frac{\theta}{2}\right) \\ \frac{\partial \psi_{tip}^{(3)}}{\partial \theta} &= \sqrt{r} \cdot \left(\frac{\sin(\theta) \cdot \cos\left(\frac{\theta}{2}\right)}{2} + \cos(\theta) \cdot \sin\left(\frac{\theta}{2}\right)\right)\end{aligned} \tag{A.18}$$

$$\begin{aligned}\frac{\partial \psi_{tip}^{(4)}}{\partial r} &= \frac{1}{2\sqrt{r}} \cdot \sin(\theta) \cdot \cos\left(\frac{\theta}{2}\right) \\ \frac{\partial \psi_{tip}^{(4)}}{\partial \theta} &= \sqrt{r} \cdot \left(-\frac{\sin(\theta) \cdot \sin\left(\frac{\theta}{2}\right)}{2} + \cos(\theta) \cdot \cos\left(\frac{\theta}{2}\right)\right)\end{aligned} \tag{A.19}$$

A.3. Calculate local coordinates from global coordinates for quadrilaterals

In some sections the calculation of the natural coordinates (r, s), for a specific quadrilateral, from global Cartesian coordinates (x, y) is required. Here, the way to calculate this is shown. Starting with Equations (1.31) and (1.32) we get:

$$\begin{aligned}&\frac{(rs - r - s + 1)}{4} \cdot \hat{\mathbf{x}}_0 + \frac{(-rs - s + r + 1)}{4} \cdot \hat{\mathbf{x}}_1 + \\ &\frac{(rs + r + s + 1)}{4} \cdot \hat{\mathbf{x}}_2 + \frac{(-rs - r + s + 1)}{4} \cdot \hat{\mathbf{x}}_3 = \mathbf{x}\end{aligned}$$

$$\begin{aligned}&rs \cdot \underbrace{\frac{(\hat{\mathbf{x}}_0 - \hat{\mathbf{x}}_1 + \hat{\mathbf{x}}_2 - \hat{\mathbf{x}}_3)}{4}}_{\mathbf{a}} + r \cdot \underbrace{\frac{(-\hat{\mathbf{x}}_0 + \hat{\mathbf{x}}_1 + \hat{\mathbf{x}}_2 - \hat{\mathbf{x}}_3)}{4}}_{\mathbf{b}} + \\ &s \cdot \underbrace{\frac{(-\hat{\mathbf{x}}_0 - \hat{\mathbf{x}}_1 + \hat{\mathbf{x}}_2 + \hat{\mathbf{x}}_3)}{4}}_{\mathbf{c}} + \underbrace{\frac{(\hat{\mathbf{x}}_0 + \hat{\mathbf{x}}_1 + \hat{\mathbf{x}}_2 + \hat{\mathbf{x}}_3)}{4}}_{\mathbf{d}} = \mathbf{x}\end{aligned}$$

$$\mathbf{a} = \begin{bmatrix} a_x \\ a_y \end{bmatrix} \qquad \mathbf{b} = \begin{bmatrix} b_x \\ b_y \end{bmatrix} \qquad \mathbf{c} = \begin{bmatrix} c_x \\ c_y \end{bmatrix} \qquad \mathbf{d} = \begin{bmatrix} d_x \\ d_y \end{bmatrix}$$

From the x - component of the equation it follows:

$$r \cdot (sa_x + b_x) + sc_x + d_x = x$$

$$\Longrightarrow r = \frac{x - sc_x - d_x}{sa_x + b_x} \tag{A.20}$$

From the y - component of the equation s can be evaluated:

$$\frac{x - sc_x - d_x}{sa_x + b_x} \cdot (sa_y + b_y) + sc_y + d_y - y = 0$$

$$sa_y x - s^2 c_x a_y - s d_x a_y + x b_y - s c_x b_y - d_x b_y +$$
$$s^2 c_y a_x + (d_y - y) \cdot s a_x + s c_y b_x + (d_y - y) \cdot b_x = 0$$

$$s^2 \cdot \underbrace{(-c_x a_y + c_y a_x)}_{e} + s \cdot \underbrace{(a_y x - d_x a_y - c_x b_y + d_y a_x - y a_x + c_y b_x)}_{f} +$$
$$\underbrace{(x b_y - d_x b_y + d_y b_x - y b_x)}_{g} = 0$$

$$\Longrightarrow s = -\frac{f}{2e} \pm \sqrt{\left(\frac{f}{2e}\right)^2 - \frac{g}{e}} \tag{A.21}$$

To evaluate if there is the '+'-sign or the '−'-sign in (A.21), firstly, r and s are calculated with the '+'-sign. If this point is inside the element ($|r| \leq 1$ and $|s| \leq 1$) this result is used. Otherwise r and s are recalculated with the '−'-sign in (A.21) and this result is used.

A.4. Span of the tip enrichment functions

By comparing the span of the displacements of the crack tip field (2.3) and (2.6), with the span of crack tip enrichment functions (3.5), they have to be equal.

From (3.5):

$$V_1 = span\left\{\sqrt{r}\sin\left(\frac{\theta}{2}\right), \sqrt{r}\cos\left(\frac{\theta}{2}\right), \sqrt{r}\sin(\theta)\sin\left(\frac{\theta}{2}\right), \sqrt{r}\sin(\theta)\cos\left(\frac{\theta}{2}\right)\right\} \tag{A.22}$$

From (2.3) and (2.6):

$$V_2 = span\left\{\sqrt{r}\sin\left(\frac{\theta}{2}\right), \sqrt{r}\cos\left(\frac{\theta}{2}\right), \sqrt{r}\cos(\theta)\sin\left(\frac{\theta}{2}\right), \sqrt{r}\cos(\theta)\cos\left(\frac{\theta}{2}\right)\right\} \tag{A.23}$$

With (A.24) and (A.25) it is shown that (A.22) and (A.23) are equal.

$$\sqrt{r}\cos(\theta)\sin\left(\frac{\theta}{2}\right) = \sqrt{r}\left[\cos^2\left(\frac{\theta}{2}\right) - \sin^2\left(\frac{\theta}{2}\right)\right]\sin\left(\frac{\theta}{2}\right) =$$
$$\sqrt{r}\left[2\cos^2\left(\frac{\theta}{2}\right) - 1\right]\sin\left(\frac{\theta}{2}\right) = \sqrt{r}\sin(\theta)\cos\left(\frac{\theta}{2}\right) - \sqrt{r}\sin\left(\frac{\theta}{2}\right) \tag{A.24}$$

$$\sqrt{r}\cos(\theta)\cos\left(\frac{\theta}{2}\right) = \sqrt{r}\left[\cos^2\left(\frac{\theta}{2}\right) - \sin^2\left(\frac{\theta}{2}\right)\right]\cos\left(\frac{\theta}{2}\right) =$$
$$\sqrt{r}\left[1 - 2\sin^2\left(\frac{\theta}{2}\right)\right]\cos\left(\frac{\theta}{2}\right) = \sqrt{r}\cos\left(\frac{\theta}{2}\right) - \sqrt{r}\sin(\theta)\sin\left(\frac{\theta}{2}\right) \tag{A.25}$$

A.5. Details using Gauss' theorem for the interaction integral

In Section 4.8.1 the Gauss' theorem is applied to Equation (4.35). One resulting term was not considered. Here it is shown that this term is zero. Therefore, the equilibrium equation (1.1), the strain-displacement relations (1.6) and (1.7), the constitutive law (1.11) and the symmetry of the stress tensor $\mathbf{S}$ and the elasticity tensor $\mathbb{C}$ is used.

$$\begin{aligned}
&\frac{\partial}{\partial x_j}\left[\sigma^{(1)}_{mn}\epsilon^{(2)}_{mn}\delta_{j1} - \sigma^{(1)}_{ij}\frac{\partial u^{(2)}_i}{\partial x_1} - \sigma^{(2)}_{ij}\frac{\partial u^{(1)}_i}{\partial x_1}\right] \\
=&\underbrace{\frac{\partial \sigma^{(1)}_{mn}}{\partial x_j}\epsilon^{(2)}_{mn}\delta_{j1}}_{I} + \underbrace{\sigma^{(1)}_{mn}\frac{\partial \epsilon^{(2)}_{mn}}{\partial x_j}\delta_{j1}}_{II} - \\
&\underbrace{\frac{\partial \sigma^{(1)}_{ij}}{\partial x_j}\frac{\partial u^{(2)}_i}{\partial x_1}}_{=0\,(1.1)} - \underbrace{\sigma^{(1)}_{ij}\frac{\partial^2 u^{(2)}_i}{\partial x_1\,\partial x_j}}_{III} - \underbrace{\frac{\partial \sigma^{(2)}_{ij}}{\partial x_j}\frac{\partial u^{(1)}_i}{\partial x_1}}_{=0\,(1.1)} - \underbrace{\sigma^{(2)}_{ij}\frac{\partial^2 u^{(1)}_i}{\partial x_1\,\partial x_j}}_{IV}
\end{aligned} \tag{A.26}$$

$$\begin{aligned}
I =& \frac{\partial \sigma^{(1)}_{mn}}{\partial x_1}\epsilon^{(2)}_{mn} = \underbrace{\mathbb{C}_{mnop}}_{=\mathbb{C}_{opmn}}\frac{\partial \epsilon^{(1)}_{op}}{\partial x_1}\epsilon^{(2)}_{mn} = \frac{\partial \epsilon^{(1)}_{op}}{\partial x_1}\sigma^{(2)}_{op} = \frac{1}{2}\left(\sigma^{(2)}_{op}\frac{\partial^2 u^{(1)}_o}{\partial x_1\,\partial x_p} + \sigma^{(2)}_{op}\frac{\partial^2 u^{(1)}_p}{\partial x_1\,\partial x_o}\right) \\
=& \frac{1}{2}\left(\sigma^{(2)}_{op}\frac{\partial^2 u^{(1)}_o}{\partial x_1\,\partial x_p} + \underbrace{\sigma^{(2)}_{po}}_{=\sigma^{(2)}_{op}}\frac{\partial^2 u^{(1)}_o}{\partial x_1\,\partial x_p}\right) = \sigma^{(2)}_{op}\frac{\partial^2 u^{(1)}_o}{\partial x_1\,\partial x_p} = \sigma^{(2)}_{ij}\frac{\partial^2 u^{(1)}_i}{\partial x_1\,\partial x_j} = IV
\end{aligned} \tag{A.27}$$

$$\begin{aligned}
II =& \frac{1}{2}\left(\sigma^{(1)}_{mn}\frac{\partial^2 u^{(2)}_m}{\partial x_j\,\partial x_n} + \sigma^{(1)}_{mn}\frac{\partial^2 u^{(2)}_n}{\partial x_j\,\partial x_m}\right)\delta_{j1} = \frac{1}{2}\left(\sigma^{(1)}_{mn}\frac{\partial^2 u^{(2)}_m}{\partial x_j\,\partial x_n} + \underbrace{\sigma^{(1)}_{nm}}_{=\sigma^{(1)}_{mn}}\frac{\partial^2 u^{(2)}_m}{\partial x_j\,\partial x_n}\right)\delta_{j1} \\
=& \sigma^{(1)}_{mn}\frac{\partial^2 u^{(2)}_m}{\partial x_1\,\partial x_n} = \sigma^{(1)}_{ij}\frac{\partial^2 u^{(2)}_i}{\partial x_1\,\partial x_j} = III
\end{aligned} \tag{A.28}$$

A.6. Derivatives of the analytical crack tip field

In Section 2.2, the analytical solution for a crack tip near field is shown. In this section the derivatives of these displacements, in the local tip coordinate system (x_1, y_1), are shown. As the displacements are given as function of (r, θ), the chain

rule is used:

$$\begin{aligned}\frac{\partial u}{\partial x_1} &= \frac{\partial u}{\partial r}\cdot\frac{\partial r}{\partial x_1} + \frac{\partial u}{\partial \theta}\cdot\frac{\partial \theta}{\partial x_1}\\ \frac{\partial u}{\partial y_1} &= \frac{\partial u}{\partial r}\cdot\frac{\partial r}{\partial y_1} + \frac{\partial u}{\partial \theta}\cdot\frac{\partial \theta}{\partial y_1}\end{aligned} \tag{A.29}$$

The derivatives of r and θ can be found with:

$$\begin{aligned}r &= \sqrt{x_1^2 + y_1^2}\\ \implies \frac{\partial r}{\partial x_1} &= \frac{x_1}{r} = \cos(\theta) \qquad (A.30)\\ \implies \frac{\partial r}{\partial y_1} &= \frac{y_1}{r} = \sin(\theta) \qquad (A.31)\end{aligned}$$

$$\begin{aligned}x_1 &= r\cdot\cos(\theta)\\ 1 &= \frac{\partial r}{\partial x_1}\cdot\cos(\theta) - r\cdot\sin(\theta)\cdot\frac{\partial \theta}{\partial x_1}\\ 1-\cos^2(\theta) &= \sin^2(\theta) = -r\cdot\sin(\theta)\cdot\frac{\partial \theta}{\partial x_1}\\ \implies \frac{\partial \theta}{\partial x_1} &= -\frac{\sin(\theta)}{r}\end{aligned} \tag{A.32}$$

$$\begin{aligned}y_1 &= r\cdot\sin(\theta)\\ 1 &= \frac{\partial r}{\partial y_1}\cdot\sin(\theta) + r\cdot\cos(\theta)\frac{\partial \theta}{\partial y_1}\\ 1-\sin^2(\theta) &= \cos^2(\theta) = r\cdot\cos(\theta)\frac{\partial \theta}{\partial y_1}\\ \implies \frac{\partial \theta}{\partial y_1} &= \frac{\cos(\theta)}{r}\end{aligned} \tag{A.33}$$

For Mode I the derivatives of u, v can be given as:

$$\begin{pmatrix}\frac{\partial u}{\partial r}\\ \frac{\partial v}{\partial r}\end{pmatrix} = \frac{K_I}{4G}\sqrt{\frac{1}{2r\pi}}(\kappa-\cos(\theta))\begin{pmatrix}\cos(\frac{\theta}{2})\\ \sin(\frac{\theta}{2})\end{pmatrix} \tag{A.34}$$

$$\begin{pmatrix}\frac{\partial u}{\partial \theta}\\ \frac{\partial v}{\partial \theta}\end{pmatrix} = \frac{K_I}{2G}\sqrt{\frac{r}{2\pi}}\left[\frac{(\kappa-\cos(\theta))}{2}\begin{pmatrix}-\sin(\frac{\theta}{2})\\ \cos(\frac{\theta}{2})\end{pmatrix} + \sin(\theta)\begin{pmatrix}\cos(\frac{\theta}{2})\\ \sin(\frac{\theta}{2})\end{pmatrix}\right] \tag{A.35}$$

For Mode II the derivatives of u, v can be given as:

$$\begin{pmatrix}\frac{\partial u}{\partial r}\\ \frac{\partial v}{\partial r}\end{pmatrix} = \frac{K_{II}}{4G}\sqrt{\frac{1}{2r\pi}}\begin{pmatrix}\sin(\frac{\theta}{2})[\kappa+2+\cos(\theta)]\\ -\cos(\frac{\theta}{2})[\kappa-2+\cos(\theta)]\end{pmatrix} \tag{A.36}$$

$$\begin{pmatrix}\frac{\partial u}{\partial \theta}\\ \frac{\partial v}{\partial \theta}\end{pmatrix} = \frac{K_{II}}{2G}\sqrt{\frac{r}{2\pi}}\begin{pmatrix}\frac{\cos(\frac{\theta}{2})}{2}[\kappa+2+\cos(\theta)] - \sin(\frac{\theta}{2})\sin(\theta)\\ \frac{\sin(\frac{\theta}{2})}{2}[\kappa-2+\cos(\theta)] + \cos(\frac{\theta}{2})\sin(\theta)\end{pmatrix} \tag{A.37}$$

Bibliography

[1] E. Anderson, Z. Bai, C. Bischof, S. Blackford, J. Demmel, J. Dongarra, J. Du Croz, A. Greenbaum, S. Hammarling, A. McKenney, and D. Sorensen. *LAPACK Users' Guide*. Society for Industrial and Applied Mathematics, Philadelphia, PA, third edition, 1999.

[2] K.-J. Bathe. *Finite Element Procedures*. Prentice-Hall, Englewood Cliffs, 1996.

[3] T. Belytschko and T. Black. Elastic crack growth in finite elements with minimal remeshing. *International Journal for Numerical Methods in Engineering*, 45(5):601–620, 1999.

[4] T. Belytschko, N. Moës, S. Usui, and C. Parimi. Arbitrary discontinuities in finite elements. *International Journal for Numerical Methods in Engineering*, 50(4):993–1013, 2001.

[5] C. Celigoj. *Methode der Finiten Elemente*. Institut für Festigkeitslehre TU Graz, Graz, 1998.

[6] C. Celigoj. *Festigkeitslehre*. Institut für Festigkeitslehre TU Graz, Graz, 2004.

[7] F. Erdogan and G. Sih. On the crack extension in plates under plane loading and transverse shear. *Journal of Basic Engineering*, 85(4):519–525, 1963.

[8] H.L. Ewalds and R.J.H. Wanhill. *Fracture Mechanics*. Edward Arnold, London, 1986.

[9] T.-P. Fries. *The eXtended Finite Element Method*. RWTH Aachen University, http://www.xfem.rwth-aachen.de, (01.03.2013).

[10] T.-P. Fries and T. Belytschko. The intrinsic XFEM: a method for arbitrary discontinuities without additional unknowns. *International Journal for Numerical Methods in Engineering*, 68(13):1358–1385, 2006.

[11] T.-P. Fries and T. Belytschko. The extended/generalized finite element method: An overview of the method and its applications. *International Journal for Numerical Methods in Engineering*, 84(3):253–304, 2010.

[12] C. Geuzaine and J.-F. Remacle. Gmsh reference manual. 2013.

[13] D. Gross and T. Seelig. *Bruchmechanik*. Springer-Verlag, Berlin, 5.Auflage, 2011.

[14] M. Hammer. *The Finite Element Method - Linear and Non-Linear Structural Analysis*. Institut für Festigkeitslehre TU Graz, Graz, 2012.

[15] R. Huang, N. Sukumar, and J.-H. Prévost. Modeling quasi-static crack growth with the extended finite element method. part II: Numerical applications. *International Journal of Solids and Structures*, 40(26):7539–7552, 2003.

[16] J.D. Hunter. Matplotlib: A 2d graphics environment. *Computing In Science & Engineering*, 9(3):90–95, 2007.

[17] B. Lawn. *Fracture of Brittle Solids*. Cambridge University Press, New York, second edition, 1993.

[18] A.N. Lowan, N. Davids, and A. Levenson. Table of the zeros of the Legendre polynomials of order 1-16 and the weight coefficients for Gauss' mechanical quadrature formula. *Bulletin of the American Mathematical Society*, 48(10):739–743, 1942.

[19] N. Moës, J. Dolbow, and T. Belytschko. A finite element method for crack growth without remeshing. *International Journal for Numerical Methods in Engineering*, 46(1):131–150, 1999.

[20] C.F. Shih and R.J. Asaro. Elastic-Plastic Analysis of Cracks on Bimaterial Interfaces: Part I—Small Scale Yielding. *Journal of Applied Mechanics*, 55:299–316, 1988.

[21] G.C. Sih, P.C. Paris, and F. Erdogan. Crack-tip stress intensity factors for plane extension and plane bending problems. *Journal of Applied Mechanics*, 29:306–312, 1962.

[22] M. Stolarska, D.L. Chopp, N. Moës, and T. Belytschko. Modelling crack growth by level sets in the extended finite element method. *International Journal for Numerical Methods in Engineering*, 51(8):943–960, 2001.

[23] N. Sukumar, N. Moës, B. Moran, and T. Belytschko. Extended finite element method for three-dimensional crack modelling. *International Journal for Numerical Methods in Engineering*, 48(11):1549–1570, 2000.

[24] N. Sukumar and J.-H. Prévost. Modeling quasi-static crack growth with the extended finite element method part I: Computer implementation. *International Journal of Solids and Structures*, 40(26):7513–7537, 2003.

[25] B. Wu, Z. Xu, and Z. Li. A note on imposing displacement boundary conditions in finite element analysis. *Communications in Numerical Methods in Engineering*, 24(9):777–784, 2008.

[26] J.F. Yau, S.S. Wang, and H.T. Corten. A mixed-mode crack analysis of isotropic solids using conservation laws of elasticity. *Journal of Applied Mechanics*, 47:335–341, 1980.